University of Alberta

Seismic Analysis and Design of Steel Plate Shear Walls

by

Anjan Kanti Bhowmick

A thesis submitted to the Faculty of Graduate Studies and Research
in partial fulfillment of the requirements for the degree of

Doctor of Philosophy

in

Structural Engineering

Department of Civil and Environmental Engineering

©Anjan Kanti Bhowmick

Fall 2009

Edmonton, Alberta

Examining Committee

Dr. Robert G. Driver, Department of Civil and Environmental Engineering

Dr. Gilbert Y. Grondin, Department of Civil and Environmental Engineering

Dr. Oya Mercan, Department of Civil and Environmental Engineering

Dr. Jozef Szymanski, Department of Civil and Environmental Engineering

Dr. Patricio F. Mendez, Department of Chemicals and Materials Engineering

Dr. Colin A. Rogers, Department of Civil Engineering and Applied Mechanics, McGill University, Canada

ABSTRACT

A nonlinear finite element model was developed to study the behaviour of unstiffened steel plate shear walls. The model was validated using the results from quasi-static and dynamic experimental programs. With the validated finite element model, the performance of 4-storey and 8-storey Type D (ductile) and Type LD (limited-ductility) steel plate shear walls with moment-resisting beam-to-column connections was studied under spectrum-compatible seismic records.

A design procedure that aims to achieve optimal seismic behaviour for steel plate shear walls was proposed. The proposed method uses the concepts of indirect capacity design principles of CAN/CSA-S16-01 to identify the infill plates that are likely to yield in the design earthquake. The proposed method was used for the design of two 4-storey and one 8-storey shear walls. Design axial forces and moments in the boundary columns for the shear walls were shown to be in good agreement with nonlinear seismic analysis results. Results also showed that some of the other capacity design methods available generally underestimate the maximum design forces in the columns, while others can be overly conservative. The effect of loading rate on the dynamic behaviour of steel plate shear walls was also investigated, as was the $P - \Delta$ effect in terms of its influence on seismic demand in shear and flexure.

A shear strength model of the infill plate with circular openings at any location was developed based on a strip model where all the strips with perforations were

partially discounted. A design method for steel plate shear walls with perforations was introduced. The method was applied for the design of boundary columns of a 4-storey steel plate shear wall with perforations. The predicted design forces in the columns for the 4-storey perforated shear wall agreed well with the forces obtained from nonlinear seismic analysis.

Finally, an improved simple formula for estimating the fundamental period of steel plate shear walls was developed by regression analysis of the period data obtained from frequency analysis of series of steel plate shear walls. In addition, the effectiveness of a shear–flexure cantilever formulation for determining fundamental periods and $P - \Delta$ effects of steel plate shear walls was studied.

ACKNOWLEDGEMENTS

TABLE OF CONTENTS

LIST OF TABLES

LIST OF FIGURES

1. INTRODUCTION

1.1 General

Steel plate shear walls (SPSWs) are a lateral force resisting system which resist both wind and earthquake forces. A SPSW consists of vertical steel plates, referred to as infill plates, which are connected to boundary beams and columns over the full height of a frame. The infill plates can be stiffened or unstiffened. Also, the surrounding steel frame may use either simple or moment resisting beam-to-column connections. A properly designed SPSW has high ductility, high initial stiffness, and high energy dissipation capacity. In comparison to commonly used reinforced concrete shear walls, steel plate shear walls are much lighter, which reduces the gravity loads and seismic loads to be transmitted to the foundation. Furthermore, the use of steel plate shear walls allows for the use of a single trade on site, the steel erection crew, which is a benefit compared to reinforced concrete shear walls with steel frames. These considerations can significantly reduce construction costs.

The design philosophy for SPSWs prior to the 1980s was to prevent shear buckling of the infill plate by using either thick infill plates or by adding stiffeners to the infill plate. After the work of Thorburn et al. (1983), the design philosophy in most jurisdictions changed to the use of thin unstiffened infill plates. In SPSWs with thin unstiffened infill plates, axial coupling of column loads is the principal mechanism for resisting the overturning moment, while the shear is resisted primarily by a diagonal tension field that develops in the infill plates after they

have buckled. This design philosophy is adopted in the current Canadian (CAN/CSA-S16-01) and American (AISC 2005) steel design standards.

Both the American and Canadian steel design standards require SPSWs to be designed according to a capacity design approach. Capacity design of structures involves pre-selecting a localized ductile fuse (or fuses) to act as the primary location for the dissipation of seismic energy. The structure must be designed so as to force the inelastic action to be concentrated at that fuse (or fuses). In SPSWs, yielding in the infill plates and plastic hinging at the end of the beams are considered the ductile fuses. Based on capacity design principles, AISC 2005 enlisted three different capacity design approaches for the design of SPSWs. These are: nonlinear pushover analysis; indirect capacity design approach, adopted from CAN/CSA-S16-01; and combined linear elastic computer programs and capacity design concepts. Berman and Bruneau (2008) proposed another capacity design method for the design of boundary columns. These capacity design methods have never been studied under real seismic loadings and, thus, there is a need for seismic evaluation of all the capacity design approaches available in the literature. The research described herein includes nonlinear seismic analysis of several multi-storey steel plate shear walls under spectrum compatible seismic records. Also, because of the expenses involved in the experimental programs to evaluate the capacity design methods, an analytical tool that can accurately predict the monotonic, cyclic and dynamic behaviour of thin unstiffened SPSWs is needed.

Despite the recent advancements in research involving design and analysis of unstiffened SPSWs, some obstacles still exist, impeding wider acceptance of the SPSW system. For example, the minimum infill plate thickness required for handling and welding purposes may be thicker than that required for a seismic design. When the capacity design approach is used, the thicker plate will induce relatively large design forces on the surrounding frame members, requiring larger beams and columns to develop the yield capacity of the infill plate..

The practical concern for utility placement is another issue to be dealt with. In case the utilities need to pass through an opening in any infill plate, according to current design practice, that opening must be heavily stiffened, making the SPSW system expensive. Therefore, work is needed to find a viable solution for having openings in the infill plates. Vian (2005) conducted experimental work on a pattern of multiple regularly spaced circular perforations in the infill plate, and Purba (2006) proposed an equation to determine the shear strength of a perforated infill plate with the specific perforation pattern proposed by Vian (2006). However, more work is needed to determine the shear strength of perforated infill plates with perforations in any location in the infill plate. Also, a simplified design method for the design of perforated SPSWs is needed.

Current design codes (NBCC 2005, NEHRP 2003) provide the same period formula for seismic design of both reinforced concrete shear walls and SPSWs,

which are known to have different dynamic properties. This empirical period formula needs to be evaluated.

1.2 Objectives and Scope

One of the main objectives of this research was to develop an analytical model for SPSWs that includes geometric and material nonlinearities and loading rate effects. The analytical model was to be verified by the results from nonlinear pushover, cyclic and dynamic tests. The validated numerical model was then used to study the seismic performances of two different steel plate shear walls, namely: Type D (ductile) and Type LD (limited ductility) plate walls, specified in CAN/CSA-S16-01.

Another main objective was to evaluate capacity design methods currently available in the literature. Nonlinear seismic analyses of multi-storey steel plate shear walls were carried out to achieve this objective. $P - \Delta$ effects and strain rate effects on the flexural demand of steel plate shear walls were also of primary interest.

With the evaluation of all available capacity design methods, there was a need for a simple and more accurate design method for SPSWs for earthquake loading. Thus, a further objective was to propose a simplified seismic design method. Nonlinear seismic analyses of three SPSWs were carried out to evaluate the effectiveness of the proposed design method.

A simplified method for the design of SPSWs with perforations was considered to be important for use by structural designers. Therefore, an important objective was to develop a simplified design method that can predict the behaviour of SPSWs with circular perforations in arbitrary locations in the panel under real seismic loadings.

Another objective of this research was to evaluate the code-specified period formula for SPSWs and propose an improved empirical formula if needed. A series of frequency analyses of SPSWs with different geometry was done to achieve this objective.

The final objective of this research work was to study the effectiveness of the use of a simple shear flexure cantilever instead of a full SPSW model for determining fundamental period, interstorey drift and $P - \Delta$ effects.

1.3 Outline of the Thesis

This section provides an overview of the manner in which the remainder of the thesis is organized.

Chapter 2 presents a brief review of previous research on unstiffened SPSWs. The review includes a summary of relevant experimental and analytical work on SPSWs. Research on perforated SPSWs is also presented.

Chapter 3 describes the finite element model that was developed to predict the behaviour of thin unstiffened SPSWs. The finite element model is validated against the test results of four different SPSWs. Pushover analysis, quasi-static cyclic analysis and dynamic analysis results are compared with the test results. The validated finite element model is then used to study the performance of Type D and Type LD steel plate walls under spectrum compatible earthquake loadings in two major cities in Canada.

Chapter 4 presents results of nonlinear seismic analyses of one 4-storey and one 15-storey SPSWs, designed according to the capacity design principles of the current Canadian standard, CAN/CSA-S16-01. The effect of loading rate on the dynamic behaviour of SPSWs is investigated. Also investigated is the $P - \Delta$ effect on seismic demand in shear and flexure.

In Chapter 5, a design procedure that aims to achieve optimal seismic behaviour for SPSWs is presented. The proposed method is used for the design of two 4-storey and one 8-storey steel plate shear walls. Design forces in the boundary columns for the three different SPSWs are compared with nonlinear seismic analysis results. Also, other capacity design approaches that have been proposed in the literature to date are evaluated in this chapter.

Chapter 6 presents a numerical study of unstiffened SPSWs with circular perforations in the infill plates. A shear strength model of the infill plate with

6

circular openings at any location is developed. Different perforation patterns in SPSWs of two different aspect ratios were analyzed to assess the proposed model. A design method for SPSWs with perforations is introduced. The method is applied for the design of boundary columns of a 4-storey SPSW with infill plate perforations.

Chapter 7 presents an evaluation of the code-specified period formula for SPSWs. A series of frequency analyses of single and multi-storey SPSWs with different geometry is carried out. An improved empirical formula developed by regression analysis of the period data obtained from these analyses is proposed. Also, the effectiveness of the use of a simple shear flexure cantilever for determining fundamental periods, interstorey drifts and $P - \Delta$ effects of SPSWs is studied.

Finally, a summary of the research and the key conclusions, as well as recommendations for future research, are presented in Chapter 8.

2. PREVIOUS RESEARCH ON STEEL PLATE SHEAR WALLS

2.1 Introduction

Numerous research programs have been conducted since the early 1970s to study the design and behaviour of steel plate shear walls. Early designs of steel plate shear walls (SPSWs) were based on the concept of preventing shear buckling of infill plates under design lateral loads, thus using heavily stiffened thin-panels and neglecting any post-buckling strength. In recent years, the idea of utilizing the post-buckling strength with the use of thin unstiffened infill plates has gained wide acceptance from researchers and designers in Canada and the United States. This chapter summarizes some of the previous research on thin unstiffened SPSWs. Research on the development of the strip model to represent the behaviour of unstiffened thin infill plates is presented first, followed by experimental and analytical research on single or multi-storey unstiffened SPSWs. Research on SPSWs with openings in the infill plates has gained attention from researchers (Roberts and Sabouri-Ghomi 1992, Vian 2005, and Purba 2006) since perforations in the infill plates can significantly reduce the design forces on boundary columns by weakening the infill plates. Also, perforated infill plates can be used to accommodate the passage of utility systems. Research on perforated SPSWs is presented.

2.2 Thorburn et al. (1983)

The first research on thin unstiffened SPSWs was done by Thorburn et al. (1983), who developed an analytical model to study their shear resistance. The model was

based on the theory of pure diagonal tension by Wagner (1931). The shear

strength of the panel prior to buckling was neglected, leaving only the tension

field action as the load resisting mechanism. In the model, known as the "strip

model", the infill plate was modelled as a series of pin-ended inclined strips

oriented in the same direction as the principal tensile stresses in the infill plate.

Each strip was assigned an area equal to the plate thickness multiplied by the

width of the strip. Fig. 2.1 shows a strip model for a typical panel. In the model,

the interior beams were assumed infinitely stiff. Fig. 2.1 shows beams with simple

connections, but other end conditions can be modelled. The angle of inclination of

the tension field was obtained using the principle of least work. Only axial energy

in the beams and columns and the energy from the tension field were considered.

The angle of inclination of the tension field, α, thus developed was:

$$\tan^4 \alpha = \left[\frac{1 + \dfrac{Lt_p}{2A_c}}{1 + \dfrac{ht_p}{A_b}} \right] \tag{2.1}$$

where L is the frame bay width, h is the frame storey height, t_p is the infill plate

thickness and A_b and A_c are cross-sectional areas of the storey beam and

column, respectively.

The researchers also conducted analytical studies to determine the number of

strips that were required to model the behaviour of the infill plate adequately, and

concluded that 10 strips would be sufficient to represent an infill panel. Thorburn

et al. (1983) also studied the use of a single equivalent diagonal brace for preliminary analysis of multi-storey shear walls. The area of the brace is derived such that the storey stiffness is the same as that for the strip model. The researchers also conducted a parametric study to investigate the influence of infill plate thickness, panel width, panel height, and column stiffness on strength and stiffness of the panel. The study showed that the parameters studied are inter-related and can influence the resulting tension field.

2.3 Timler and Kulak (1983)

Timler and Kulak (1983) performed a test on a single-storey large-scale SPSW specimen to verify the strip model proposed by Thorburn et al. (1983). The specimen consisted of a pair of single-storey, one-bay, SPSWs with pinned joints at the four extreme corners. The specimen was loaded to both service and ultimate levels. A cyclic loading up to the allowable deflection limit was also performed.

Timler and Kulak (1983) recognized that the bending stiffness of the columns affects the value of the angle of inclination of the tension field. Thus Eq. (2.1), originally developed by Thorburn et al. (1983), was revised as follows:

$$\tan^4 \alpha = \left[\frac{1 + \dfrac{Lt_p}{2A_c}}{1 + ht_p \left(\dfrac{1}{A_b} + \dfrac{h^3}{360 I_c L} \right)} \right] \tag{2.2}$$

where I_c is the moment of inertia of the column and the other variables were defined earlier. Timler and Kulak (1983) demonstrated reasonable agreement

between the predicted angles of inclination with the measured angles of inclination during the test.

Timler and Kulak (1983) modelled their test specimen using the strip model to analyse it. Good correlation was found between predicted and test results of the infill plate stresses, axial strains, and the load-deflection response. The strip model proposed by Thorburn et al. (1983) and the angle of inclination of the tension field proposed by Timler and Kulak (1983) have been adopted by both the Canadian standard, CAN/CSA S16-09 (CSA 2009) and the American specification (AISC 2005).

2.4 Roberts and Sabouri-Ghomi (1992)

Roberts and Sabouri-Ghomi (1992) conducted a series of quasi-static cyclic loading tests on unstiffened steel plate shear panels with centrally placed circular openings. The specimens had a constant depth, d, of 300 mm, width, b, of either 300 mm or 450 mm and panel thickness, h, of either 0.83 mm or 1.23 mm. The test setup consisted of the shear panel clamped between pairs of stiff, pin-ended frame members. Two diagonally opposite pinned corners were connected to the hydraulic grips of a 250 kN servo-hydraulic testing machine, where the loading was applied. For the diameter of the central circular opening, D, four different values (0, 60, 105, and 150 mm) were selected. The schematic of a typical test specimen is shown in Fig. 2.2. Based on the quasi-static test results, the researchers recommended that strength $\left(V_{yp,perf}\right)$ and stiffness $\left(K_{perf}\right)$ of a

11

perforated panel can be conservatively approximated by applying a linear reduction factor to the strength $\left(V_{yp}\right)$ and stiffness $\left(K_{panel}\right)$ of a similar solid panel.

$$\frac{V_{yp,perf}}{V_{yp}} = \frac{K_{perf}}{K_{panel}} = \left[1 - \frac{D}{d}\right] \tag{2.3}$$

The researchers also developed a theoretical model for predicting the hysteretic characteristics of unstiffened steel plate shear panels. The model was modified by the linear reduction factor, obtained by using Eq. (2.3), for perforated shear panels. A comparison with the test results of perforated shear panels showed that the theoretical model gave reasonable but conservative estimates of the test results.

2.5 Xue and Lu (1994)

Xue and Lu (1994) conducted a numerical study on a three-bay, twelve-storey frame designed for code specified seismic loading. Four different frame configurations having identical frame members in all cases, but different connection arrangements in each, were considered. For each case, the exterior bays had moment resisting beam-to-column connections and the interior bay had infill plates in every storey. Two different beam-to-column connections at the interior bay, full moment connections (**F)** or partial moment (shear type) connections (**P)** and two different arrangements for connecting the infill plate to the boundary members in a panel (connecting to both beams and columns, **GC**, or connecting only to beams, **G**) made four different frame-wall systems: **F-GC**, **F-G, P-GC,** and **P-G**. For comparison, upper and lower bound cases of frame-shear

wall systems were also included in the analyses. The upper bound case consisted of frames with all moment resisting connections for beam-to-column connections and all the infill plates in every storey connected with both the beams and columns. The infill plates in the upper bound case were not assumed to buckle under applied load. The lower bound case consisted of a frame with simple beam-to-column in the interior bay and with no infill plates.

The six frame-wall systems were modelled using elastic beam elements for beams and columns and four-node shell elements with large deformation capacity for infill plates. The initial imperfections introduced in the infill plates consisted of the superposition of several shear buckling modes of the infill plates. Lateral loads were applied monotonically at each floor and no gravity loads were applied. Pushover (base shear vs. top displacement) curves for different frame-wall systems showed that infill plates in the interior bay increased the lateral stiffness of the system significantly, but the type of beam-to-column connection in the interior bay had a minimal effect on lateral stiffness of the system. The **F-GC** system had a lateral stiffness as high as the upper bound case, but its columns were required to resist a substantial portion of the storey shear, which might cause early damage or failure of critical columns. The frames with infill plates connected to the beams only (**P-G** systems) were found to have stiffness slightly lower than the stiffness of the **F-GC** systems. Based on all the analysis results, Xue and Lu (1994) recommended that **P-G** systems be used. No tests were performed to verify the conclusions.

2.6 Driver et al. (1997; 1998)

Driver et al. (1997, 1998) conducted quasi-static cyclic testing on a large-scale, four-storey, single bay SPSW specimen. The specimen had moment resisting beam-to-column connections and the unstiffened infill plates were welded to fish plates that were also welded to the boundary members. The test specimen, as shown in Fig. 2.3, was 7.5 m high and 3.05 m wide between column centrelines, with the first storey height of 1.93 m and a typical storey height of 1.83 m for the remaining stories. The infill plates for the first and second storey were nominally 4.8 mm thick. For the third and fourth storey, infill plate thicknesses of 3.4 mm were used. Gravity loads were applied to the tops of the columns and equivalent cyclic lateral loads were applied at each floor level, as per the requirements of ATC-24 (Applied Technology Council 1992). The storey shear versus storey deformation of the first panel was used to control the test.

A total of 30 load cycles were applied to the test specimen, out of which 20 cycles were in the inelastic range. The test specimen was found to have high initial stiffness, excellent ductility and high energy dissipation capability. After the ultimate strength was attained, the deterioration of the load-carrying capacity was gradual and stable. The maximum deflection attained by the lowest storey prior to failure of the specimen was nine times the yield deflection.

Driver et al. (1997) developed a finite element model to analyse their test specimen. Beams and columns were modelled with beam elements and infill

plates were modelled with shell elements. Initial imperfections based on the first buckling mode of the infill plate were included in the finite element model. Experimentally-obtained residual stresses for the boundary members were also included in the model. Because of convergence problems, geometric nonlinearity was not included up to the ultimate load. Both static pushover and cyclic analyses were performed. For the pushover analysis, an excellent prediction of the ultimate strength was observed, but it overestimated the initial stiffness slightly. For the cyclic analysis, the load vs. displacement curves had good agreement with the test data, but they did not capture the pinching of the hysteresis loops developed during the test.

Driver et al. (1997) extended the strip model to include inelastic behaviour in the analysis of their test specimen. Each infill plate was replaced by 10 diagonal pin-ended strips. Inelastic behaviour in both the inclined tension strips and in the boundary members was modelled. Although the strip model slightly underestimated the elastic stiffness of the test specimen, excellent agreement was obtained with the ultimate strength.

2.7 Lubell et al. (2000)

Lubell et al. (2000) conducted quasi-static cyclic testing for two single-storey steel plate shear walls specimen (SPSW1 and SPSW2) and one 4-storey specimen (SPSW4). The two single storey specimens are depicted in Fig. 2.4. In all specimens, the beam-to-column connections were moment resisting connections.

All beams and columns were S75×8 sections and all infill plates were 1.5 mm thick. The only difference between the SPSW1 and SPSW2 specimens was that the top beam of specimen SPSW2 consisted of two S75×8 sections, fully welded together. This was done to better anchor the tension field developed in the infill plate. For the same reason, a S200×34 section was used at the top beam of the SPSW4 specimen. It was found during fabrication of SPSW1 that the initial out-of-plane displacement of the infill plate was 26 mm. To minimise the out-of plane displacements, cautions were taken during fabrication of the other two specimens. Thus, the maximum out-of-plane displacement observed for SPSW2 and SPSW4 was less than 5 mm.

All the specimens were tested under quasi-static cyclic loading. The load history followed the procedures recommended in ATC-24 (Applied Technology council 1992) guidelines. The single storey specimens were loaded at the top of the panel and for the SPSW4 specimen, equal lateral loads were applied in each storey. Also for the 4-storey specimen, a constant gravity load of 13.5 kN was applied in each storey. All the specimens showed well-defined load–deformation envelopes, high initial stiffness, and stable hysteresis behaviour. Specimen SPSW2 showed a significant increase in stiffness and capacity compared to specimen SPSW1, mainly due to the use of a stiffer beam in SPSW2 and large initial out-of-plane deformations in SPSW1. Significant "pull-in" of the columns was observed in all specimens due to their low flexural stiffness. A less desirable yielding sequence was observed for specimen SPSW4 where columns yielded before significant

16

yielding in the infill plates. This resulted in a state of global instability and termination of test at a first storey displacement of $1.5\delta_y$, where δ_y is the yield displacement at the first storey. The researchers stated that an increased overturning moment in the multi-storey specimen resulted in high axial forces and moments in the columns and thereby altered the yielding sequence (columns yielding before infill plates). Thus, they recommended that design standards should require that SPSWs be analysed as a whole, as the behaviour of a single isolated panel is different than a panel in a multi-storey SPSW.

Lubell et al. (2000) also conducted a series of numerical analyses of the test specimens using a nonlinear frame analysis program. The capacities of all the test specimens were predicted reasonably well, but the elastic stiffness was significantly overestimated for the SPSW1 and SPSW4 specimens. Based on the results obtained from the analyses, Lubell et al. (2000) concluded that the design standard at that time, CAN/CSA S16.1-M94, did not address design-related issues like the effect of large overturning moments, the influence of aspect ratio, and the potential for undesirable yielding sequences of the shear wall components for multi-storey SPSWs.

2.8 Rezai (1999)

Rezai (1999) conducted shake-table testing on a quarter-scale, 4-storey SPSW to study the seismic performance of multi-storey SPSWs. The 4-storey shake table specimen is shown in Fig. 2.5. The columns were made of $B100\times9$ sections in

every storey. Measured member properties for B100×9 section are given in the literature (Rezai 1999). All beam-to-column connections were full moment connections and all the infill plates were 1.5 mm thick. At each storey, steel plates were placed on the beams to provide a storey mass of 1700 kg. The specimen was braced in the out-of-plane direction. Before doing the shake table testing, Rezai (1999) conducted low-amplitude vibration test on the 4-storey specimen to determine its frequency. The fundamental frequency of the shake table specimen was obtained as 6.1 Hz in the longitudinal direction. The test specimen was subjected to a number of site-recorded and synthetically generated ground motions at varying intensities. The limited capacity of the shake table prevented a significant inelastic response from the specimen. Thus, the interpretations and recommendations by the researcher were based on the response of the system mainly in the elastic range.

Rezai (1999) found that the first mode was the primary mode of vibration with very little contribution from higher modes. From load–deformation plots of all four storey levels, it was found that that majority of the energy was dissipated by the first storey. Also, the first storey was dominated mostly by shear deformations, while the top storey acted as a rigid body rotating about the first storey. Furthermore, it was found that the flexural strain generated in the intermediate level beams was negligible. Thus, it was concluded that loads in the infill plates at the top and bottom of an inter-storey beam counteract each other.

Rezai (1999) also conducted a series of analyses on the test specimens of Lubell et al. (2000) and the shake table specimen. Based on these analytical studies, an important conclusion was that even though the column sections used were very small hot-rolled sections, they contributed significantly in developing the tension field in the infill plates. It was also found that the premature column yielding and the formation of plastic hinges in the columns resulted in a less ductile behaviour. The use of lower yield strengths for the infill plates in comparison to the yield strengths of boundary members was suggested to ensure yielding in the infill plates first.

2.9 Behbahanifard et al. (2003)

Behbahanifard et al. (2003) conducted quasi-static cyclic testing on a three-storey SPSW specimen, as shown in Fig. 2.6, consisting of the upper three stories of the Driver et al. (1997) specimen. Although the second storey infill plate buckled elastically during the previous test, there was no sign of damage (yielding). The loading sequence was similar to that used in the test by Driver et al. (1997). The specimen reached its ultimate capacity at a first storey displacement of $7\delta_y$, where δ_y is the yield displacement at the first storey of three-storey test specimen. After that, the strength started to decrease gradually due to the formation of tears in the lower storey infill plate. Overall, the specimen showed high initial stiffness, excellent ductility, and high energy dissipation capability.

A nonlinear finite element model based on the explicit formulation was developed in ABAQUS (Hibbitt et al. 2007) to simulate the monotonic and cyclic behaviour of both Behbahanifard et al. (2003) and Driver et al. (1997) specimens. A four node shell element with reduced integration (ABAQUS element S4R) was used for the beams, columns and infill plates. Residual stresses were not included in the finite element model for simplicity. For the cyclic analyses, a kinematic hardening material model was included to simulate the Bauschinger effect. The researchers reported that with the use of ABAQUS/Explicit, convergence was easily achieved. Excellent agreement was observed between the test results and the results from the finite element analyses. However, the capacity was slightly underestimated during the analysis (12% for three-storey specimen and 7.8% for four-storey specimen).

With the validated finite element model, a parametric study was conducted to investigate some non-dimensional parameters affecting the behaviour of a single storey SPSW. Ten non-dimensional parameters were identified, from which four are discussed here: aspect ratio $\left(\dfrac{L}{h}\right)$; ratio of axial stiffness of infill plate to column axial stiffness$\left(\dfrac{t_p L}{2 A_c}\right)$; a parameter relating to column flexibility parameter, ω_h, as defined in CAN/CSA S16-09; and a parameter related to initial imperfection magnitude. The researchers found that a decrease in the aspect ratio would generally increase the capacity of SPSWs. An increase in the axial stiffness ratio led to an increase in the stiffness of the shear wall. As the column flexibility

parameter decreased, the column lateral stiffness increased relative to the panel

stiffness. It was also demonstrated that initial out-of-plane imperfections could

significantly influence the initial stiffness of the shear panel. For imperfection

sizes larger than 1% of $\sqrt{Lh}$, the stiffness reduction was found to be noticeable

and it was recommended that it be accounted for in the design. Thus, it was

suggested that imperfections be limited in practice to 1% of $\sqrt{Lh}$.

2.10 Berman and Bruneau (2003)

Using the concept of plastic analysis and the strip model, Berman and Bruneau

(2003) derived equations to calculate the ultimate strength of single and multi-

storey SPSWs with simple or rigid beam-to-column connections. For a single

storey SPSW with simple beam-to-column connections, shown in Fig. 2.7, the

assumed collapse mechanism gives a storey shear strength, V_{yp} identical to the

expression given in CAN/CSA S16-01 for probable storey shear strength:

$$V_{yp} = 0.5F_{yp}t_pL\sin 2\alpha \tag{2.4}$$

where F_{yp} is the yield strength of the infill plate and all other parameters have

been defined earlier. Equation 2.4 was modified for a frame with rigid beam-to-

column connections by adding the components of internal work from plastic

moments in the columns and (or) beams.

To calculate ultimate strengths of multi-storey SPSWs, two types of failure

mechanism, as shown in Fig. 2.8, were assumed: (1) soft storey mechanism, and

(2) yielding of all infill plates and plastic hinging at the ends of all beams (except

for the top and bottom storey where plastic hinging is also allowed at the columns) formed simultaneously. These two mechanisms help the design engineer to estimate the ultimate strength of single or multi-storey SPSW and investigate the possibility of soft storey mechanisms.

Berman and Bruneau (2003) also looked at the design of SPSWs using the provisions of CAN/CSA S16-01. It was observed that for calculating infill plate thickness, the storey shear, V_s, found from the equivalent lateral force method, should be multiplied by a system overstrength factor, Ω_s, between 1.1 to 1.5. Thus, the minimum infill plate thickness required to resist storey shear is:

$$t = \frac{2V_s\Omega_s}{F_y L \sin 2\alpha} \tag{2.5}$$

where F_y is the nominal yield strength of the infill plate.

2.11 Berman and Bruneau (2005)

Berman and Bruneau (2005) conducted quasi-static testing of three specimens using light gauge cold-formed steel for the infill plate material. The prototype SPSWs were designed as seismic retrofits for a hospital structure (Yang and Whittaker 2002) with an emphasis given to minimising their impact on existing framing. Since the minimum infill plate thickness available is often greater than that required to resist design lateral forces, the light gauge material was selected to create a system just strong enough to resist the design seismic loading. Two of the specimens had flat infill plates (thickness of 0.9 mm), while the third was

designed with a corrugated infill plate with a thickness of 0.7 mm. Connection of the infill plates to the boundary frames is achieved through the use of bolts in combination with industrial strength epoxy or welds. A Type B steel deck, with the corrugations orientated at 45° from the horizontal, was used for the corrugated infill plate.

The bay width and storey height of the specimens were designed to be 3660 mm and 1830 mm, respectively (i.e., approximately 0.5 scale from the prototypes). Strip models were developed for each specimen and used to design the boundary frame members to remain elastic. In the case of the flat infill plates (Specimens F1 and F2), two alternatives were developed. The connection for Specimen F1 relied on industrial strength epoxy, which was determined to have a lap shear strength of approximately 17.2 MPa and a handling time of roughly 30 min. The infill plate was fully welded for Specimen F2. In the SPSW with corrugated infills (Specimen C1), the corrugated infill was connected to the boundary frame using the epoxy. As corrugated metal deck is available in only 910 mm or 610 mm widths, the infill of Specimen C1 was made up of four sections, as shown in Fig. 2.9. These sections were connected to each other using 1.6 mm diameter steel pop rivets spaced at 100 mm on centre. From coupon tests of the infill material, yield stresses of 152, 214, and 330 MPa were obtained for Specimens F1, F2, and C1, respectively.

The hysteresis curves for corrugated panel specimen C1 and flat panel specimen F2, along with pushover curves obtained from strip models of the specimens are shown in Fig. 2.10. The corrugated infill panel exhibited unsymmetric hysteresis loops, since tension field action only developed in the direction of the corrugations. It was thus recommended that two walls with opposed orientation of corrugations be used in a given structural line to achieve symmetric system behaviour. The specimen utilizing a flat infill and a welded connection to the boundary frame (specimen F2) reached a ductility ratio of 12 and drift of 3.7% and showed a reasonable agreement in initial stiffness and base shear strength with the monotonic pushover of a strip model, as shown in Fig. 2.10(b). Also, specimen F2 was significantly more ductile than the other two and failure was the result of fractures in the infill adjacent to the fillet weld used to connect the infill to the boundary frame.

2.12 Vian (2005)

Vian (2005) conducted quasi-static cyclic tests on three single-storey, single bay SPSW specimens. The first specimen had rigid beam-to-column connection with reduced beam sections (RBS) on the beams, and a solid infill plate of low yield strength (LYS) steel. The other two specimens had the same boundary frame properties as the first specimen, and either multiple regularly spaced circular perforations in the infill plate or reinforced quarter-circle cut-outs in the upper corners of the infill plate. The last two specimens were intended to accommodate the need for utility systems to pass-through the infill plate. The solid panel,

24

perforated, and cut-out corner-reinforced specimens were designated as S2, P, and CR specimens, respectively. The two specimens, P and CR, are shown in Figs. 2.11 and 2.12, respectively.

The SPSW specimens had a width of 4000 mm, centre-to-centre of columns, and a depth of 2000 mm. The infill plate used in the three specimens had a thickness of 2.6 mm with yield and ultimate stresses of 165 MPa and 305 MPa, respectively. The perforated specimen had staggered holes arranged at a 45° angle spaced at 300 mm centre-to-centre along both the vertical and horizontal directions to provide a panel strip width, S_{diag}, equal to 424 mm. The number of 200 mm diameter perforations along the diagonal strip was equal to 4. For the cut-out corner specimen, quarter-circle cut-outs of 500 mm radius at the upper corners of the infill plate were used. To reinforce along the cut-out edges, arch sections 160 mm wide by 19 mm thick were selected. In addition, another solid panel specimen (S1) was built and tested prior to the fabrication of the remaining three specimens mainly to investigate the fabricator's workmanship in using seam welds. Vian (2005) observed that substantial deficiencies in fabrication and inadequate overall quality of workmanship occurred. The problems were corrected for the other three specimens (S2, P and CR).

Quasi-static cyclic loading was applied for the three specimens. Specimen S2 and P were tested to a maximum interstorey drift of 3%, while specimen CR was tested to a maximum interstorey drift of 4%. During cyclic testing, all specimens

exhibited behaviour in which beam plastic hinging was located at the connection locations. This showed the effectiveness of RBS connections in SPSW beams and was recommended (Vian 2005) to control boundary frame yielding during a significant earthquake. The detailed perforated SPSW specimen (P) exhibited ductile behaviour during testing and thus showed that this system is a viable alternative to a solid panel SPSW, without the need for stiffeners around the perforations. The perforated layout was also recommended for use in SPSW applications where the minimum available plate thickness is larger than required. The cut-out reinforced corner specimen also performed well during testing and appeared to be an effective solution for SPSWs to allow for the passage of utilities.

Vian (2005) also conducted finite element analyses on the three tested specimens. In general, good agreement was observed between the test results and the hysteresis curves obtained from the analysis. The analytical model of the perforated SPSW was further extended to consider perforations in the infill plates with diameters of 100, 150, 200 mm. The results were compared to the results for individual perforated strips having the same perforation diameters. It was reported that the elongation predicted by the finite element model of an individual perforated strip and the full SPSW model, for monitored maximum strain, was significantly different and thus further research was recommended.

2.13 Purba (2006)

Purba (2006) conducted a series of finite element analyses to investigate the behaviour of unstiffened thin SPSWs having openings in the infill plate. The two designs, namely the perforated infill plate and the cut-out corner SPSW proposed by Vian (2005), were investigated. Similar to Vian (2005), individual perforated strips having a size of 2000 mm by 400 mm with 4 perforations along the strip length and perforation diameters, $D,$ from 10 mm to 300 mm were first analyzed to develop a fundamental understanding of the behaviour of complete perforated SPSW.

With the behaviour of individual perforated strips known, a series of 4000 mm by 2000 mm single-storey perforated SPSWs having multiple perforations were modelled. Shell elements were used to model both the infill plates and the boundary frame members. Nonlinear pushover analyses were carried out for the single-storey perforated SPSWs. Variations in perforation diameter and infill plate thickness were considered in the analyses. Purba (2006) found that the results from the individual perforated strip analysis can accurately predict the behaviour of complete perforated SPSW provided the holes diameter is less than 60% of the strip width $\left(\dfrac{D}{S_{diag}} \le 0.6 \right)$. It was found that no interaction exists between adjacent strips that could affect the stress distribution within an individual strip.

Purba (2006) also examined the applicability of using the equation (Eq. 2.3) proposed by Roberts and Sabouri-Ghomi (1992) to approximate the strength of a perforated infill plate with multiple perforations. Based on his analysis results, he concluded that shear strength of an infill plate of a SPSW having multiple regularly spaced circular perforations throughout the infill plate can be calculated by multiplying the shear strength of a solid infill plate by a factor $\left(1 - 0.7\dfrac{D}{S_{diag}}\right)$.

Purba (2006) also investigated two cut-out corner SPSW designs having flat-plate and T-section reinforcement along the cut-out edges. It was observed that there was very small difference in the shear strength of the infill plate. Thus, the flat-plate (with a minimum fish plate) was considered to be adequate to reinforce the cut-out edges.

2.14 Berman and Bruneau (2008)

Berman and Bruneau (2008) proposed a capacity design method for the design of boundary columns. In their method, a linear model of the column on elastic supports was first used to determine the axial forces in the beams. A uniform plastic collapse mechanism, proposed earlier by Berman and Bruneau (2003), was assumed to estimate the lateral seismic loads that cause full infill plate yielding and plastic hinging of the beams at their ends. Simple column free body diagrams, as shown in Fig. 2.13 for a generic 4-storey SPSW, was then used to determine the design column axial forces and moments. The free body diagrams include

28

distributed loads representing the web plate yielding at story i, ω_{xci} and ω_{yci}, moments from plastic hinging of the beams, M_{prli} and M_{prri}, axial forces from the beams, P_{bli} and P_{bri}, applied lateral seismic loads obtained from the plastic collapse mechanism considered, F_i, and base reactions for those lateral seismic loads, R_{yl}, R_{xl}, R_{yr}, and R_{xr}. The researchers explained how the various force components of the free body diagrams are to be determined.

To demonstrate the effectiveness of the proposed capacity design method, Berman and Bruneau (2008) designed two 4-storey SPSWs, one with constant infill plate thickness, SPSW-C, and the other with variable plate thickness, SPSW-V. Column design loads were also calculated using two other available capacity design approaches, namely the Indirect Capacity Design (ICD) approach and the combined linear elastic computer programs and capacity design concept (LE+CD), as described in the 2005 AISC seismic provisions for structural steel buildings (AISC 2005). Column axial loads and moments from the three capacity design approaches were compared with those from pushover analyses for both SPSW-C and SPSW-V. The proposed procedure was shown to give column design loads that are significantly closer to the nonlinear static pushover results than the two pre-existing procedures. Furthermore, the proposed procedure was able to capture important aspects of SPSW behaviour such as moment–axial force interaction in beams, and proper distribution of beam axial load to the right and left columns.

Berman and Bruneau (2008) concluded that the proposed capacity design procedure would provide reasonable column design forces for SPSWs that are expected to yield over their entire height, which restricts it typically to shorter SPSWs. They noted that this procedure will likely be overly conservative for tall SPSWs where simultaneous yielding of the web plates over the entire SPSW height is unlikely. In those situations, it was recommended that the column axial forces obtained from this proposed procedure be reduced (following a procedure similar to that proposed by Redwood and Channagiri (1991)) to account for some infill plates remaining partially elastic while others yield. However, they recommended that at each story the columns be designed to resist the moments generated by yielding of the web plates at that level and the corresponding frame moments.

2.15 Summary

Experimental and analytical research on thin unstiffened SPSWs has shown that the SPSW system possesses high initial stiffness, ultimate strength, and ductility, as well as stable hysteresis curves and a large energy dissipation capacity. To date, most of the analytical research on SPSWs is limited to nonlinear quasi-static analysis. Thus, minimal research has been conducted to characterise the nonlinear dynamic (seismic) behaviour of SPSWs.

Current Canadian and American seismic design provisions require that SPSWs be designed according to the capacity design approach. The capacity design methods

currently available in the literature have never been investigated based on seismic analysis.

Finally, researchers have recently demonstrated the use of an array of perforations in the infill plates to accommodate utility access and also to reduce the strength demand for the boundary framing members. However, the proposed design method is limited to a specific perforation layout only. Also, a capacity design method for the design of boundary columns, with perforations in the adjacent infill plates, is not currently available.
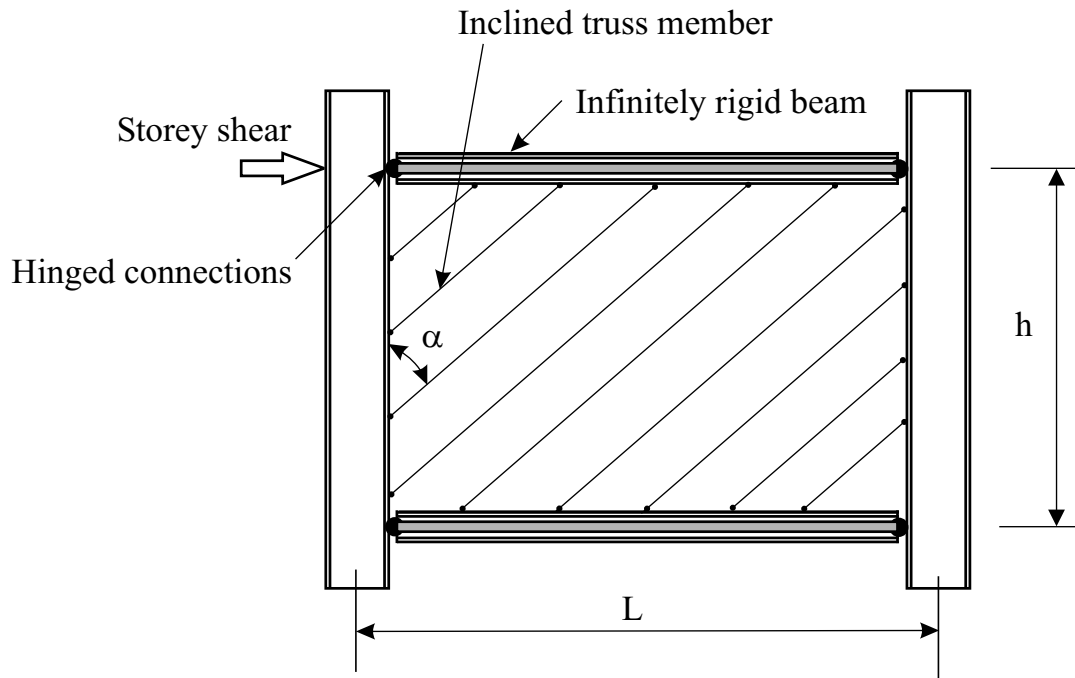
Fig. 2.1 Strip Model (Thorburn et al. 1983)
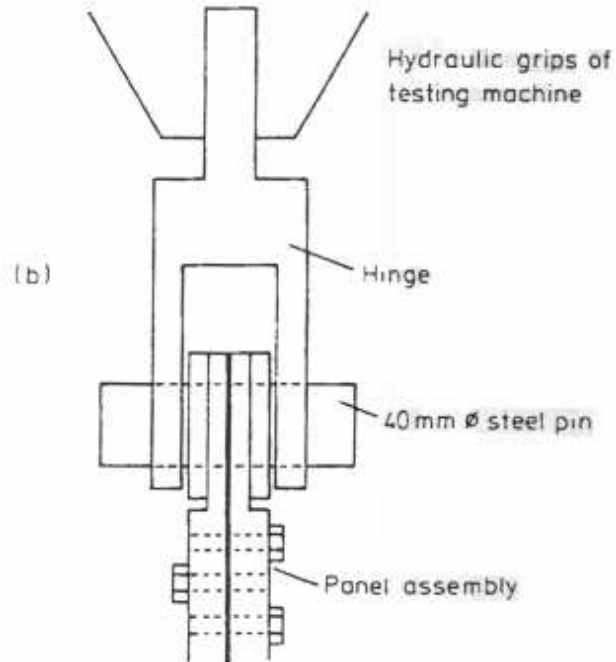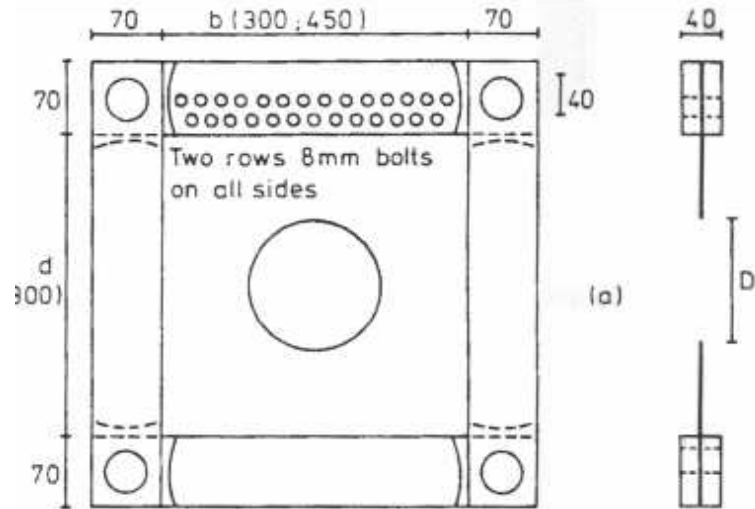
Fig. 2.2 Schematic of Test Specimen (Roberts and Sabouri-Ghomi 1992)
(a) Perforated Shear Panel and (b) Hinge
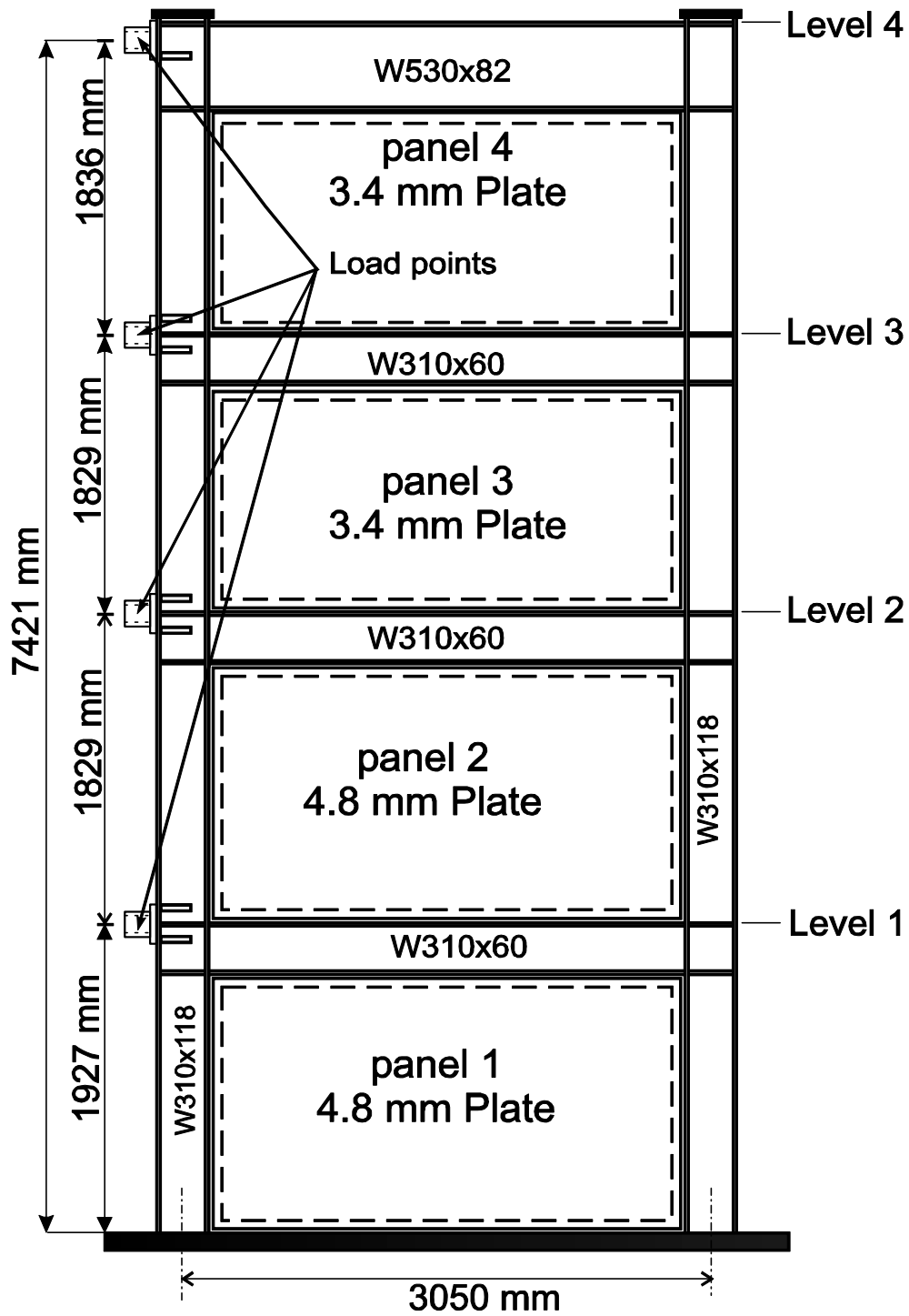
Fig. 2.3 Four-storey test specimen (Driver et al. 1997)
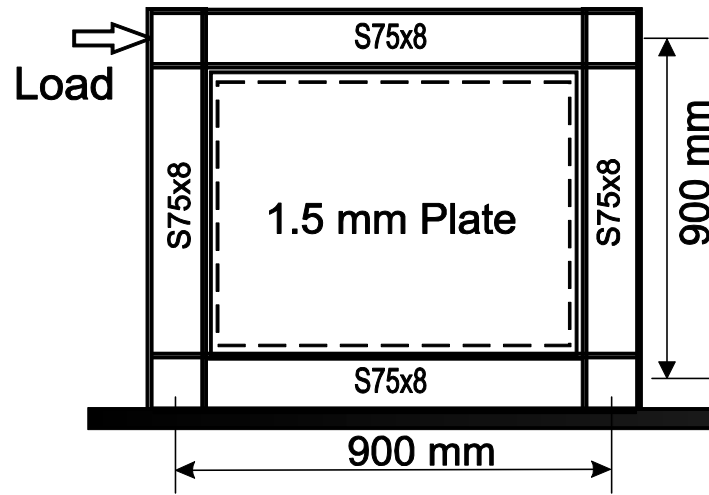
(a)
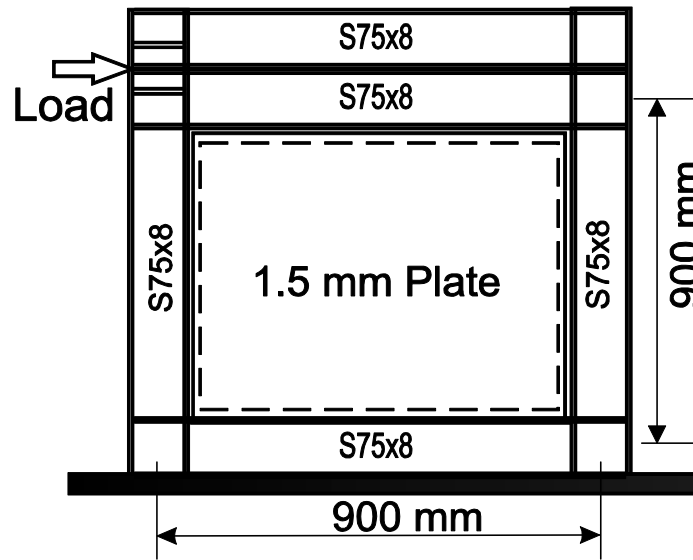
(b)

Fig. 2.4 Single storey test specimens (Lubell et al. 2000): (a) SPSW1, and (b)

SPSW2
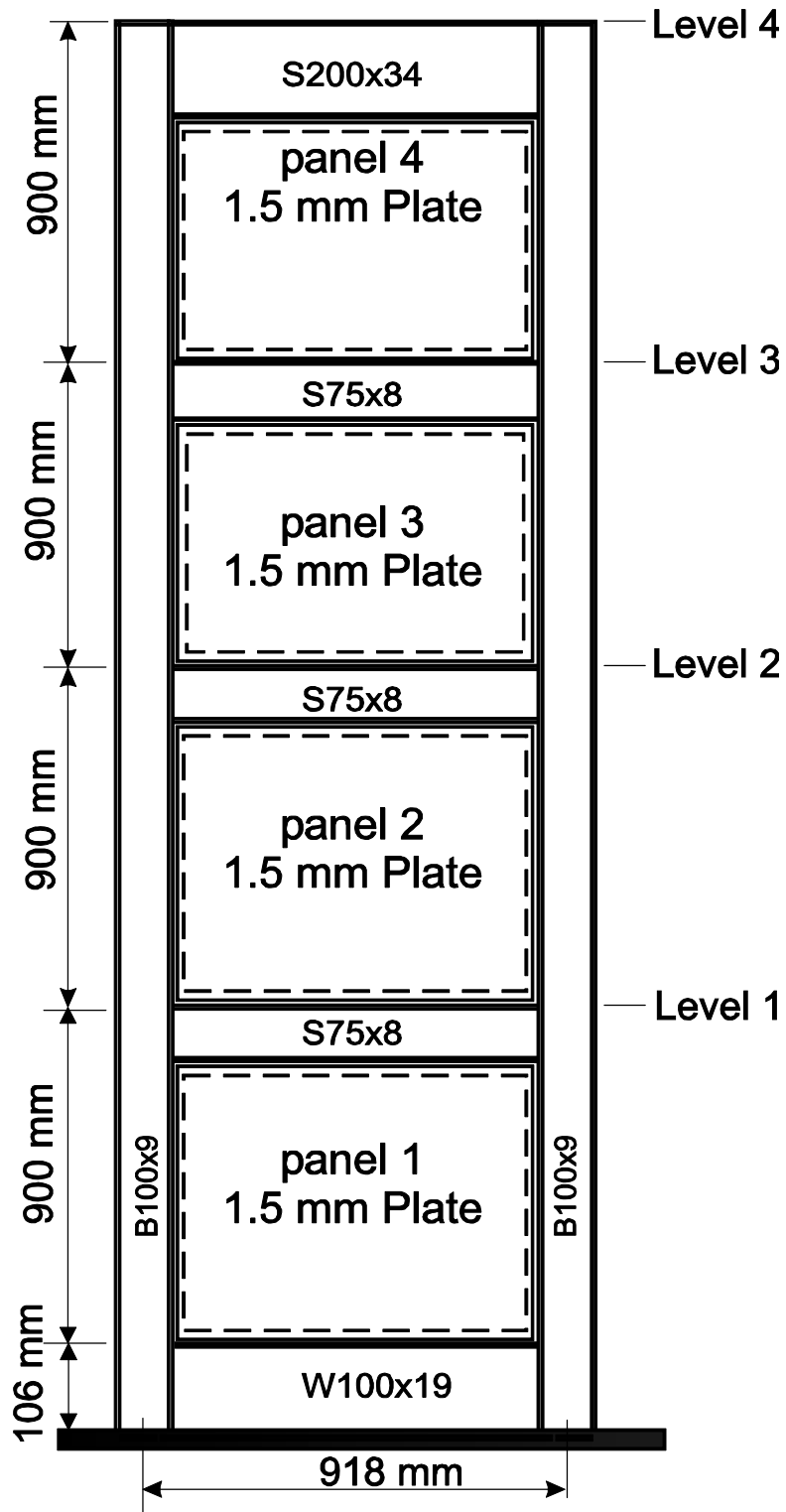
Fig. 2.5 Four-storey shake table test specimen (Rezai 1999)
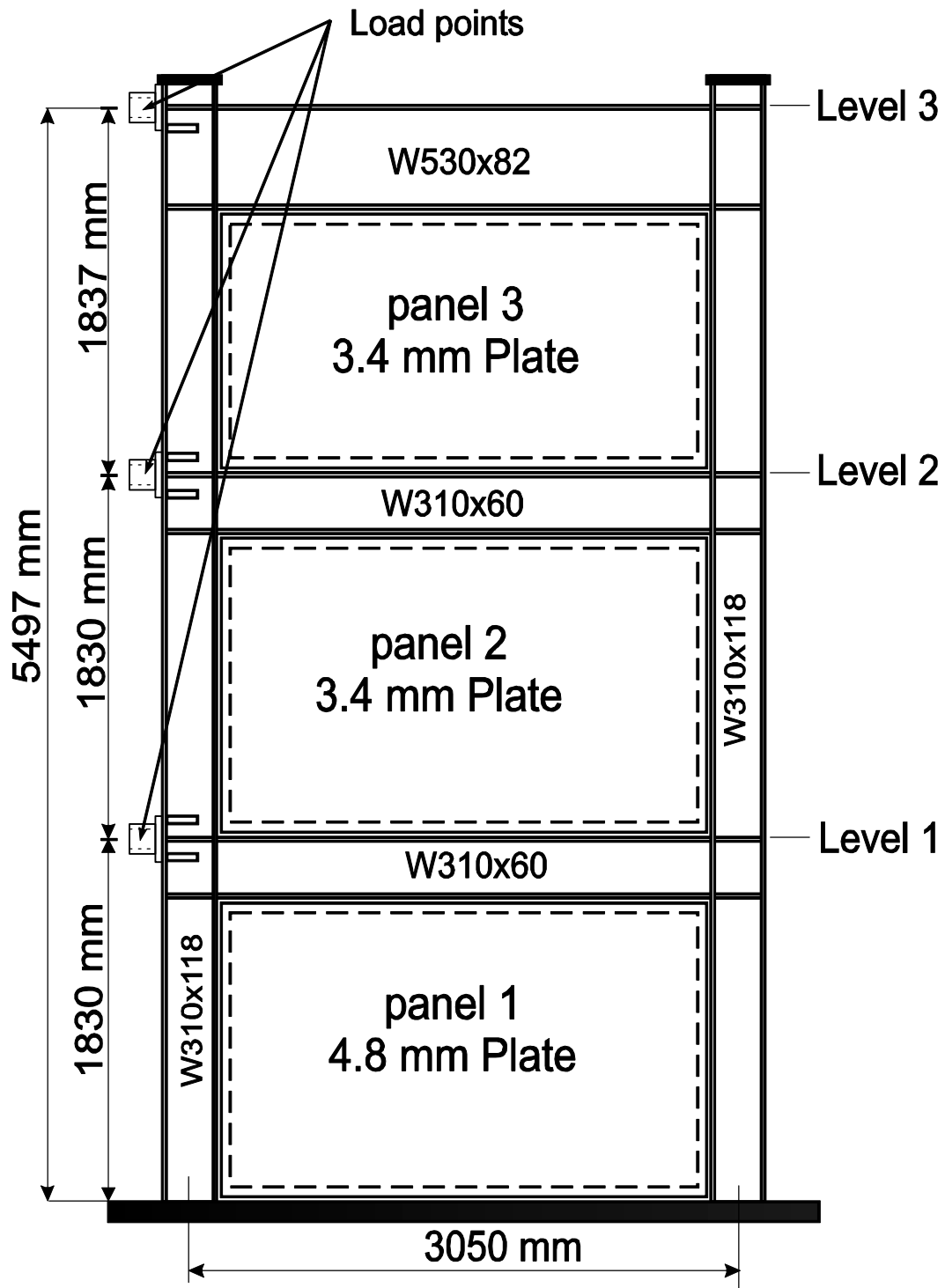
Fig. 2.6 Three-storey test specimen (Behbahanifard et al. 2003)
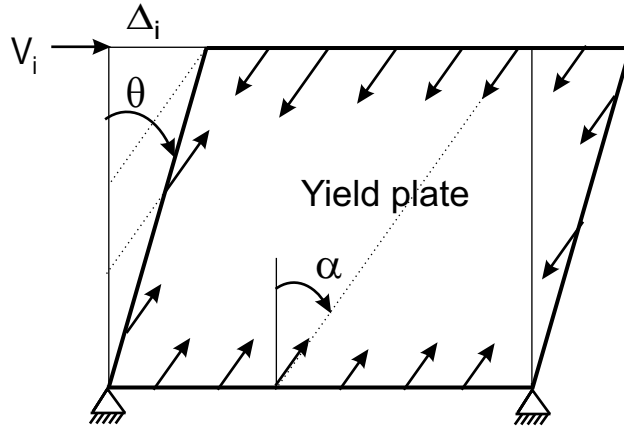
Fig. 2.7 Single storey SPSW collapse mechanism (Berman and Bruneau 2003)

(a)

(b)
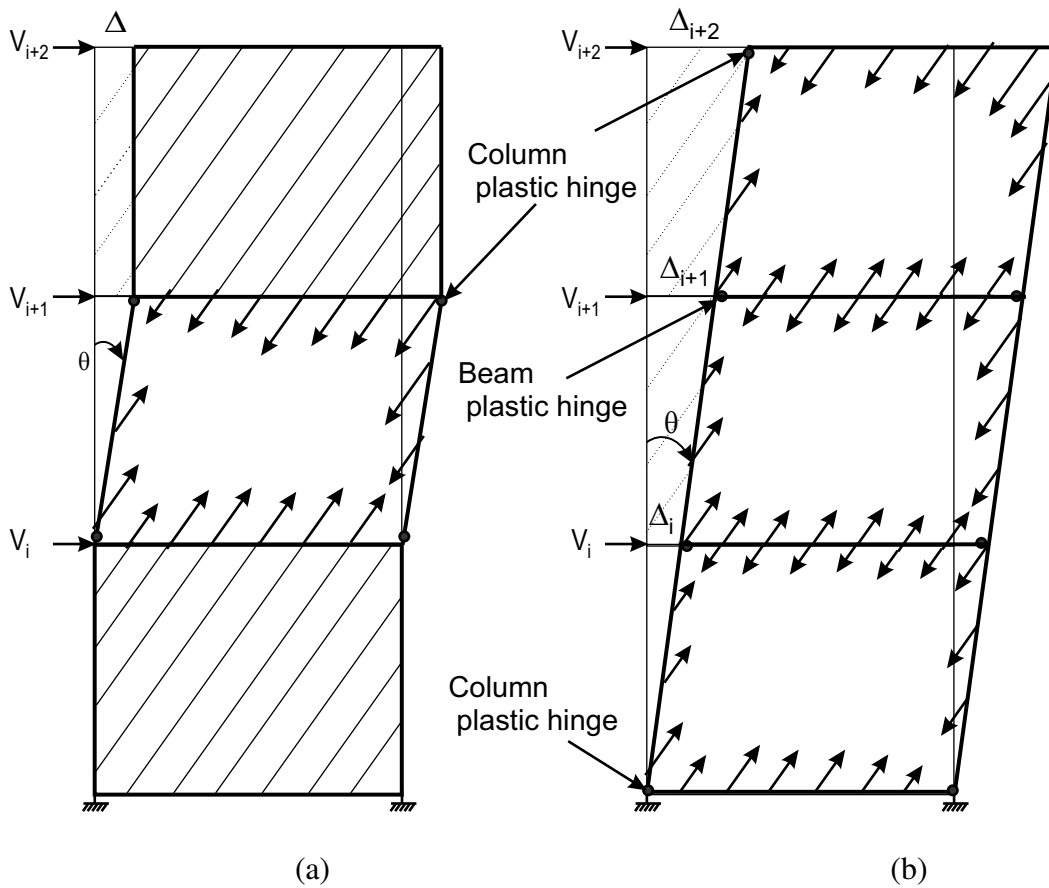
Fig. 2.8 Multi-storey SPSW collapse mechanisms: (a) Soft storey mechanism, and (b) Unified collapse mechanism (Berman and Bruneau 2003)
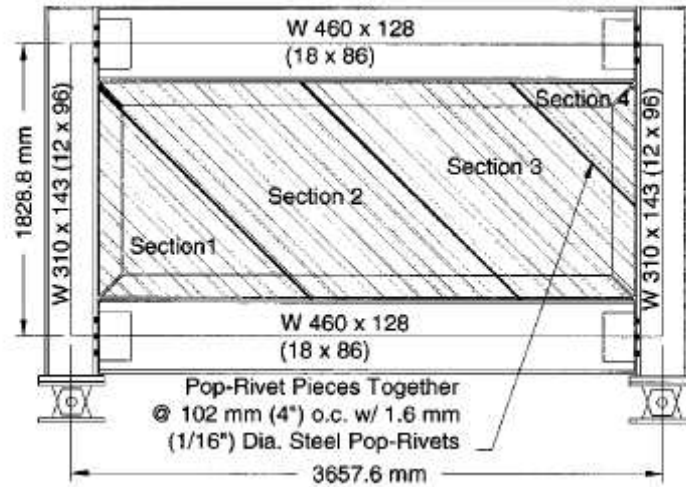
Fig. 2.9 Corrugated infill specimen (Berman and Bruneau 2005)
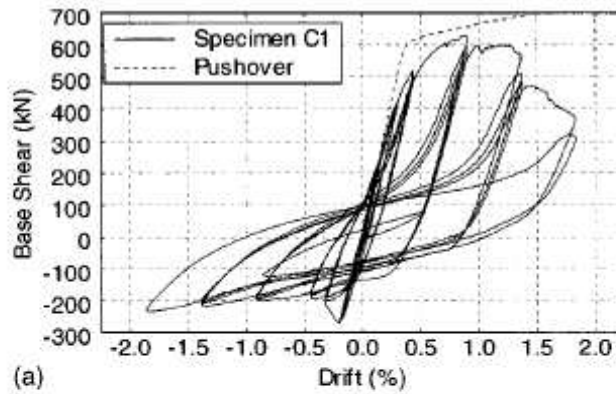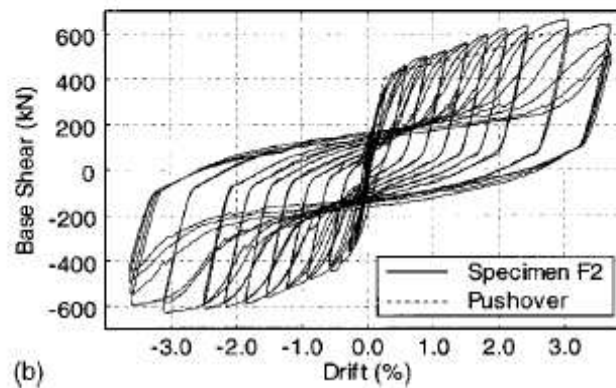
Fig. 2.10 Test hystereses and pushover curves: (a) Specimen C1 and (b) Specimen F2 (Berman and Bruneau 2005)
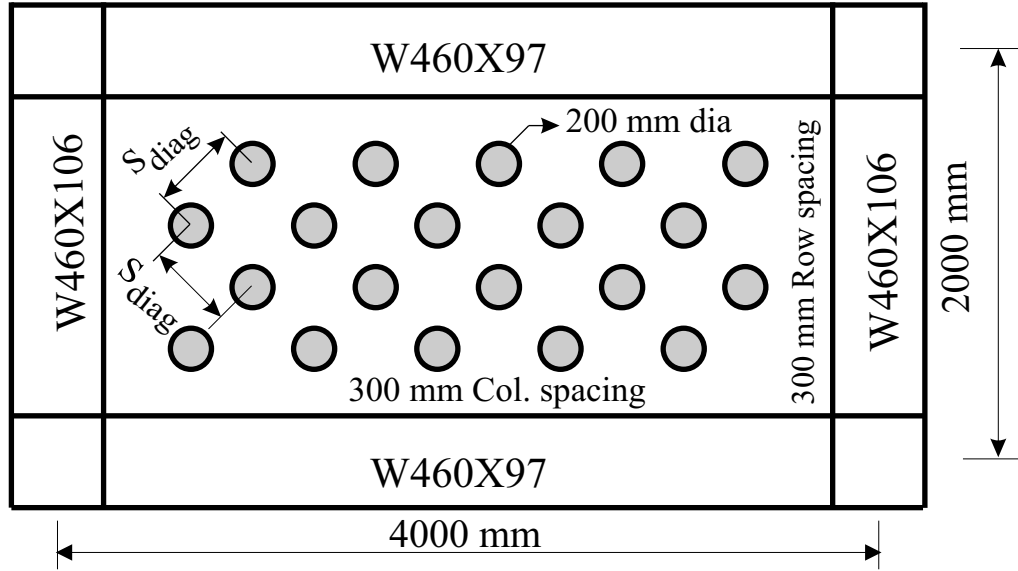
Fig. 2.11 Perforated SPSW specimen (Vian 2005)
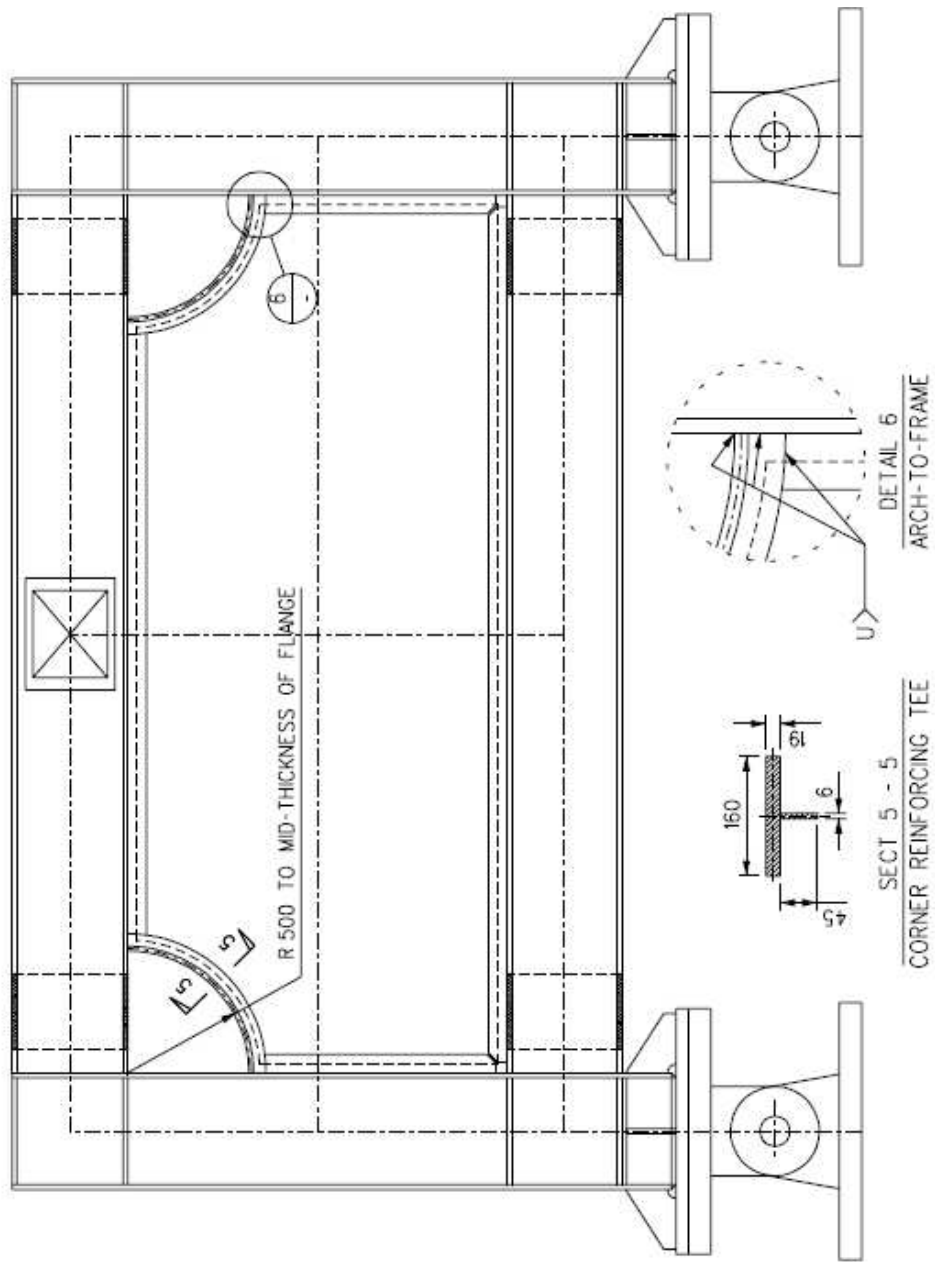
Fig. 2.12 Cut-out corner reinforced SPSW specimen (Vian 2005)
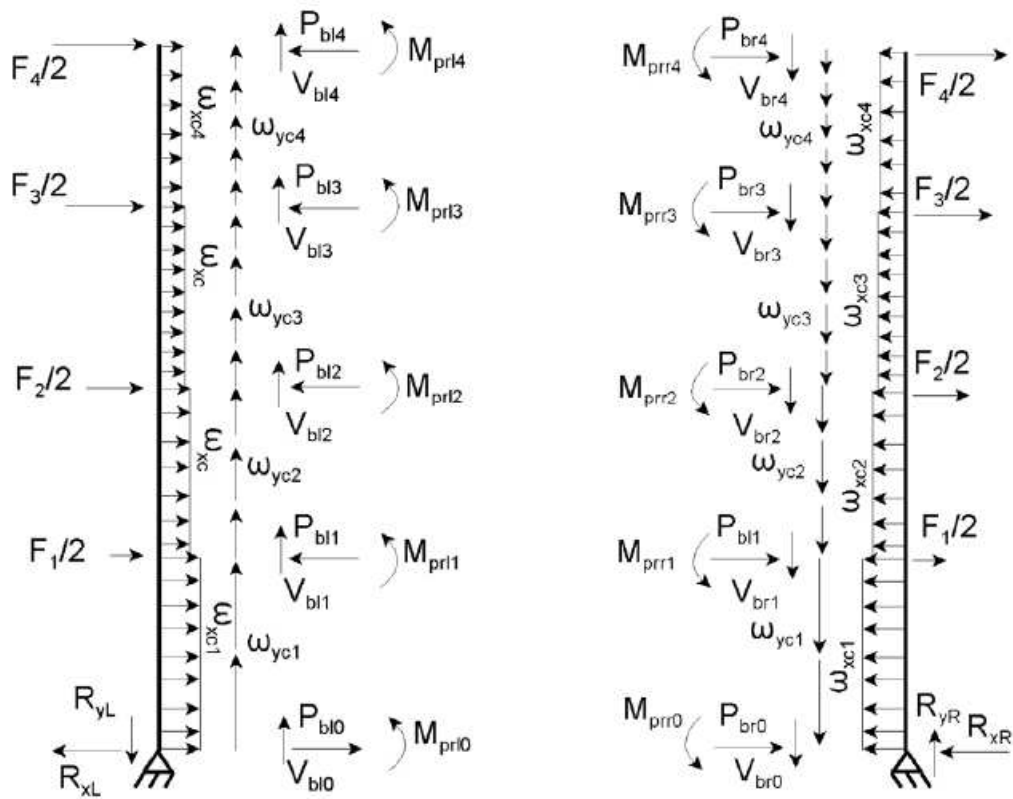
Fig 2.13 Column free body diagrams (Berman and Bruneau 2008)

References

AISC. 2005. Seismic provisions for structural steel buildings. American Institute of Steel Construction, Chicago, IL.

Applied Technology Council. 1992. Guidelines for cyclic seismic testing of components of steel structures. ATC-24, Redwood City, CA.

Behbahanifard, M.R., Grondin, G.Y., and Elwi, A.E. 2003. Experimental and numerical investigation of steel plate shear walls. Structural Engineering Report No. 254, Dept. of Civil and Environmental Engineering, University of Alberta, Edmonton, AB.

Berman, J. W. and Bruneau, M. 2003. Plastic analysis and design of steel plate shear walls. Journal of Structural Engineering, ASCE, 129(11): 1148-1156.

Berman, J. W. and Bruneau, M., 2005. Experimental investigation of light-gauge steel plate shear walls. Journal of Structural Engineering, ASCE, 131(2): 259-267.

Berman, J. W., and Bruneau, M. 2008. Capacity design of vertical boundary elements in steel plate shear walls. Engineering Journal, AISC, first quarter, pp. 57-71.

CSA. 2009. Limit states design of steel structures. CAN/CSA S16-09, Canadian Standards Association, Toronto, ON.

CSA. 2001. Limit states design of steel structures. CAN/CSA S16-01, Canadian Standards Association, Toronto, ON.

Driver, R.G., Kulak, G.L., Kennedy, D.J.L., and Elwi, A.E. 1997. Seismic behaviour of steel plate shear walls. Structural Engineering Report No. 215,

Dept. of Civil and Environmental Engineering, University of Alberta, Edmonton, AB.

Driver, R.G., Kulak, G.L., Kennedy, D.J.L., and Elwi, A.E. 1998. Cyclic test of four storey steel plate shear wall. Journal of Structural Engineering, ASCE, 124(2): 112-120.

Hibbitt, Karlsson, and Sorensen. 2007. ABAQUS/Standard User's Manual. Version 6.7, HKS Inc., Pawtucket, RI.

Lubell, A.S., Prion, H.G.L., Ventura, C.E., and Rezai, M. 2000. Unstiffened steel plate shear wall performance Under Cyclic Load. Journal of Structural Engineering, ASCE, 126(4): 453-460.

NRCC. 2005. National Building Code of Canada. Canadian Commission on Building and Fire Codes, National Research Council of Canada, Ottawa, ON.

Purba, R. H. 2006. Design recommendations for perforated steel plate shear walls. M.Sc. Thesis, State Univ. of New York at Buffalo, Buffalo, N.Y.

Rezai, M. 1999. Seismic behaviour of steel plate shear walls by shake table testing. PhD Dissertation, Dept. of Civil Engineering, University of British Columbia, Vancouver, BC.

Roberts, T.M. and Sabouri-Ghomi, S. 1992. Hysteretic characteristics of unstiffened perforated steel plate shear panels. Thin Walled Structures, 14: 139-151.

Thorburn, L.J., Kulak, G.L., and Montgomery, C.J. 1983. Analysis of steel plate shear walls. Structural Engineering Report No. 107, Dept. of Civil Engineering, University of Alberta, Edmonton, AB.

Timler, P.A., and Kulak, G.L. 1983. Experimental study of steel plate shear walls. Structural Engineering Report No. 114, Dept. of Civil Engineering, University of Alberta, Edmonton, AB.

Vian, D. 2005. Steel plate shear walls for seismic design and retrofit of building structures. PhD dissertation, State Univ. of New York at Buffalo, Buffalo, N.Y.

Wagner, H. 1931. Flat sheet metal girders with very thin webs, Part I – General theories and assumptions. Technical memo No. 604, National Advisory Committee for Aeronautics, Washington, DC.

Xue, M. and Lu, L-W. 1994. Interaction of infilled steel shear wall panels with surrounding frame members. Proceedings, Structural Stability Research Council: reports on current research activities: June 20, 1994, Lehigh University, Bethlehem, PA.

Yang, T.Y., and Whittaker, A.S. 2002. MCEER demonstration hospitals– mathematical models and preliminary results. Technical Report, Multidisciplinary Center for Earthquake Engineering Research, State University of New York at Buffalo, Buffalo, NY.

3. FINITE ELEMENT ANALYSIS OF STEEL PLATE SHEAR WALLS[1]

3.1 Introduction

Steel plate walls (SPSWs) are increasingly being used as the primary lateral load resisting system in buildings. They consist of steel plates installed vertically within building frames and connected to the surrounding beams and columns. The steel infill plates may be stiffened or unstiffened and the surrounding steel frame may use simple or moment-resisting beam-to-column connections. In thin unstiffened SPSWs, infill plates tend to buckle with a very small applied lateral load. Indeed, they may often be considered pre-buckled based on fabrication tolerances, welding distortion, and deformations of the frame under gravity loads. At the point of buckling, the load-resisting mechanism changes from in-plane shear to an inclined tension field. The tension field action developed in the infill plates is capable of resisting additional shear until they reach the material yield strength. Thus, design and analysis of unstiffened SPSWs are based on the post-buckling strength of the infill panels.

Kulak and co-investigators at the University of Alberta pioneered the research on thin unstiffened steel plate walls in the early 1980s. Thorburn et al. (1983) proposed a simplified model to analyze thin SPSWs. This model, generally called the "strip model," is acknowledged as a valid means of analysis of SPSWs in the Canadian steel design standards, CAN/CSA S16-01 (CSA 2001) and CAN/CSA S16-09 (CSA 2009). The strip model neglects the panel buckling resistance and

---

[1] A version of this chapter has been accepted for publication in the *Canadian journal of civil engineering*

thus the dominant action is the post-buckling strength from the diagonal tension field. The strip model represents the panels as a series of discrete pin-ended diagonal strips, oriented in the direction of the principal tension, that are capable of transmitting tension forces only. Each strip is assigned an area equal to the product of the strip width and the plate thickness. Using least work principles, Timler and Kulak (1983) derived an expression to predict the angle of inclination of the tension strips. Although the strip model results in a good representation of the elastic behaviour of SPSWs, it has been reported (Driver et al. 1997) to underestimate the stiffness slightly.

Elgaaly et al. (1993), Driver et al. (1997), Rezai (1999) and other researchers have used finite element formulations including geometric and material nonlinearities to analyze SPSWs. They used shell elements for the infill plates and beam/frame elements for boundary columns and beams. In general, the results of the finite element analyses showed a load versus deflection behaviour somewhat stiffer than the experimental findings and also with the use of beam/frame elements for boundary members it was not possible to capture any local buckling in the boundary members. Behbahanifard et al. (2003) proposed a finite element approach based on an explicit dynamic formulation. It was shown that the model could predict the inelastic behaviour of a SPSW well for both the monotonic and quasi-static cyclic loading cases. A special loading frame was used in the model to carry out a displacement controlled analysis. Implementation of this loading frame can be time consuming for taller SPSWs and it is suitable for proportional

loading only. Kharrazi et al. (2005) proposed an analytical model that considers the shear and bending behaviour of the SPSW systems individually. The model was applied to the test specimens of Driver et al. (1998) and Behbahanifard et al. (2003). In both the cases, the model predicts the initial stiffness well, but provides a significantly low estimate of capacity.

This chapter describes the development of a finite element model that includes both geometric and material non-linearities. Damping and strain rate effects are also incorporated. The model is validated by comparing the finite element analysis results with the observed behaviour of three specimens tested quasi-statically, which consisted of different configurations and loading conditions, and one specimen tested dynamically.

SPSWs designed for seismic loads according to the 2005 National Building Code of Canada (NRCC 2005) may be classified as Type D (ductile) or Type LD (limited ductility) plate walls. Clause 27 of CAN/CSA S16-01 describes the design requirements for these two plate wall types. The design of Type D plate walls is based on the capacity design philosophy, which involves pre-selecting a localized ductile fuse (or fuses) to act as the primary location for the dissipation of seismic energy. In SPSWs, it is tension yielding in the infill plate, occurring under the action of the storey shear, that is considered to be the ductile and desirable mode of energy dissipation. Plastic hinges may also form in the beams and at the column bases. The other elements of the structure must be designed to withstand

48

the loads delivered to them by yielding of the fuses. Type LD plate walls are designed to dissipate a limited amount of seismic energy through yielding of the infill plates and supporting members. In the design of Type LD plate walls according to CAN/CSA S16-01, the capacity design approach need not be used. Instead, they are only required to meet the non-seismic requirements of Clause 20. Type LD plate walls are limited to 60 m in height. Comparisons of the performance of Type D and Type LD SPSWs under earthquake loading have never been conducted explicitly. With the finite element model developed, this chapter presents the results of non-linear dynamic analyses performed on 4-storey and 8-storey Type D and Type LD SPSWs when subjected to spectrum compatible earthquake ground motions of Vancouver and Montreal.

3.2 Selection of finite element analysis technique

Due to the highly non-linear nature of the problem and severe convergence difficulties in implicit analysis, an explicit scheme (ABAQUS/Explicit) was found to provide an accurate solution (Behbahanifard et al. 2003) for quasi-static applications. In an explicit formulation, the solution is obtained without iteration. With proper control of the kinetic energy, the explicit approach can be used for quasi-static loading cases. The dynamic explicit formulation uses the central difference method, which is a conditionally stable algorithm.

It was observed in the current research that seismic analyses using dynamic explicit formulations lead to impractically small time increments. With the inclusion of small stiffness damping, the situation became worse, resulting in a

very computationally expensive analysis. Therefore, the implicit time integration method implemented in ABAQUS/Standard (Hibbitt et al. 2007), was used for this research project. The method uses the Hilber-Hughes-Taylor operator, which is an extension of the trapezoidal rule (Hilber et al. 1978). This operator is unconditionally stable, which is of great value when studying non-linear structural systems. With implicit time integration, sometimes it is difficult to obtain a solution for a static analysis when the system is highly non-linear. However, non-linearities are usually more easily accounted for in dynamic analysis than in static analysis because the inertia terms provide mathematical stability to the system, making the method more robust. Thus, an automatic time incrementation scheme is adopted within the implicit dynamic integration method. To determine whether a dynamic simulation is producing an appropriate quasi-static response, the work done by the external forces should be nearly equal to the internal energy of the system, while the kinetic energy remains bounded and small.

3.3 Characteristics of the finite element model

3.3.1 Geometry and initial conditions

The as-built dimensions of specimens tested in laboratories were used for creating the finite element models. However, the fish plates used in the test specimens to connect the infill plates to the boundary members were not modelled. Instead, infill plates were considered to be connected directly to the beams and columns. All steel plate walls tested would have had some initial infill plate imperfections resulting from various sources such as welding of the infill plate to the beams and columns, floor beam deflections, and fish plate connection eccentricity. Any

initial out-of-plane deformations can significantly affect the initial behaviour as compared to a perfectly flat plate. Therefore, initial imperfections of the infill plates were considered in the finite element model. The infill plate was taken to have an initial imperfection pattern corresponding to the first buckling mode of the plate wall loaded in a way similar to that used in the respective test. For the magnitude of initial imperfections, a value of $2w$, where w is the infill plate thickness, was selected.

3.3.2 Element selection

The beams, columns, and infill plates were modelled using a general purpose four-node doubly-curved shell element with reduced integration (ABAQUS element S4R). The element S4R accounts for finite membrane strains and large rotations. This element has six degrees of freedom per node: three translations (u_x, u_y, u_z) and three rotations $(\theta_x, \theta_y, \theta_z)$ defined in a global coordinate system. The S4R element is based on an isoparametric formulation. This element uses one integration point on its mid-surface to form the element internal force vector. Reduced integration elements are used as they give accurate results and significantly reduce running time if the elements are not distorted locally. The element size was selected from a mesh refinement study.

3.3.3 Material properties

Stress versus strain responses obtained from tension coupon tests of different parts of the SPSW were used when reported by the original researchers. Otherwise, estimated values were used. The von Mises yield criterion was adopted for the analyses presented here. The associated flow rule was used to

51

obtain the plastic strain increment. For all the monotonic pushover analyses, a non-linear isotropic hardening model was used. Such a model is adequate for monotonic loading. For quasi-static cyclic loading and seismic loading that involves a significant number of strain and stress reversals, the Bauschinger effect becomes potentially important. Thus, for these two loading cases, a kinematic hardening rule was used in the analysis. Rayleigh proportional damping with a damping ratio of 5%, which is commonly used for building with partition walls, was selected for the seismic analyses (except for the dynamic analysis of the Rezai (1999) specimen, where 3% damping ratio was used to reflect the use of an unclad steel frame).

3.3.4 Strain-rate model

The strain rate model incorporated in the finite element analysis is the Cowper-Symonds overstress power law (Cowper and Symonds 1957):

$$\dot{\varepsilon}_p = D \left(\frac{\sigma_D}{\sigma_S} - 1 \right)^q \tag{3.1}$$

where $\dot{\varepsilon}_p$ is the plastic strain rate; σ_D and σ_S are the dynamic and static yield stresses, respectively; and D and q are material parameters to be determined from test data. These material parameters for the initial yield of mild steel under dynamic loading are $D = 40.4 \text{ sec}^{-1}$ and $q = 5$ (Cowper and Symonds 1957).

3.4 Displacement control analysis

A displacement control solution strategy is used in this work for all quasi-static analyses. For this study, a subroutine was used to carry out the displacement control analysis. This ABAQUS subroutine allows displacement control, while

52

maintaining the lateral loads equal during the loading process. The top storey displacement is used as the control parameter and the analysis is stopped when the displacement reaches a specified limit.

3.5 Validation of finite element model

The finite element model was validated by comparing published test results with the corresponding analysis results. A 4-storey specimen tested by Driver et al. (1998), a 3-storey specimen tested by Behbahanifard et al. (2003), and a single storey SPSW specimen tested by Lubell et al. (2000) were modelled using the method outlined above. Pushover analyses were carried out and the resulting curves are compared to the corresponding envelope of hysteresis curves obtained from the physical tests. The model is also validated using a quasi-static cyclic analysis of the specimen tested by Driver et al. (1998). Finally, the finite element approach is used for dynamic analysis of a 4-storey SPSW specimen tested by Rezai (1999), where analytical responses are compared with shake table test results.

3.5.1   Pushover analysis and results

3.5.1.1 Driver et al. (1998) specimen

The large-scale 4-storey SPSW test specimen of Driver et al. (1998) was modelled and a pushover analysis carried out. The published material properties were used for the specimen. Initial imperfections corresponding to the first buckling mode with a peak amplitude of 10 mm $(\approx 2w)$ were used. In the first loading step, gravity loads were applied to the top of each column that were then kept constant for the remainder of the analysis. Equal horizontal in-plane forces

were applied at each beam level, as in the test, and the analysis was carried out until the displacement at the top of the plate wall reached a target value of 140 mm, obtained from the envelope of hysteresis curves of the physical test. The geometry of the 4-storey SPSW, along with the finite element mesh, is shown in Fig. 3.1. The measured and predicted base shears are plotted against the first storey drift in Fig. 3.2. The figure indicates that the finite element model predicts the initial stiffness and post-yield response of the shear wall very well. The ultimate capacity of the specimen was underestimated by about 7.5%. The history of different types of energy developed during the pushover analysis is presented in Fig. 3.3. The internal and external energies are equal and the kinetic energy is negligible relative to the internal energy. This indicates that the analysis has been carried out in a quasi-static condition.

3.5.1.2 Behbahanifard et al. (2003) specimen

The top three panels of the specimen tested by Driver et al. (1998), were retested after removing the damaged bottom panel. Therefore, the finite element model used the same material properties as used for the Driver et al. (1997) specimen. In order to reflect accurately the damage that resulted from the test of the 4-storey specimen, the initial imperfections were measured in the bottom panel of the three-storey specimen, which had suffered some permanent deformation; the peak out-of-plane magnitude was approximately 39 mm. The measured initial imperfections were mapped onto the finite element mesh. The remaining two storeys used initial imperfections corresponding to the first buckling mode, with a peak amplitude of 10 mm. The base shear versus first storey drift curve is

presented in Fig. 3.4. The initial stiffness is predicted well and the peak capacity of the test specimen is under-predicted by about 7.8%.

3.5.1.3 Lubell et al. (2000) specimen

Lubell et al. (2000) tested two single storey specimens. Only one specimen, designated as SPSW2, is analysed here. Based on material test data presented by Lubell et al. (2000), a static yield strength of 380 MPa was selected for the beams and columns, while the infill plate yield strength was taken as 320 MPa. A monotonic pushover analysis was conducted with a lateral load applied along the centreline of the top beam. The displacement of a node at that level was monitored and the analysis was terminated when the maximum lateral deflection reached 50 mm, obtained from the envelope of hysteresis curves of the physical test. Figure 3.5 compares the pushover analysis curve to the envelope of the test specimen (SPSW2) hysteresis curve. It is observed that the model agrees well with the test results. The initial stiffness was predicted very well and the capacity was underestimated by only 3.1%.

3.5.2   Quasi-static cyclic analysis and results

Further validation of the finite element model was carried out by comparing cyclic analysis results with the test results of the cyclic test conducted by Driver et al. (1998). As for the push-over analysis described above, the gravity load was applied first at the top of each column and kept constant for the rest of the analysis. A cyclic displacement history was applied by increasing the displacement of the first panel by an amount equal to a multiple of the yield displacement (δ_y, $2\delta_y$, $3\delta_y$, $4\delta_y$, $5\delta_y$, and $6\delta_y$; where δ_y is the first panel yield

displacement obtained from a pushover analysis of 4-storey SPSW). Also, at each displacement level, the SPSW was cycled two times to get a stable hysteresis response. Hysteresis curves obtained from the finite element analysis were compared with the test results. Figure 3.6 shows the finite element predictions for the first storey drift. In general, there is good agreement between the test results and the finite element analysis. Both the predicted capacity and stiffness of the SPSW are in excellent agreement with the test results. The hysteresis curves generated by the analysis show slightly less pinching than observed during the test.

3.5.3 Dynamic analysis of 4-storey SPSW tested by Rezai (1999)

A non-linear dynamic analysis has been conducted for the 4-storey SPSW specimen tested on a shake table. The specimen had a storey height of 900 mm and an overall width of 1016 mm. All the frame connections were full moment connections. In the finite element model the storey gravity loads were represented as lumped masses at each floor. About 1700 kg of mass was applied at each floor, resulting in a total mass of 6800 kg applied on the specimen. As no imperfection data were available, initial imperfections corresponding to the first buckling mode with a peak amplitude of $2w$ (=3 mm) was used in the finite element model. Before the dynamic analysis was conducted, a frequency analysis was carried out to calculate the fundamental period. The fundamental natural frequency for the first mode (translational) was calculated as 6.71 Hz, which is 10% higher than the test result (6.1 Hz). No attempt was made to match the test frequency exactly. A critical damping ratio of 3% was selected for this SPSW test. To account for the

strain rate effect, the Cowper-Symonds overstress power law, presented earlier, was included in the finite element analysis. Three different earthquake records were used for the test: 1992 Landers, 1992 Petrolia, and 1994 Northridge. In the test, shake table runs were taken as a percentage of the peak ground acceleration of the selected reference earthquake. This means that the "140% Tarzana" run would be a run where the peak acceleration of the desired input earthquake motion was 140% of the recorded value of the reference Tarzana Hill record of 1994 Northridge earthquake.

Due to limited input and output test data availability, only the 140% Tarzana Hill earthquake record was used for the dynamic analysis. As in the shake table test, the displacement versus time history (Rezai 1999) was applied at the base of the specimen. Figure 3.7 shows the input ground displacement history of the 140% Tarzana Hill earthquake applied at the shake table. Figure 3.8 shows a comparison of the displacement at the top of the frame relative to the ground as recorded during the shake table test and the predicted relative displacement from the non-linear dynamic analysis. In Fig. 3.9, the dynamic storey displacement envelopes from the test and the analysis are compared. Overall, the finite element model is in excellent agreement with the shake table test results. The maximum top storey displacement was underestimated by less than 1%. However, it is recalled that Rezai's test specimen remained elastic during the test and thus validation for the available dynamic test program was only for the elastic range.

The validations presented above demonstrate that the finite element model can reliably be used for seismic analysis of SPSW systems.

3.6 Seismic performance of SPSWs

3.6.1   Design of Type D and Type LD SPSWs

A 4-storey and an 8-storey building are used to evaluate the seismic performance of steel plate walls. The hypothetical symmetrical office building is assumed to be located in two different cities, Vancouver and Montreal, and has a total plan footprint area of 2014 m^2. The building has two identical SPSWs provided to resist lateral forces in each direction; thus, each shear wall will resist one half of the design seismic loads (torsion neglected). Each shear wall panel is 7.6 m wide, measured from centre to centre of columns, and has an aspect ratio of 2.0 (storey height of 3.8 m). The building is assumed to be founded on rock (site class B according to NBCC 2005). A dead load of 4.26 kPa was used for each floor and 1.12 kPa for the roof. The live load on all floors was taken as 2.4 kPa. The nominal yield strength of the beams, columns and infill plates of the SPSWs was assumed to be 350 MPa and all steel members were assumed to have a modulus of elasticity of 200 000 MPa. A ductility-related force modification factor, R_d, of 5.0 and an overstrength force modification factor, R_o, of 1.6 were used in the design of the Type D plate walls as per NBCC 2005. Similarly, for designing the Type LD plate walls, force modification factors of $R_d = 2.0$ and $R_o = 1.5$ were used. The NBCC 2005 load combination $D + 0.5L + E$ (where $D =$ dead load, $L =$ live load and $E =$ earthquake load) was considered for floors and for the

roof, the load combination $D + 0.25S + E$ (where $S =$ snow load) was considered.

While designing Type D and Type LD SPSWs with moment-resisting beam-to-column connections, it is observed that in any seismic region, the differences in the design of Type D and LD plate walls are: (1) the use of capacity design provisions for Type D plate walls, and (2) a difference in the force modification factors for the two systems. (This assumes that the equation for period specified in the NBCC that is a function only of the building height is used.) The design seismic base shear is given by (NBCC 2005):

$$V = \frac{S(T_a)M_v I_E W}{R_d R_o} \geq \frac{S(2.0)M_v I_E W}{R_d R_o}$$
(3.2)

where $S(T_a)$ is the design spectral acceleration, expressed as a ratio of gravitational acceleration, for the fundamental lateral period of vibration of the structure, T_a; M_v is an amplification factor to account for higher mode effects on the base shear; I_E is an importance factor for the structure; W is the total dead load plus 25% of the design snow load, 60% of the storage load, and the full contents of any tanks. All the factors except R_d and R_o are the same for Type D and LD plate walls, and the design base shear for a typical Type LD plate wall is therefore always about 8/3 (= 2.67) times higher than that of a Type D plate wall. Thus, the base overturning moment, M_f, for a Type LD plate wall is always approximately 2.67 times higher than that for a Type D plate wall. According to the capacity design provisions in CAN/CSA S16-01, design column axial forces

in Type D SPSWs can be obtained from gravity loads combined with an overturning moment magnified by an amplification factor, B, defined as:

$$B = \frac{V_{re}}{V}$$ (3.3)

where V_{re} is the probable shear resistance at the base of the wall, and V is the factored lateral seismic force at the base of the wall obtained from NBCC 2005.

The probable shear resistance of the wall $\left(V_{re}\right)$ is given by(CSA 2001):

$$V_{re} = 0.5 R_y F_y wL \sin 2\alpha$$ (3.4)

where R_y is the ratio of the expected to nominal steel yield strength (specified as 1.1 in CAN/CSA S16-01); w is the infill plate thickness; L is the bay width; α is the angle of the tension field developed in the infill plate and is obtained from CAN/CSA S16-01. The amplification factor need not be taken as greater than the ductility-based force modification factor, R_d. In addition to gravity loads, which are the same in the Type D and Type LD plate walls for a certain building, the design axial load components for the base columns are $\dfrac{BM_f}{L}$ for Type D plate walls and $\dfrac{M_f}{L}$ for Type LD walls. For buildings with eight storeys or fewer, the design usually is not governed by the drift limit. In these cases, for a Type D plate wall with an amplification factor, B, approximately equal to 2.67, capacity design provisions in CAN/CSA S16-01 will result in almost the same framing members as Type LD plate walls, where capacity design is not applied. This observation helps in the selection of the infill plate thickness. For all 4-storey

SPSWs, a 3 mm infill plate thickness was selected even though a thinner plate would theoretically be adequate, as this is considered the minimum practical thickness using conventional welding practice and for handling considerations. In the design of the 8-storey Type D SPSW in Vancouver, a 3 mm infill plate gives an amplification factor of 2.67 for capacity design provisions, resulting in storey columns similar to those in the Type LD SPSW. Thus, for the 8-storey Type D and Type LD SPSWs in Vancouver, a constant thickness of 4.5 mm instead of 3 mm was selected for the infill plates. For the 8-storey Type D and Type LD SPSWs in Montreal, a constant infill plate thickness of 3 mm was used. It is noted that the capacity design requirements for the Type D SPSWs will typically result in heavier frame members than for the Type LD walls, where capacity design need not be considered, due to the substantial overstrength of the infill plate even when the practical minimum thickness is selected.

Both CAN/CSA S16-09 and CAN/CSA S16-01 have provisions for the stiffness of the columns to ensure the development of an essentially uniform tension field in the infill plate. The required limit on the flexibility parameter, ω_h, is given as:

$$\omega_h = 0.7h \sqrt[4]{\frac{w}{2LI_c}} \leq 2.5 \qquad (3.5)$$

All the boundary columns selected in this study are class 1 sections and satisfy this column flexibility requirement. Consistent with the philosophy of the column flexibility parameter (Eq. 3.5), Dastfan and Driver (2008) proposed a boundary

member flexibility parameter, ω_L, for the design of the top panel boundary elements:

$$\omega_L = 0.7 \sqrt[4]{\left(\frac{h^4}{I_c} + \frac{L^4}{I_b}\right)\frac{w}{4L}} \leq 2.5 \qquad (3.6)$$

where I_b is the moment of inertia of the top beam; I_c is the moment of inertia of the top storey columns; and h is the storey height. The top beams selected for this investigation also meet the flexibility limit expressed by Eq. (3.6). Intermediate beams in all Type D and Type LD plate walls were selected for the same beam-to-column relative stiffness $\left(\dfrac{I_b/L}{2I_c/h}\right)$: 0.20 for the 4-storey and 0.10 for the 8-storey SPSWs. The final column and beam sections satisfy the beam-column design requirements of CAN/CSA S16-01. Tables 3.1 and 3.2 present the final columns and beams for the 4- and 8-storey Type D and Type LD SPSWs.

3.6.2   Finite element model

For the seismic analysis, a dummy gravity column is added to the finite element model that is made of bar elements and connected to the plate wall at every floor with pin ended rigid links. The dummy gravity column is designed to carry half of the total remaining mass in every floor without introducing additional lateral stiffness to the system. In the finite element analysis, the storey gravity loads were represented as lumped masses on the columns at every floor. A 5% Rayleigh proportional damping ratio is selected for all the seismic analyses. An elasto-plastic stress versus strain curve is adopted. A yield strength of 385 MPa was

selected for infill plates, and for the beams and columns a yield strength of 350 MPa was used.

3.6.3 Earthquake ground motions

Commentary J of NBCC 2005 recommends the use of spectrum compatible earthquake records while doing time history analyses. Because this procedure was adopted in the following work, the number of seismic records required to investigate the behaviour is minimized. Therefore, only four seismic records are chosen for the time history response analysis. These are: (1) N-S component of the El-Centro earthquake of 1940; (2) Petrolia station record from the 1992 Cape Mendocino earthquake; (3) Parkfield 1966 earthquake record; and (4) Nahanni, Canada 1985 earthquake record. The selected ground motions are shown in Fig. 3.10. Response spectra of all four acceleration records are developed by numerically integrating the response of a 5% damped elastic oscillator. Figures. 3.11 and 3.12 show the response spectra for the four selected seismic records, along with the design spectra of Vancouver and Montreal determined from the spectral acceleration values available from the Geological Survey of Canada. The seismic records are modified using the SYNTH program (Naumoski 2001) to make them spectrum compatible for Vancouver and Montreal. The spectrum compatible earthquake records for Vancouver and Montreal are presented in Figs. 3.13 and 3.14 respectively. All four spectrum compatible earthquake records lead to very similar response spectra. This was observed for both Vancouver and Montreal. Only the modified (spectrum compatible) response spectra for the

Parkfield 1966 earthquake record and the design spectra for Vancouver and Montreal are shown in Fig. 3.15.

3.6.4 Seismic response of SPSWs

Nonlinear time step dynamic analyses of the Type D and Type LD SPSWs were performed using ABAQUS. Table 3.3 presents peak seismic response parameters for the Type D and Type LD 4-storey SPSWs computed from non-linear time history analyses under the four selected spectrum compatible seismic records for Vancouver. The average roof displacement demand from the four analyses for the 4-storey Type LD wall is only about 1.08 times the average displacement demand of the Type D SPSW in Vancouver. On average, the seismic overturning moment at the base of the Type D wall is about 1.21 times the base moment of Type LD wall. Table 3.3 also shows that the average dynamic base shear for Type D SPSW is 1.13 times the average dynamic base shear of Type LD SPSW. As shown in Table 3.4, for spectrum compatible seismic records for Montreal, the average overturning moment at the base for the Type D wall is 1.14 times the average base moment of the Type LD wall. The dynamic base shear for both Type D and Type LD SPSWs in Montreal are much lower than the probable shear resistance of 4350 kN, calculated using Equation 3.4. This is why there was no yielding in the infill plates of the 4-storey Type D and Type LD walls under spectrum compatible records in Montreal. For Vancouver, dynamic shears at the bottom two storeys are higher than the probable storey shear resistance of 4350 kN and thus the bottom two infill plates were yielded. Moreover, in the case of the 4-storey Type LD

64

SPSW in Vancouver, one lower storey column experienced a significant amount of yielding. Figure 3.16 shows the extent of yielding in the 4-storey Type D and Type LD SPSWs at the time when base shear is maximum under the Parkfield 1966 spectrum compatible earthquake record in Vancouver. It is observed that in the case of the 4-storey Type D wall, yielding only occurred in the infill plates and the boundary frames remained essentially elastic. Thus, for this wall, seismic energy was dissipated through yielding in the infill plates, whereas for the 4-storey Type LD SPSW, there was some energy dissipation through plastification in the lower storey columns.

Tables 3.5 and 3.6 present peak seismic response parameters of the Type D and Type LD 8-storey SPSWs in Vancouver and Montreal, respectively, computed from non-linear time history analyses. The average displacement demand for the 8-storey Type LD wall is about 1.13 times higher for Vancouver and 1.11 times higher for Montreal than the average displacement demands of the Type LD SPSWs. Seismic demand for overturning moment at the base of the Type D wall in Vancouver is about 1.25 times higher than the average base moment of the Type LD wall. For SPSWs in Montreal (Table 3.6), the average overturning moment demand at the base for the Type D wall is 1.36 times the average base moment of the Type LD wall. The dynamic shears for both the Type D and Type LD SPSWs in Montreal are much lower than the probable shear resistance of 4350 kN. Thus, the behaviours of the Type D and Type LD SPSWs designed for Montreal were fully elastic. It should be noted that unlike the 8-storey SPSWs in

Vancouver, where 4.5 mm infill plates were used, an infill plate thickness of 3 mm was selected for all the floors in the 8-storey SPSWs in Montreal, expecting some yielding in the infill plates. For Vancouver, inelastic shears for the four bottom floors exceed the probable storey shear resistance of 6548 kN and thus the infill plates for the bottom 4-storeys showed signs of yielding. The remaining framing members behaved almost elastically.

To observe the performances of 8-storey SPSWs under a severe earthquake in both Vancouver and Montreal, time history analyses were carried out for an earthquake record of amplitude of 2.0 times the amplitude of the spectrum compatible Parkfield 1966 earthquake record. This modified earthquake record will be termed as the "severe" Parkfield earthquake for simplicity. Figure 3.17 shows the envelopes for peak interstorey drifts, storey shears, and bending moments for the 8-storey Type D and Type LD steel plate walls in Montreal and Vancouver for the severe Parkfield earthquake record. Though interstorey drift ratios increase with an increase in the amplitude of the earthquake record, they are significantly lower than the NBCC drift limit. Thus, it seems unlikely that the interstorey drift limit would govern the design of typical low to medium rise (8-storey or lower) SPSWs. Figure 3.17(c) also shows that the moment demand at the base in the 8-storey Type D wall in Vancouver is 1.06 times higher than the base moment demand for the Type LD wall. For Montreal, the base moment for the Type D wall is about 1.39 times higher than that of the Type LD wall. The distribution of dynamic shears in Fig. 3.17(b) confirms that even for the applied

severe Parkfield earthquake record in Montreal, the behaviour of the 8-storey Type LD SPSW is almost elastic as storey shears are lower than the probable storey shear resistance of 4350 kN. Only the bottom two infill plates are partially yielded. Figure 3.18 shows the extent of yielding in the bottom four storeys of the 8-storey Type D and Type LD SPSWs in Vancouver, when the base shear is at its maximum value. It is observed that in case of the 8-storey Type D wall, yielding is only in the infill plates, while the boundary frames remained essentially elastic with the exception of some yielding in the outer flanges at the column base. This is because the Type D SPSW was designed using the capacity design approach. For the 8-storey Type LD SPSW, though the right column experienced significant yielding in the first and fourth floor, limited plastification in the left column and partially elastic infill plates prevented the development of any soft storey. Thus, both the Type D and Type LD SPSWs were capable of withstanding the severe Parkfield earthquake.

3.7 Conclusions

A non-linear finite element approach is found to be very effective to study the behaviour of SPSWs. The finite element model developed is able to provide very good predictions for quasi-static and dynamic analyses of SPSW specimens with different geometry and configurations. For quasi-static tests, the model captured all essential features of the test specimens analysed: initial stiffness, peak load, and the post-peak behaviour. For the dynamic test of the 4-storey SPSW, the

model provided excellent representations of the in-plane frequencies and storey displacements.

Nonlinear dynamic analyses have been performed to study the performance of 4-storey and 8-storey SPSWs. Two different design considerations—ductile (Type D) and limited ductility (Type LD) plate walls, as defined in the edition of CAN/CSA S16-01 were considered in this study. The main findings of the study are follows:

(1) SPSWs with moment-resisting beam-to-column connections provide excellent structural performance in terms of stiffness and ductility. For the severe Parkfield earthquake selected for this study, the 8-storey Type LD SPSW in Vancouver experienced significant yielding in first, second, and fourth storey columns (right column). However, no soft storey was developed because of the limited plasticity in the other (left) column and partially elastic infill plates. Thus, the system behaved in a robust manner.

(2) The seismic analyses show that Type D SPSWs perform in a more ductile manner than Type LD walls. For the 8-storey Type D SPSW in Vancouver under the severe Parkfield earthquake, yielding started at the base of one column only after five bottom storey infill plates were yielded. In any case, no yielding in either column in any intermediate floor was observed. Conversely, yielding was observed in the columns at intermediate floors prior to any yielding in the infill plates for the 8-storey Type LD SPSW in Vancouver.

(3) The analyses show that the ductility demand in the 4-storey and 8-storey Type D and Type LD SPSWs under spectrum compatible records in Montreal is very low. Even under the severe (two times) Parkfield 1966 earthquake record, the behaviour of the 8-storey Type LD wall (with 3 mm infill plate thickness in every storey) was fully elastic. Since 3 mm is a very small thickness if handling and welding issues are considered, the Type LD SPSW with moment-resisting beam-to-column connections can in general be used for low to medium rise (8-storey or lower) buildings in a seismic region like Montreal or lower.

(4) The interstorey drift distributions obtained from all inelastic time history analyses conducted were well within the 2005 NBCC limit of 2.5% of the storey height, so low to medium rise buildings with SPSWs are unlikely to be governed by drift considerations.

(5) Since capacity design principles are not used in the design of Type LD SPSWs, in high seismic regions there is always a chance of plastic hinge formation in the boundary columns in any intermediate floor. This was observed in the analysis of the 8-storey Type LD SPSW in Vancouver under the severe Parkfield earthquake record. Plastification in boundary columns other than at the base may trigger a soft storey mechanism. Thus, it is recommended that Type LD SPSWs not be used for medium to high rise (over 8-storey) buildings in high seismic regions until the lack of capacity design requirements for this type of SPSW is rectified.

(6) As has been widely discussed in the literature, again the difficulty of optimizing the design of SPSWs due to the minimum practical infill plate thickness has been highlighted. That is, in many realistic design situations the theoretical required infill plate thickness for an optimal design is too thin to be practical.

Table 3.1 Summary of 4-storey Type D and Type LD SPSW properties

Region	SPSW type	Column section	Intermediate beam section	Top beam section
Vancouver	Type D	W310X253	W410X132	W760X434
Vancouver	Type LD	W310X143	W410X74	W760X434
Montreal	Type D	W310X202	W410X100	W760X434
Montreal	Type LD	W310X129	W410X74	W760X434

Table 3.2 Summary of 8-storey Type D and Type LD SPSW properties

Region/ SPSW	Column sections			beam sections		Top beam section
	1-3	4-6	7-8	1-3	4-7	
Vancouver Type D	W360X677	W360X551	W360X262	W460X235	W460X193	W760X582
Vancouver Type LD	W360X463	W360X216	W360X122	W410X149	W410X100	W760X582
Montreal Type D	W360X382	W360X314	W360X122	W410X149	W410X114	W760X434
Montreal Type LD	W310X226	W310X158	W310X129	W410X67	W410X67	W760X434

Table 3.3 Maximum inelastic response parameters of Type D and Type LD 4-storey SPSW in Vancouver

Earthquake records	Type D SPSW			Type LD SPSW		
	Roof displacement (mm)	Base shear (kN)	Base moment (kN·m)	Roof displacement (mm)	Base shear (kN)	Base moment (kN·m)
El Centro 1940	71.2	5711	57 140	74.6	4951	48 920
Petrolia 1992	72.5	5764	56 700	80.4	4830	47 660
Nahanni 1985	71.4	5713	57 790	79.6	5032	47 430
Parkfield 1966	72.1	5825	60 540	76.8	5507	47 830

Table 3.4 Maximum inelastic response parameters of Type D and Type LD 4-storey SPSW in Montreal

Earthquake records	Type D SPSW			Type LD SPSW		
	Roof displacement (mm)	Base shear (kN)	Base moment (kN·m)	Roof displacement (mm)	Base shear (kN)	Base moment (kN·m)
El Centro 1940	34.1	2702	27 150	30.7	2338	21 670
Petrolia 1992	30.3	3061	25 750	41.1	2726	26 460
Nahanni 1985	40.2	3263	32 890	43.6	2676	27 450
Parkfield 1966	35.3	3136	28 410	34.7	3208	24 240

Table 3.5 Maximum inelastic response parameters of Type D and Type LD 8-storey SPSW in Vancouver

Earthquake records	Type D SPSW			Type LD SPSW		
	Roof displacement (mm)	Base shear (kN)	Base moment (kN·m)	Roof displacement (mm)	Base shear (kN)	Base moment (kN·m)
El Centro1940	164.8	7586	164 100	191.5	6446	132 700
Petrolia 1992	167.5	7798	164 600	188.4	7242	132 200
Nahanni 1985	154.0	7505	155 100	176.4	6625	124 500
Parkfield 1966	162.6	8236	163 500	176.3	6984	129 800

Table 3.6 Maximum inelastic response parameters of Type D and Type LD 8-storey SPSW in Montreal

Earthquake records	Type D SPSW			Type LD SPSW		
	Roof displacement (mm)	Base shear (kN)	Base moment (kN·m)	Roof displacement (mm)	Base shear (kN)	Base moment (kN·m)
El Centro 1940	61.5	1923	35 390	73.3	1450	25 400
Petrolia 1992	61.1	2447	37 500	63.9	1474	25 900
Nahanni 1985	60.3	2017	34 850	68.2	2289	28 400
Parkfield 1966	66.1	2029	40 330	72.5	1824	29 100
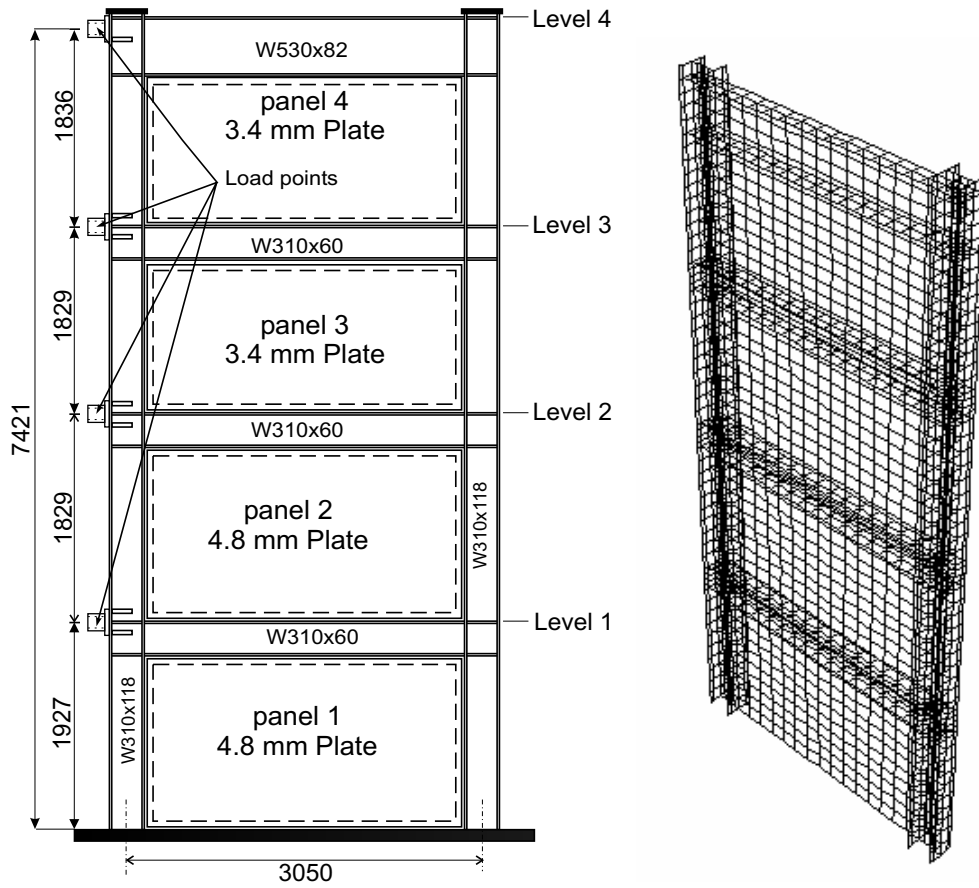
Fig. 3.1 Test specimen of Driver et al. (1998) and FE mesh
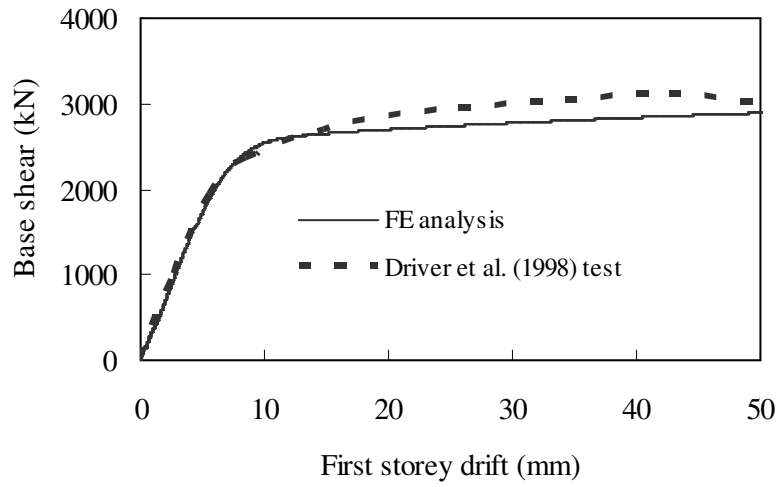
Fig. 3.2 Comparison of pushover analysis with test results of Driver et al. (1998)
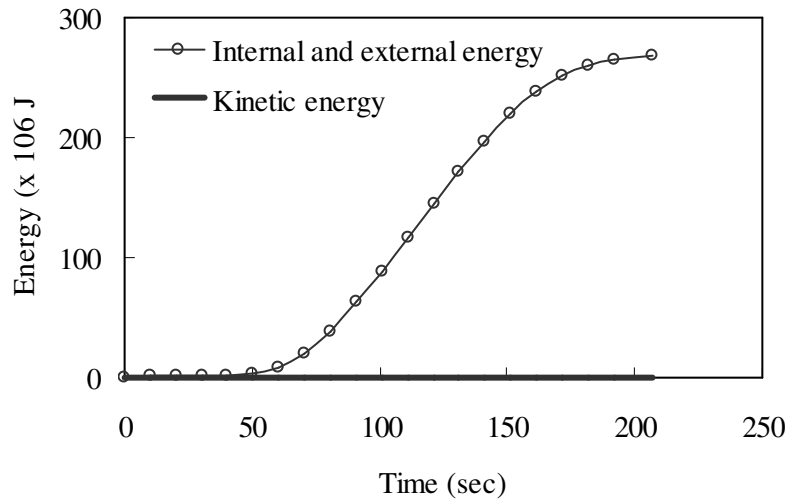
Fig. 3.3 Energy history of the pushover analysis of 4-storey SPSW of Driver et al.
(1998)
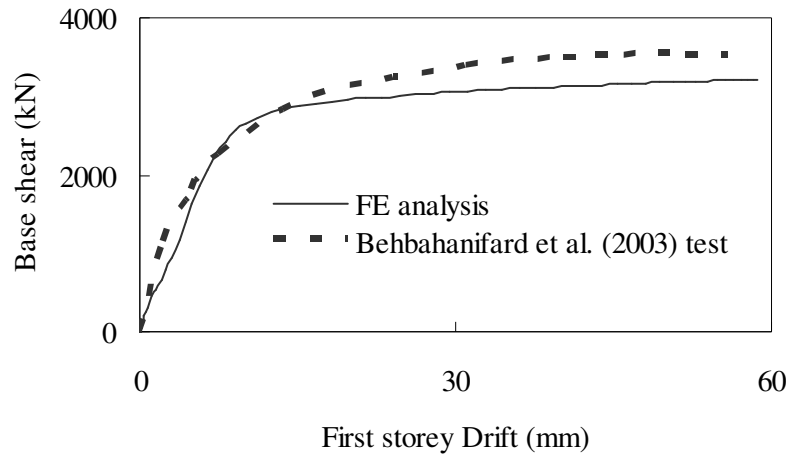
Fig. 3.4 Comparison of pushover analysis with test results of Behbahanifard et al. (2003)
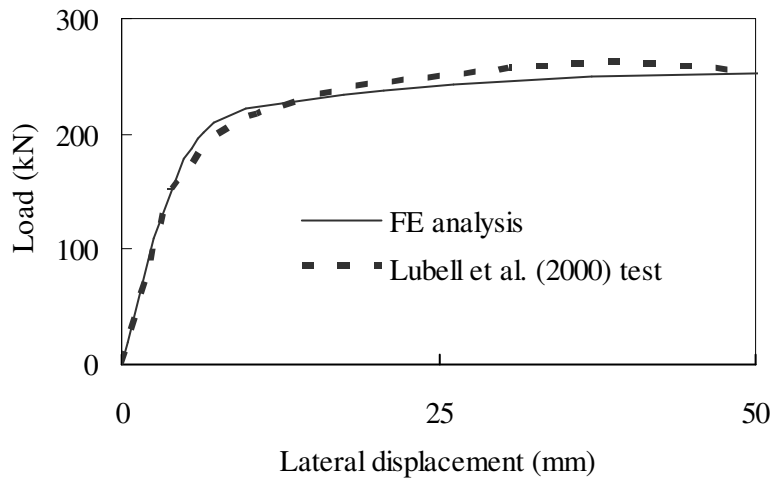
Fig. 3.5 Comparison of pushover analysis with test results of Lubell et al. (2000)
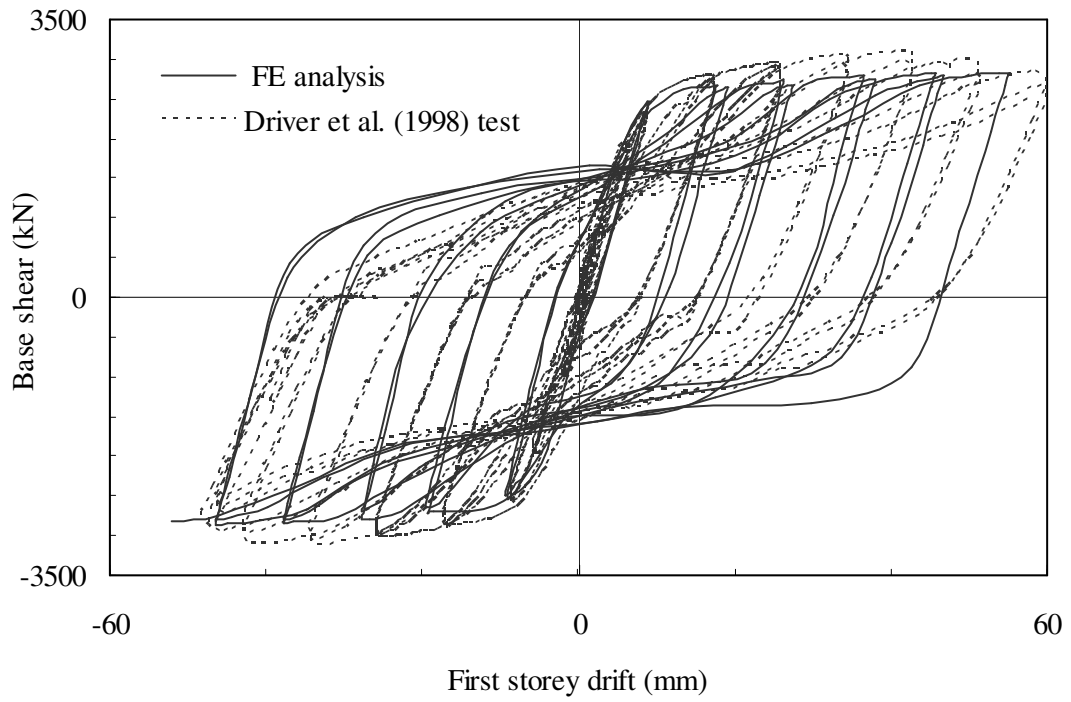
Fig. 3.6 Comparison of hysteresis curve with test results of Driver et al. (1998)
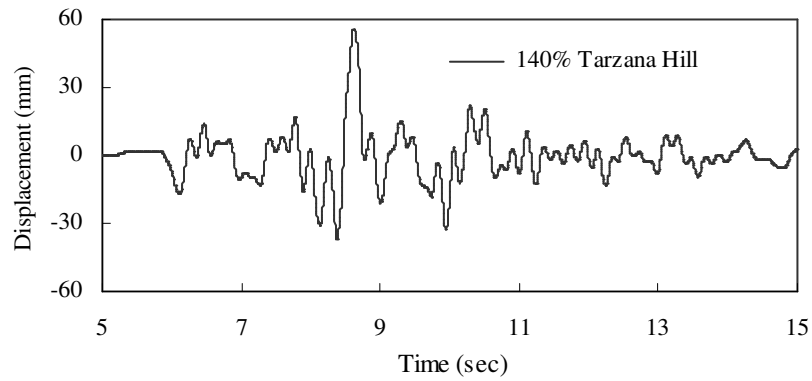
Fig. 3.7 Input table displacement for Rezai (1999) specimen
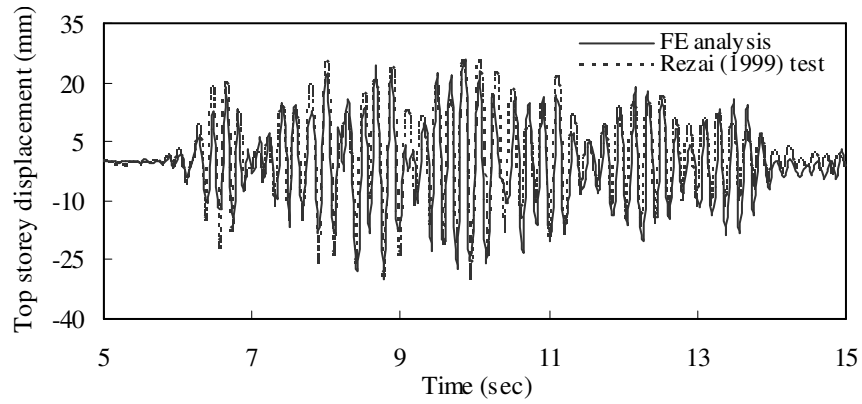
Fig. 3.8 Comparison of top storey displacement history for Rezai (1999) test
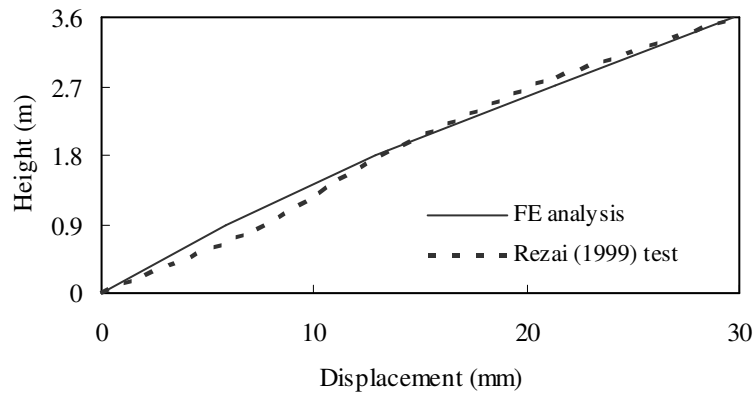
Fig. 3.9 Comparison of storey displacement envelope for Rezai (1999) specimen

77
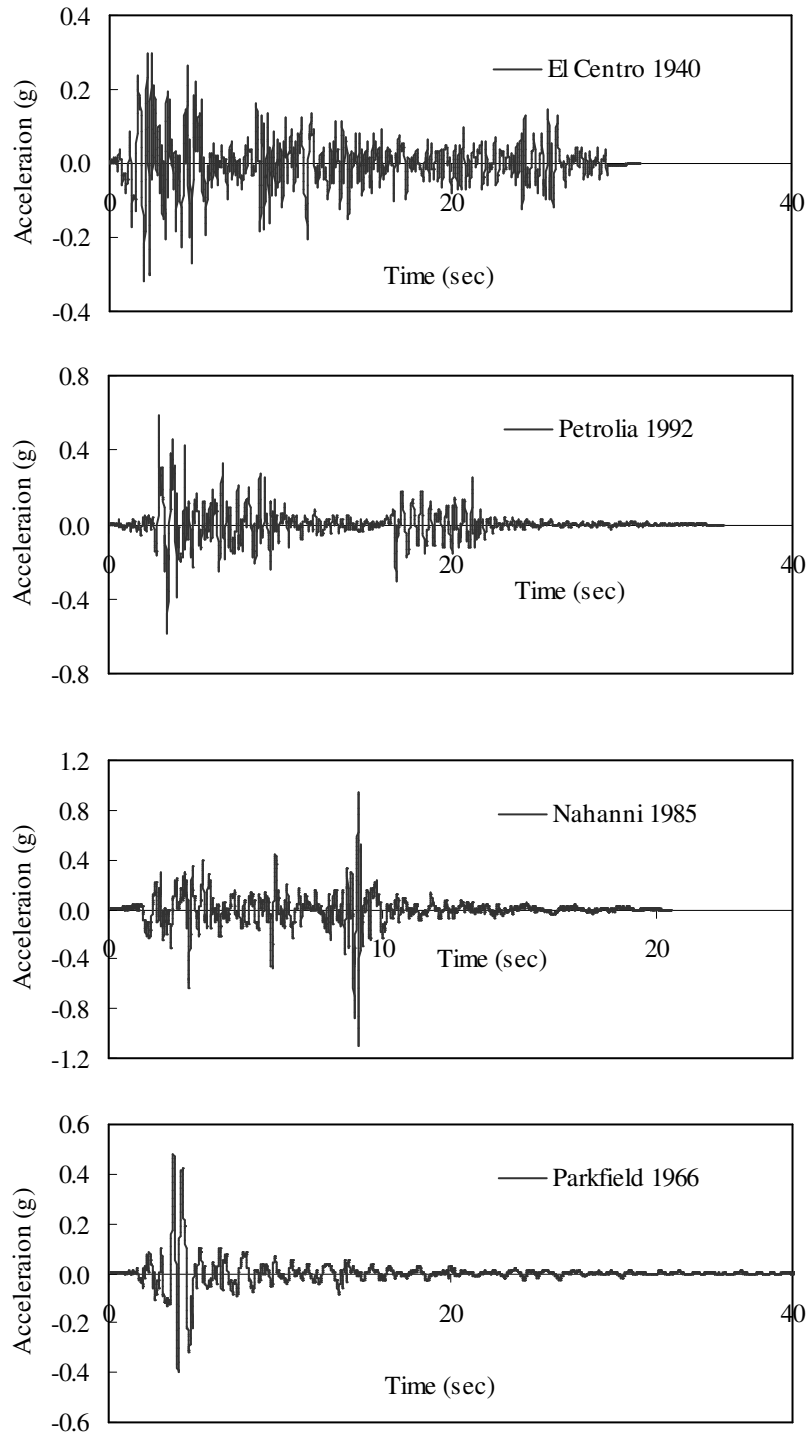
Fig. 3.10 Selected ground motions for seismic analysis
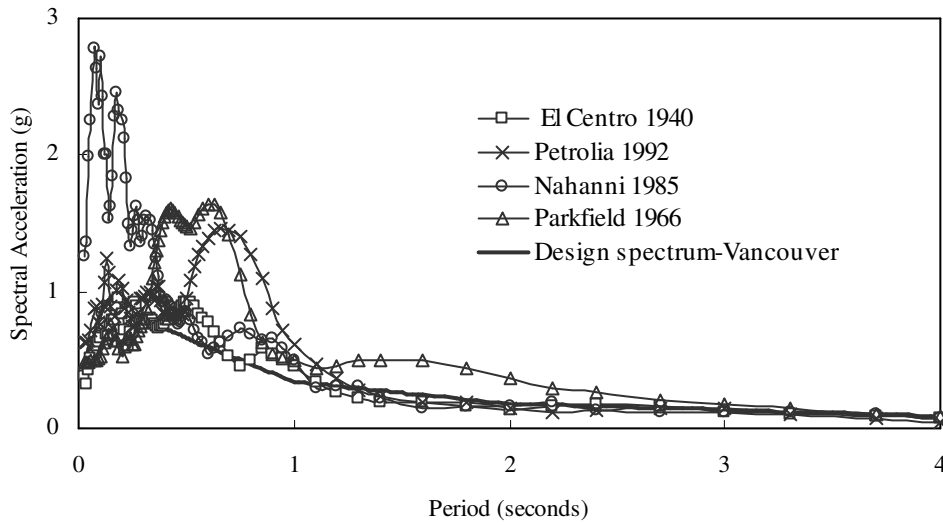
Fig. 3.11 5% damped absolute acceleration spectra of the selected ground motions
and design spectra of Vancouver
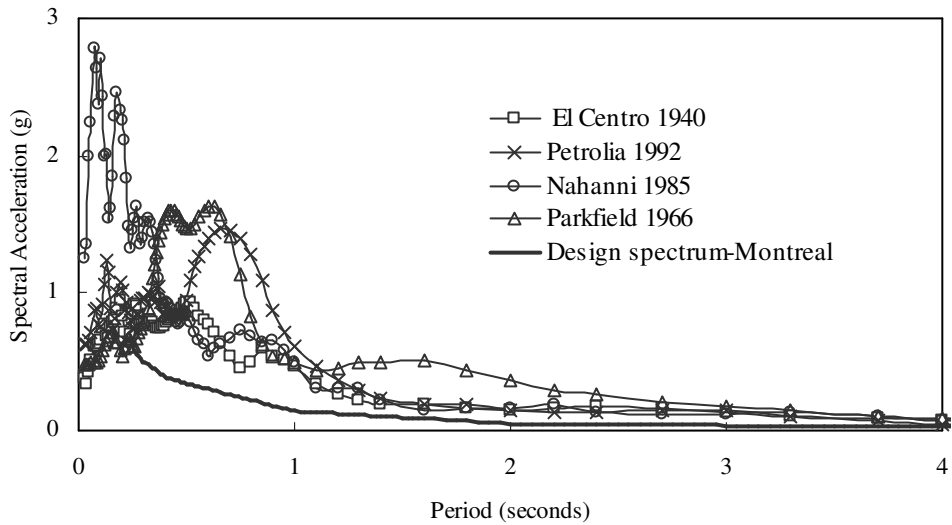
Fig. 3.12 5% damped absolute acceleration spectra of the selected ground motions
and design spectra of Montreal
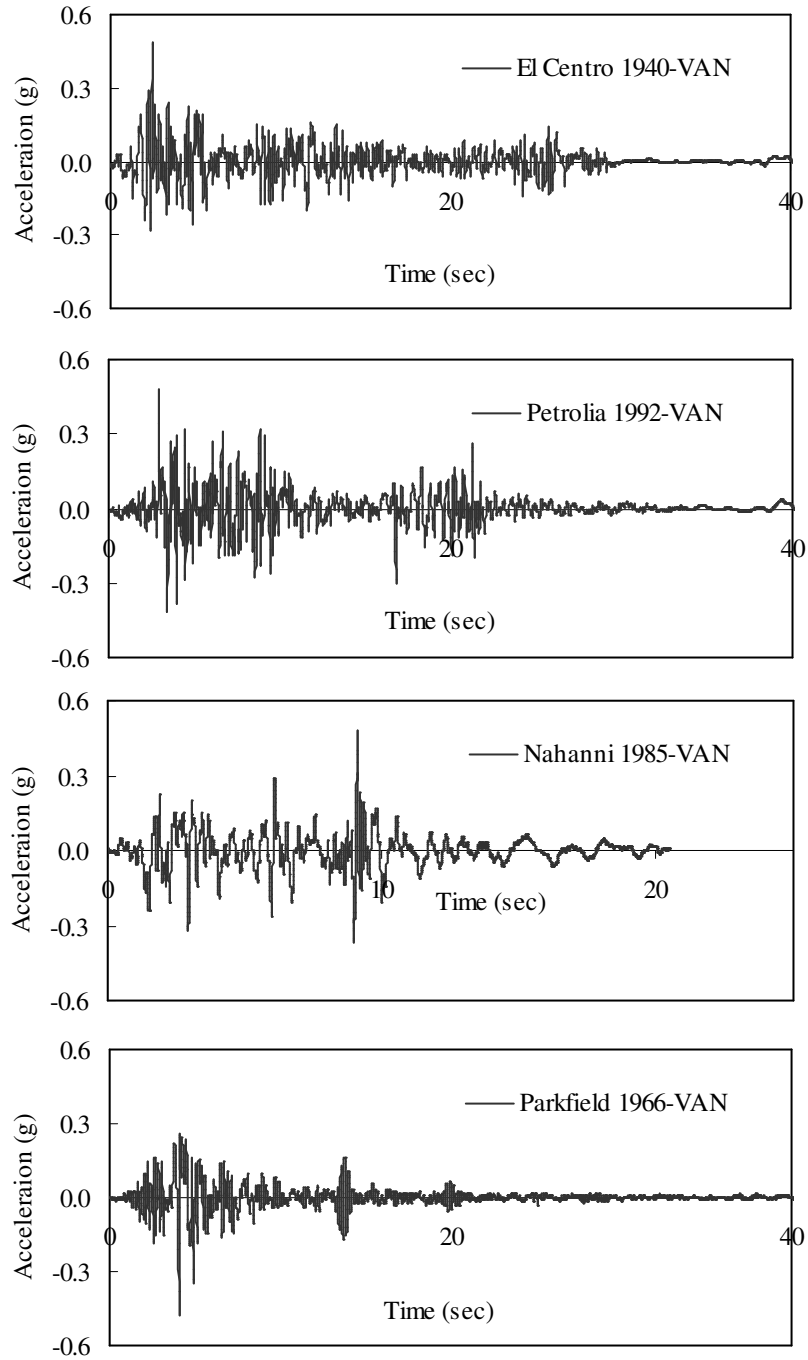
Fig. 3.13 Spectrum compatible seismic records to Vancouver

80
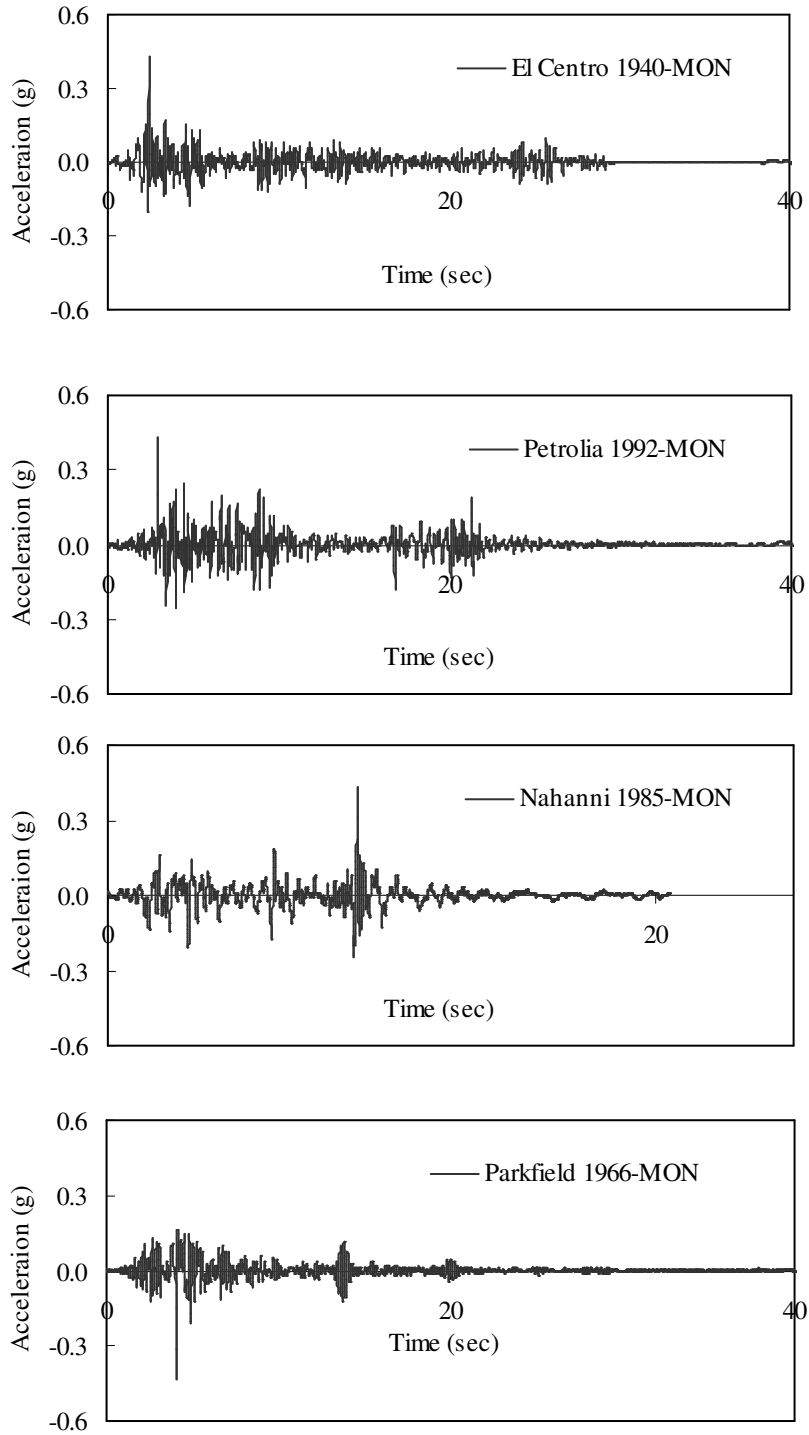
Fig. 3.14 Spectrum compatible seismic records to Montreal
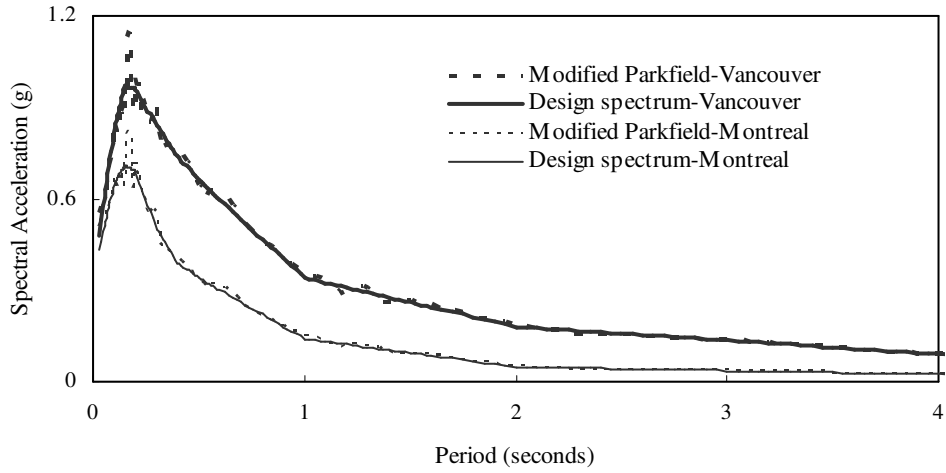
Fig. 3.15 Acceleration spectra for spectrum compatible Parkfield 1966 earthquake record

No yielding

Yielding

Type D SPSW

Type LD SPSW
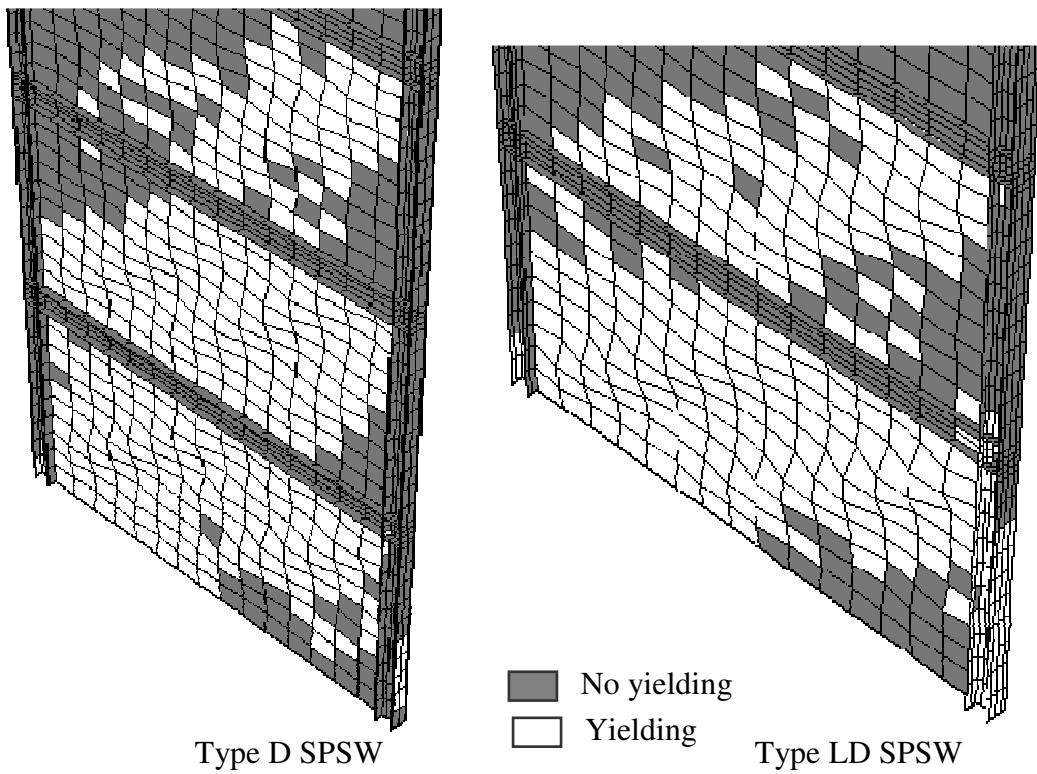
Fig. 3.16 FE mesh of 4-storey SPSWs under Parkfield earthquake (Vancouver) at the time of maximum shear
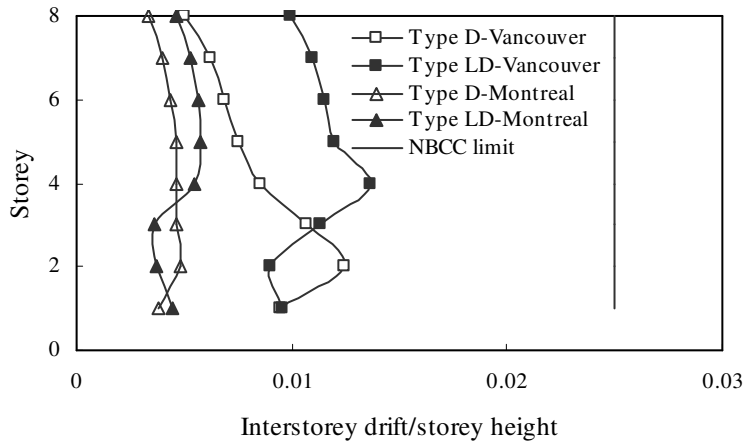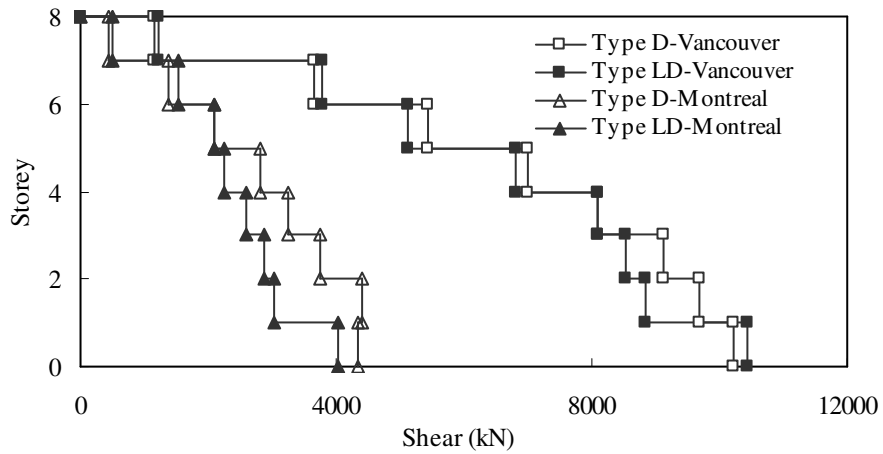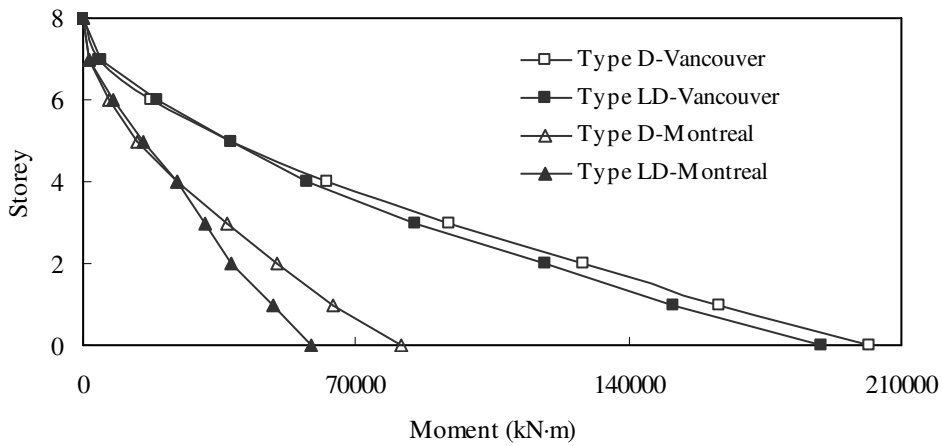
Fig. 3.17 Inelastic response of 8-storey SPSWs under 2.0 Parkfield earthquake:
(a) peak interstorey drifts; (b) peak storey shear forces and (c) peak bending
moments

No yielding

Yielding

Type D SPSW   Type LD SPSW
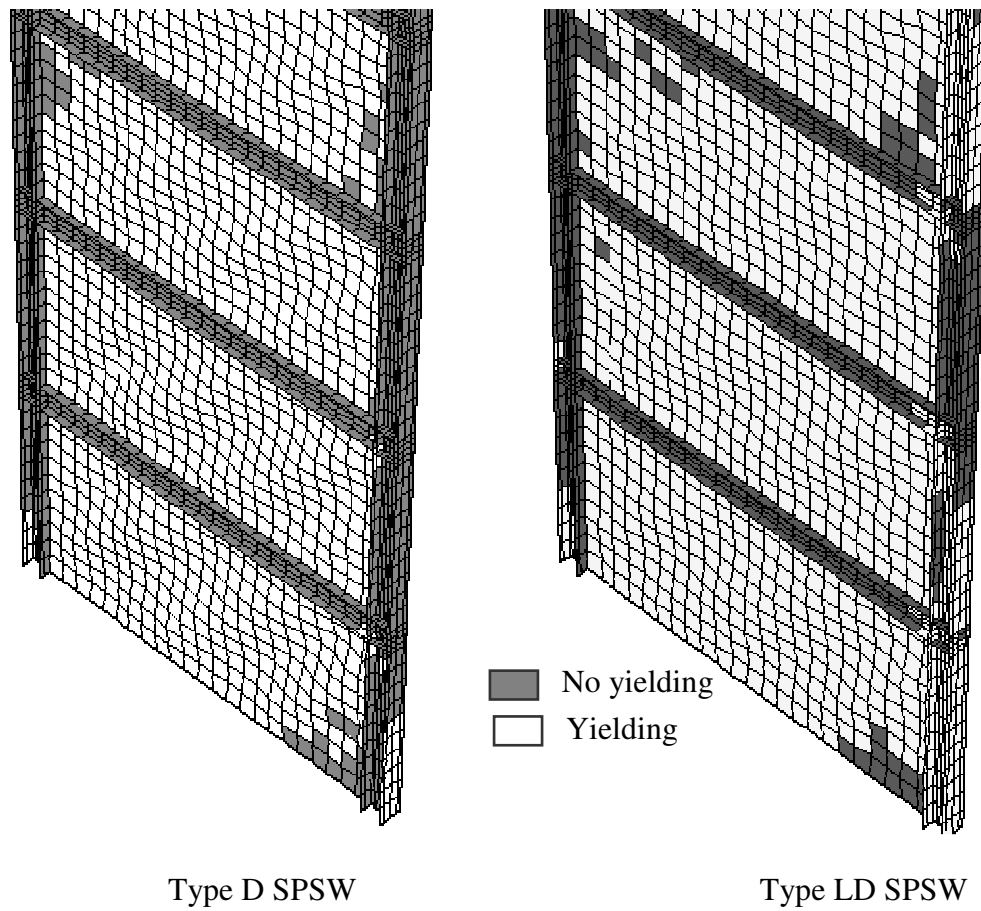
Fig. 3.18 FE mesh of 8-storey SPSWs under 2.0 Parkfield earthquake at the time
of maximum shear (Vancouver)

References

Behbahanifard, M.R., Grondin, G.Y., and Elwi, A.E. 2003. Experimental and numerical investigation of steel plate shear walls. Structural Engineering Report No. 254, Dept. of Civil and Environmental Engineering, University of Alberta, Edmonton, AB.

CSA. 2009. Limit states design of steel structures. CAN/CSA S16-09, Canadian Standards Association, Toronto, ON.

CSA. 2001. Limit states design of steel structures. CAN/CSA S16-01, Canadian Standards Association, Toronto, ON.

Cowper, G.R. and Symonds, P.S. 1957. Strain hardening and strain rate effects in the impact loading of cantilever beams. Brown University Division of Applied Mathematics, Report No. 28, Providence, RI.

Dastfan, M. and Driver, R.G. 2008. Flexural stiffness limits for frame members of steel plate shear wall systems. *In* Proceedings of 2008 Annual Structural Stability Research Council Conference, April 2-5, Nashville, TN, pp. 321-334.

Driver, R.G., Kulak, G.L., Kennedy, D.J.L., and Elwi, A.E. 1997. Seismic behaviour of steel plate shear walls. Structural Engineering Report No. 215, Dept. of Civil and Environmental Engineering, University of Alberta, Edmonton, AB.

Driver, R.G., Kulak, G.L., Kennedy, D.J.L., and Elwi, A.E. 1998. Cyclic test of four storey steel plate shear wall. Journal of Structural Engineering, ASCE, 124(2): 112-120.

Elgaaly, M., Caccese, V., and Du, C. 1993. Postbuckling behavior of steel-plate shear walls under cyclic loads. Journal of Structural Engineering, ASCE, 119(2): 588-605.

Hibbitt, Karlsson, and Sorensen. 2007. ABAQUS/Standard User's Manual. Version 6.7, HKS Inc., Pawtucket, RI.

Hilber, H.M., Hughes, T.J.R., and Taylor, R.L. 1978. Collocation, dissipation and 'overshoot' for time integration schemes in structural dynamics. Earthquake Engineering and Structural Dynamics, 6: 99-117.

Kharrazi, M.H.K. 2005. Rational method for analysis and design of steel plate walls. PhD Dissertation, Dept. of Civil Engineering, University of British Columbia, Vancouver, BC.

Lubell, A.S., Prion, H.G.L., Ventura, C.E., and Rezai, M. 2000. Unstiffened steel plate Shear Wall performance Under Cyclic Load. Journal of Structural Engineering, ASCE, 126(4): 453-460.

Naumoski, N. 2001. Program SYNTH- generation of artificial accelerogram history compatible with a target spectrum. User's manual. Dept. of Civil Engineering, University of Ottawa, Ottawa, ON.

NRCC. 2005. National Building Code of Canada. Canadian Commission on Building and Fire Codes, National Research Council of Canada, Ottawa, ON.

Rezai, M. 1999. Seismic behaviour of steel plate shear walls by shake table testing. PhD Dissertation, Dept. of Civil Engineering, University of British Columbia, Vancouver, BC.

Thorburn, L.J., Kulak, G.L., and Montgomery, C.J. 1983. Analysis of steel plate
shear walls. Structural Engineering Report No. 107, Dept. of Civil
Engineering, University of Alberta, Edmonton, AB.

Timler, P.A., and Kulak, G.L. 1983. Experimental study of steel plate shear walls.
Structural Engineering Report No. 114, Dept. of Civil Engineering, University
of Alberta, Edmonton, AB.

4. SEISMIC ANALYSIS OF STEEL PLATE SHEAR WALLS CONSIDERING STRAIN RATE AND $P - \Delta$ EFFECTS[2]

4.1 Introduction

Steel plate shear walls (SPSWs) have been accepted widely as a very effective system for resisting lateral loads due to wind and earthquakes. A conventional SPSW consists of vertical infill plates connected to the surrounding beams and columns. Although infill plates have been designed to prevent buckling before yielding by providing either stiffeners or sufficient thickness, modern steel plate shear walls are usually thin and unstiffened. In an unstiffened SPSW, axial coupling of column loads is the principal mechanism for resisting the overturning moment, while the shear is resisted primarily by a diagonal tension field that develops in the infill plates after they have buckled.

Experimental and analytical research on steel plate shear walls has focused mainly on static and quasi-static cyclic loading conditions. This chapter presents the results of a comprehensive study pertaining to seismic design and analysis of a typical 15-storey and a 4-storey steel plate shear wall.

One of the seismic design requirements in the current AISC provisions (AISC 2005) and Canadian steel design standard CAN/CSA S16-01 (CSA 2001) is that steel plate shear walls be designed under capacity design principles. Capacity design of structures involves pre-selecting a localized ductile fuse (or fuses) to act

---

[2] A version of this chapter has been published in the *Journal of constructional steel research*, 65(5): 1149-1159

as the primary location for the dissipation of seismic energy. The structure must be designed so as to force the inelastic action to be concentrated at the energy dissipators, which are detailed to behave in a ductile and stable manner. All other structural elements are protected against actions that could cause failure by providing them with sufficient strength so as to behave essentially elastically under forces consistent with the development of the maximum feasible forces in the designated fuses, with due account given to the overstrength of the energy dissipators (Paulay and Priestley 1992). In SPSWs, it is tension yielding in the infill panels, occurring under the action of the storey shear, that is considered to be the ductile and desirable mode of energy dissipation, although some energy dissipation by the boundary frame is inevitable.

Research on inelastic seismic response of structures (Gupta and Krawinkler 2000, Montgomery 1981, Tremblay et al. 1999) has shown that $P-\Delta$ effects are significant on flexible structures and do amplify the lateral displacements. The additional deformations result in an increase in ductility demand. Seismic provisions, including those in the 2005 National Building Code of Canada (NRCC 2005), specify limits on the expected interstorey drifts in a structure, with a view to limiting the nonstructural damage, as well as controlling the impact of the $P-\Delta$ forces on seismic performance. Considerable research has been done on how to take $P-\Delta$ effects into account. The non-mandatory commentary to NBCC 2005 endorses a method based on the stability approach recommended by (Paulay and Priestley 1992) to account for $P-\Delta$ effects. Analyses were carried out to

assess the influence of $P - \Delta$ effects on steel plate shear walls. Also, stability approaches proposed in the recommended seismic design provisions of the National Earthquake Hazards Reduction Program (NEHRP 2000) and the NBCC 2005 commentary are evaluated.

The loading rate effect in seismic analysis is an important aspect to be considered. In some previous research on seismic analysis (Mahin et al. 1972, Wallace and Krawinkler 1989), the loading rate effect was considered negligible, as moderate velocities were assumed. However, after the 1994 Northridge and 1995 Kobe earthquakes, where the recorded velocities were very high, researchers started emphasizing the importance of the load rate effect, which is a possible cause of unexpected failure of steel structures (Gioncu 2000). Manjoine (1944) conducted strain-rate tests on mild steels at room temperature for strain rates from 9.5 x 10^{-7} /sec to 3 x 10^2 /sec. These test results indicated that yield stress increased with an increase of strain rate, especially for strain rates greater than 10^{-1} /sec. However, the modulus of elasticity was found not to be influenced by the strain-rate variation. More recent research on strain rate effects (Kaneko 1997, Nakamura et al. 1999) has confirmed the previous results of (Manjoine 1944). Researchers, (Gioncu 2000, Kaneko 1997), have observed that strain rates usually vary from 10^{-1} /sec to 0.5×10^2/sec for near field earthquakes. Current Canadian and American seismic provisions do not have any clause to account for loading rate effects. This chapter presents a study on a typical 4-storey and a 15-storey steel plate shear wall to assess the importance of strain rate effects on its dynamic

flexural demand over the shear wall height. The steel plate shear walls have been designed in accordance with the NBCC 2005 and CAN/CSA S16-01 requirements and are analyzed for ground motions compatible with Vancouver, Canada.

4.2 Seismic design of steel plate shear walls

The equivalent static force procedure was used in the design of the steel plate shear walls for this study. NBCC 2005 permits this approach for a regular structure with a total height less than 60 m and a fundamental period less than 2 s, with certain restrictions on the method of determining the period. The design seismic base shear in NBCC 2005 is given by

$$V = \frac{S(T_a)M_v I_E W}{R_d R_o} \geq \frac{S(2.0)M_v I_E W}{R_d R_o} \tag{4.1}$$

where $S(T_a)$ is the design spectral acceleration, expressed as a ratio of gravitational acceleration, for the fundamental lateral period of vibration of the structure, T_a; M_v is an amplification factor to account for higher mode effects on the base shear; I_E is an importance factor for the structure; W is the total dead load, plus 25% of the design snow load and 60% of the storage load and the full contents of any tanks; R_d is a ductility-related force modification factor that reflects the capability of a structure to dissipate energy through inelastic deformation; and R_o is an overstrength-related force modification factor that accounts for the dependable portion of the reserve strength in a structure designed according to the NBCC 2005 seismic provisions. The design provisions also state that for structures with $R_d \geq 1.5$, the base shear need not be taken as being greater

than two-thirds of the value calculated for $T_a = 0.2$ s, but with M_v taken as 1.0. Thus

$$V \leq \frac{2}{3} \frac{S(0.2) I_E W}{R_d R_o} \qquad (4.2)$$

The base shear thus calculated is distributed over the height of the structure in proportion to the mass concentrated at each storey. The resulting expression for the force at any floor level x, F_x, is given by

$$F_x = (V - F_t) \frac{W_x h_x}{\sum\limits_{i=1}^{n} W_i h_i} \qquad (4.3)$$

where F_t is an additional lateral force applied at the top floor and its value is a function of the fundamental period of the structure; W_i and W_x are the portions of W assigned to level i or x, respectively; h_i and h_x are the height from the base to storey level i or x, respectively. With the loads at every floor calculated, the structure is designed to resist the effects caused by the equivalent static seismic forces. For a given base shear, the largest overturning moments are produced when the shear is distributed according to the first vibration mode. The moments become proportionately smaller when higher modes become influential. Since the NBCC 2005 base shear distributions are based predominantly on the first mode, the resulting moments at the storey levels need to be adjusted. Therefore, an overturning moment reduction coefficient, J_x, which depends on the fundamental

period and the height of level x, is applied. Thus, the overturning moment at level x, M_x, is

$$M_x = J_x \sum_{i=x}^{n} F_i \left(h_i - h_x \right)$$ (4.4)

NBCC 2005 requires that seismic-induced shears and overturning moments calculated at each storey level be amplified to account for the $P - \Delta$ effect. According to the recommendation in the NBCC commentary, the design storey shear, V_x^*, at any level is thus taken as

$$V_x^* = V_x \left(1 + \theta_{x,NBCC} \right)$$ (4.5)

where $\theta_{x,NBCC} = \dfrac{P_x \Delta_{mx}}{R_o V_x h_{sx}}$ is the stability factor; P_x is the total gravity load on the structure at and above the level x under consideration; Δ_{mx} is the maximum inelastic interstorey drift of the storey immediately below level x, and h_{sx} is the storey height immediately below level x. The NBCC commentary suggests that the $P - \Delta$ effect can be neglected if the stability factor is less than 0.10 and recommends that the structure be stiffened if $\theta_{x,NBCC} > 0.40$.

In the seismic design provision of the NEHRP 2000, the $P - \Delta$ effect is accounted for by increasing the storey shear by

$$V_x^* = V_x \Big/ \left(1 - \theta_{x,NEHRP} \right)$$ (4.6)

where $\theta_{x,NEHRP} = \dfrac{P_x \Delta_{ex}}{V_x h_{sx}}$ is the stability factor; P_x is as defined above; and Δ_{ex} is the elastic interstorey drift corresponding to the shear V_x, occurring in the storey immediately below level x. The NEHRP provisions specify that the $P - \Delta$ effects

may be neglected if the stability factor $\theta_{x,NEHRP}$ is less than 0.10. The provisions for $P - \Delta$ effects in the international building code 2000 (ICC 2000) are identical to those in the NEHRP provisions.

Once the design shear and moments are estimated, the steel plate shear wall is designed according to the capacity design provisions specified in CAN/CSA S16-01. AISC 2005 adopted a similar approach as an indirect capacity design approach for the design of steel plate shear walls. Capacity design for steel plate shear walls is based on tension yielding of the infill plate prior to the columns attaining their factored capacity. To ensure this, the column moments and axial forces obtained from an elastic analysis are magnified by an amplification factor, B, defined as

$$B = \frac{V_{re}}{V} \tag{4.7}$$

where V_{re} is the probable shear resistance at the base of the wall; and V is the factored lateral seismic force at the base of the wall obtained from NBCC 2005. The probable shear resistance of the wall (V_{re}) is given by

$$V_{re} = 0.5 R_y F_y w L \sin 2\alpha \tag{4.8}$$

where R_y is the ratio of the expected steel yield strength to the nominal yield strength of the material (specified as 1.1 in CAN/CSA S16-01, but R_yF_y must be taken as at least 385 MPa); w is the infill plate thickness; L is the bay width; α is the angle of the tension field developed in the infill plate and is obtained from CAN/CSA S16-01. The amplification factor, B, need not be taken as greater than

the ductility-based force modification factor, R_d, implying that if the overstrength of the infill plate is sufficiently high, the expected behaviour throughout the wall will be essentially elastic. Therefore, no further amplification in the seismic force beyond R_d is required.

Both CAN/CSA S16-09 and CAN/CSA S16-01 provide the following equation to ensure that the columns in steel plate shear walls are sufficiently stiff to develop an essentially uniform tension field in the adjacent infill plate

$$\omega_h = 0.7 h_s \sqrt[4]{\frac{w}{2LI_c}}$$ (4.9)

ω_h is the column flexibility parameter and must not exceed 2.5. This flexibility limit leads to a minimum column moment of inertia, I_c, as follows

$$I_c \geq \frac{0.00307 w h_s^4}{L}$$ (4.10)

In order to achieve a sufficiently uniform tension field in the top panel, consistent with the philosophy of equation (4.9), Dastfan and Driver (2008) have proposed a boundary member flexibility parameter, ω_L, for the design of the boundary elements in the top and bottom panels as follows

$$\omega_L = 0.7 \sqrt[4]{\left(\frac{h^4}{I_c} + \frac{L^4}{I_b}\right)\frac{w}{4L}}$$ (4.11)

where ω_L must not exceed the value of 2.5 in the top panel and 2.0 in the bottom; and I_b is the moment of inertia of the top beam (or bottom beam, if present).

4.3 Selection of steel plate shear wall system

The building considered in this study is a hypothetical symmetrical office building located in Vancouver, Canada. As a four storey building it has a total height of 15.2 m and as a 15-storey building it has a total height of 57.0 m from the ground level (3.8 m storey height). As shown in Fig. 4.1, the building has two identical steel plate shear walls provided to resist lateral forces along one direction. It is assumed that each shear wall resists one-half of the design seismic loads (for simplicity, torsion is neglected). Each shear wall panel is 7.6 m wide, measured from centre to centre of columns, and has an aspect ratio of 2.0. The building is assumed to contain a foundation built on rock (site class B according to NBCC 2005). The gravity loads applied on each column of the steel plate shear wall include dead, live, and snow loads. A dead load of 4.26 kPa is used for each floor and 1.12 kPa for the roof. The live load on all floors is taken as 2.4 kPa. Snow loads applied at the roof are calculated following the provisions of NBCC 2005, without drifting. A ductility-related force modification factor, R_d, of 5.0 and an overstrength force modification factor, R_o, of 1.6 are used in the design, as prescribed by NBCC 2005. Table 4.1 and Table 4.2 summarize the calculations of the storey shears and overturning moments in the 15-storey and 4-storey steel plate shear walls, respectively. The NBCC 2005 load combination $D + 0.5L + E$ (where $D =$ dead loads, $L =$ live loads and $E =$ earthquake loads) was considered for intermediate floors and for the roof, the load combination $D + 0.25S + E$ (where $S =$ snow loads) was considered. For the design of the steel plate shear walls, an infill plate thickness of 3.0 mm was assumed to be the

minimum practical thickness based on handling and welding considerations. The nominal yield strength of the boundary beams, columns and infill plates was assumed to be 350 MPa and all steel members were assumed to have a modulus of elasticity of 200 000 MPa. Because the infill plate is the primary energy dissipating component of the seismic system, according to the capacity design approach, the boundary members were designed for a probable infill plate yield strength of $R_y F_y$ of 385 MPa, where R_y is taken as 1.1.

The boundary columns selected satisfied all the CAN/CSA S16-01 requirements for strength and stiffness. Intermediate beams were designed based on the factored dead and live loads assuming the tension field forces on either side of the beam would balance each other. Final design forces were obtained from a linear elastic analysis of the steel plate shear wall. Storey drifts at each level (Δ_x in Table 4.1 and Table 4.2) obtained from the linear elastic analysis were multiplied by $R_d R_0$ to account for the inelastic action and then checked against the allowable interstorey drift limit. Table 4.1 presents the anticipated inelastic interstorey drift (Δ_{mx}) that varies from 28.7 mm to 77.0 mm for the 15-storey steel plate shear wall, which is well below the NBCC 2005 and NEHRP 2000 drift limit of $0.025 h_{sx}$ (95 mm). The inelastic interstorey drift for the 4-storey steel plate shear wall, as observed in Table 4.2, varies from 11.9 mm to 24.0 mm, well below the drift limit. The final column and beam sections satisfied the beam-column design requirements of CAN/CSA S16-01 and the columns were selected in three storey lifts.

97

Stability factors to account for $P-\Delta$ effects in NBCC and NEHRP are calculated using Equations 5 and 6, respectively, and presented in Table 4.3. Storey shears increased for $P-\Delta$ effects are also compared. The NBCC approach for $P-\Delta$ effects is more conservative (higher shear forces), mainly because the inelastic interstorey drift is considered rather than the elastic drift as in the NEHRP provisions. For the NBCC method, the amplification factor for storey shear ranges from 1.09 to 1.30 for the 15-storey SPSW and 1.01 to 1.05 for the 4-storey SPSW. Conversely, the NEHRP provisions suggest that $P-\Delta$ effects are small, with maximum amplification factors of 1.06 for the 15-storey SPSW and 1.01 for the 4-storey SPSW. For this study, it was decided to neglect $P-\Delta$ effects in the design of the steel plate shear wall to permit the study of a weaker shear wall that is more vulnerable to $P-\Delta$ effects in a non-linear seismic analysis. Table 4.4 presents the final columns and beams for the 15- and 4-storey steel plate shear walls.

4.4 Inelastic seismic time history analyses

4.4.1   Frequency analysis

A nonlinear finite element model was developed for analysing the SPSWs. Details of the finite element model are presented in Chapter 3. The finite elemnt model was used to conduct a frequency analysis, in ABAQUS (Hibbitt et al. 2007), for the 4-storey and 15-storey SPSWs to determine periods of vibration and corresponding mode shapes, both with and without $P-\Delta$ effects. Table 4.5 presents estimates of the first four in-plane fundamental periods for both of the

finite element models, with and without $P - \Delta$ effects. As expected, including the gravity loading in the analysis softens the structure and thus lengthens the periods of vibration, although this effect is insignificant in the 4-storey wall. Also, with higher modes the $P - \Delta$ effects become smaller because with the increase in mode number, the modal elastic stiffness of the steel shear wall increases more rapidly than the modal geometric stiffness.

NBCC 2005 and NEHRP 2000 adopted the identical empirical expression for estimation of fundamental period

$$T = 0.05(h_n)^{3/4} \tag{4.12}$$

where h_n is the height of the building in metres. Table 4.5 shows that the computed fundamental period of the 15-storey steel shear wall, including $P - \Delta$ effects, is 2.9 times larger than the NBCC and NEHRP estimate. For the 4-storey steel plate shear wall the computed fundamental period is 1.5 times the NBCC and NEHRP estimate. Thus, the code specified empirical expression for fundamental period provides a higher spectral acceleration and so is a conservative estimate.

4.4.2 Ground motion time histories

When dynamic time history analysis is used to assess the structural response, NEHRP 2000 recommends the use of at least three time histories to explore expected seismic performance. NBCC 2005 does not specify any number of time histories to use, but it emphasizes the used of spectrum compatible earthquake records. Spectrum compatibility is considered a desirable characteristic where the

response spectrum from the earthquake records should match with the design site specified response spectrum for certain periods of interest. The four seismic records used in Chapter 3 are also chosen for the time history response analysis. As recommended in NBCC 2005, the seismic records were modified using the software SYNTH (Naumoski 2001) to make them spectrum compatible. The SYNTH program first computes the spectrum for the real acceleration time history. In order to match the computed spectrum with the target spectrum, the computed spectrum is then raised and suppressed iteratively by corresponding modification of the Fourier coefficients.

4.4.3   Inelastic response in shear wall

Nonlinear time step dynamic analyses of the steel shear wall were performed for two building heights and four seismic records. Figure 4.2 presents the envelope of interstorey drift, storey shears, and bending moments obtained from inelastic time history analyses of the 15-storey steel plate shear wall. To compare with the current CAN/CSA S16-01 approach, strain rate effects were not included in the analysis. The effect of strain rate will be discussed later.

Figure 4.2 (a) shows that the interstorey drift ratios obtained from inelastic time history analyses are significantly less than interstorey drift limit specified by NBCC 2005. The infill plates at the upper levels were designed with overstrengths much greater than those at the lower storeys. Infill plates with high overstrength do not contribute much to the system ductility. Thus, the seismic drift demands on the upper stories are less.

Fig. 4.2 (b) shows that for all ground motions, the NBCC 2005 static base shear force distribution is much lower than those of the dynamic shear distributions. This is because of the overstrength resulting from using thicker infill plates than required to resist storey shears. The average shear force developed at the base of the steel plate shear wall from the time history analyses, 6357 kN, is about 47% higher than the probable shear resistance calculated by using equation 8. The shear strength prediction for steel plate shear walls in CAN/CSA S16–01 is based on fully yielded tension strips at an angle similar to the diagonal tension field, neglecting the contribution from the boundary framing members and possible interaction between adjacent strips. Driver et al. (1997) discussed several aspects of the system behaviour that are neglected by dividing the plate into individual strips that may be significant in the determination of both strength and stiffness. To estimate these contributions to shear strength, a nonlinear static pushover analysis was conducted for the NBCC 2005 seismic forces. The pushover analysis was carried out for a target roof displacement of 445 mm, which is the average of the peak roof displacements obtained from time history seismic analyses presented in Table 4.6. The pushover analysis was carried out with the NBCC 2005 recommended equivalent static force distribution. The maximum infill plate shear in the pushover analysis was found at the second storey, with the second storey infill plate fully yielded. The second storey shear (infill plate only) from the pushover analysis was (4350/4075 =1.067) 6.7 % higher than the probable panel shear resistance estimated by CAN/CSA S16-01. Since no dynamic

101

amplification exists in the pushover analysis, this 6.7% shear can be attributed to other factors not accounted for by the strip model.

From all the time history analyses, the average shear contribution from the boundary column members at the base was obtained from the finite element analysis as 1940 kN, namely, about 30% of total average base shear from the seismic time history analyses. Thus, it is observed that the current Canadian code overlooks a significant amount of shear strength contributed by the surrounding framing members. In total, the shear strength is underestimated by approximately 36%. Thus, for this 15-storey steel plate shear wall the dynamic amplification factor for shear at the base can be estimated from $V_{dyn}/1.36BV$, where V_{dyn} is the average dynamic base shear from the inelastic seismic analyses; B and V are as defined in equation 7. The dynamic amplification factor for shear thus calculated at the base is 1.15. This dynamic shear force amplification is likely caused by higher modes of vibration. The NBCC 2005 proposed a base shear adjustment factor for higher mode effect, M_v, for this 15-storey shear wall of only 1.01.

Figure 4.2 (c) shows that the dynamic moment envelopes are almost linear. But the seismic demands for flexure at the base and a few of the lower storeys are significantly underestimated by the code. This is mainly due to two reasons: the use of high overstrength infill plates on the upper floors and the use of an amplification factor that does not include the significant amount of shear strength contributed by the boundary columns. This leads to an underestimation of axial

forces and local bending moments in the boundary columns at the base of the frame.

Figure 4.3 shows the seismic envelopes for axial force and bending moment for the boundary columns. As stated in CAN/CSA S16-01, the axial forces in the boundary columns are obtained from a moment envelope for the shear wall. According to CAN/CSA S16-01, the local bending moments in the columns are obtained from an elastic analysis multiplied by the amplification factor, B. Both axial forces and bending moments are significantly underestimated by the capacity design approach in CAN/CSA S16-01.

To investigate the effect of infill plates overstrength in the upper floors, the 15-storey steel plate shear wall was redesigned with the same overstrength in every storey with the first storey infill plate thickness of 3 mm. This was done by adjusting all other infill plate thicknesses to the thicknesses required to get the same overstrength as the first storey infill plate. Figure 4.4 shows that with the use of same overstrength infill plates at every storey, the flexural demand in the shear wall goes down as well as the axial load demand in the boundary columns. The flexural demand in the boundary columns does not change significantly as a result of this design change. Moreover, in the upper floors the column flexural demands become slightly higher since the thinner infill plates contribute less to the moment carrying capacity.

Figure 4.5 shows the envelopes for peak interstorey drifts, storey shears, and bending moments for the 4-storey steel plate shear wall. The interstorey drift

ratios for the 4-storey SPSW obtained from the seismic analyses are much lower than the NBCC 2005 drift limit. From nonlinear seismic analyses, as explained above for the 15-storey steel plate shear wall, the average shear strength contribution at the base for the boundary columns for the 4-storey steel plate shear wall is estimated as 12%. This results in a lower estimated value of amplification factor, B, for the capacity design approach. Figure 4.5 (c) also shows that the seismic moment demand at the base is underestimated in the current standard by about 22%. Figure 4.6 shows both axial forces and column moments are underestimated by the current capacity design approach in CAN/CSA S16-01.

4.5 Strain rate effect on seismic response

The 4- and 15-storey steel plate shear walls were reanalyzed considering strain rate effects. In Tables 4.6 and 4.7, the absolute peak inelastic roof displacements, base shears, and base overturning moments of the 15- and 4-storey steel plate shear walls are presented with and without the strain rate effect. In the case of the 15-storey steel plate shear wall, in Table 4.6, the average increase in flexural demand at the base of the wall is only 4% and the increase in roof displacement is only 2%. The increase in seismic demand is very small for the 15-storey wall as the maximum strain rate estimated from the analysis is only 0.043/sec and it occurs for the Petrolia earthquake record. For the 4-storey steel plate shear wall, in Table 4.7, the maximum increase in roof displacement and base overturning moment is about 15% when the strain rate model is included in the analysis. This maximum increase is obtained for the El Centro earthquake, as the strain rate

observed for El Centro (0.098 /sec) is greater than the strain rates observed for the other three earthquake records. On average the strain rate effect increases the flexural demand by about 11%. To assess the severity of the strain rate effect, the spectrum compatible El Centro 1940 earthquake was amplified 1.5 and 2.0 times and then applied at the base of the steel plate shear wall. Only the 15-storey steel plate shear wall with and without strain rate effects is analyzed. The results are presented in Fig. 4.7. It is observed that with an increase in intensity of earthquake, the strain rate effect on the seismic demand at the base of the steel plate shear wall increases. The flexural demand increases from 1% to 21% when the El Centro earthquake record is amplified by 1.5. The maximum strain rates for the spectrum-compatible El Centro and 1.5 El Centro records were 0.029/sec and 0.066/sec, respectively. Thus, for seismic design in Vancouver, the strain rate has a small effect in the inelastic seismic demand of steel plate shear walls. However, for larger earthquakes this effect may need to be considered.

4.6 $P - \Delta$ effect on seismic response

The $P - \Delta$ effect is always greater for taller structures. Thus, for this research work only the 15-storey steel plate shear wall is analyzed to assess the $P - \Delta$ effect on the seismic behaviour. As explained above, the mass of half the building was placed on a leaning dummy column. The typical floor mass applied at each floor of the leaning column was 192 MN and 62 MN at the roof level. Figure 4.8 shows the inelastic seismic response of the 15-storey shear wall for the El Centro earthquake record. The inelastic response of the wall is characterized by

the roof displacement, the base shear, and the base overturning moment. The analysis was conducted with and without $P - \Delta$ effects included. The results shown in Fig. 4.8 indicate that $P - \Delta$ effects are very small in this case. An increase in top storey displacement demand of only about 3.7% is observed. The flexural demand at the base of the steel shear wall is increased by only 1.7%. To highlight the relative importance of any $P - \Delta$ effect in the case of higher intensity earthquakes, the steel plate shear wall was reanalyzed with amplified records of 1.5 and 2.0 times the El Centro earthquake history. The peak response parameters are presented in Table 4.8, where it is shown that the increase or decrease in the response parameters due to the $P - \Delta$ effects is very small. These results indicate that $P - \Delta$ effects for low- and mid-rise structures are not important for steel plate shear walls that are stiff enough to meet the NBCC 2005 interstorey drift limit.

4.7 Conclusions

A typical 4-storey and 15-storey steel plate shear wall for a building located in Vancouver and designed according to the NBCC 2005 and CAN/CSA S16-01 seismic provision were analyzed under four spectrum compatible ground motions. Strain rate effects and $P - \Delta$ effects on the inelastic seismic responses were evaluated. The analyses also provided information on the displacement and force demand on the ductile lateral load resisting system. The key findings from this study are as follows:

(7) The current capacity design approach in CAN/CSA S16-01 underestimates the probable shear strength at the base of the steel plate shear wall. From inelastic dynamic analyses, it was observed that flexural seismic demand at the base of the steel plate shear wall is underestimated in the current code. This is because current practice does not include the shear strength contribution from the boundary columns. It should be noted that in a taller steel plate shear walls where the boundary columns are large at the bottom storeys, the columns may carry a larger portion of the total shear strength. Due to an underestimation in probable shear strength at the base, a lower value of the amplification factor B is estimated, which leads to a lower value of bending moment at the base of the steel plate shear wall. The analytical work also show that for the same reason, axial force and bending moment demands in the boundary columns are underestimated. Thus, it is recommended that the contribution of the columns to the shear strength of the shear wall system be included at the design stage.

(8) The interstorey drifts obtained from the inelastic time history analyses were well within the limit of $0.025h_{sx}$ prescribed by NBCC 2005/NEHRP 2000.

(9) High overstrength infill plates do not contribute significantly to the system ductility. Thus, when it is practical, the thickness of the infill plate should be adjusted to reduce the overstrength variation over the building height.

(10) Strain rate has an effect in the dynamic response of steel plate shear walls. With higher strain rates the ductility of the steel plate shear wall

reduces and the average flexural demand at the base of the wall is increased. For seismic design of a steel plate shear wall in Vancouver, the strain rate effect increased the overturning moment by about 11% for the 4-storey and about 4% for 15-storey steel plate shear wall.

(11) The NBCC 2005 approach for accounting for $P - \Delta$ effects is more stringent than the NEHRP 2000 approach. According to the current Canadian stability factor approach, the flexural capacity of the steel plate shear wall had to be increased by as much as 30% in one storey. The inelastic seismic analysis of the shear wall designed without any amplification for $P - \Delta$ effects showed that the $P - \Delta$ effect on the response of the structure is very small. Thus, the stability approach in NBCC 2005 seems overly conservative and could be omitted if the shear wall meets the code specified inter storey drift limit.

Table 4.1 Seismic loads and forces for the 15-storey steel plate shear wall

Storey	W_x (kN)	h_x (m)	F_x (kN)	V_x (kN)	J_x	M_x (kN·m)	Δ_x (mm)	Δ_{mx} (mm)
1	8520	3.8	15.1	1800	0.893	62800	3.6	28.7
2	8520	7.6	30.3	1790	0.904	57500	8.7	41.2
3	8520	11.4	45.4	1760	0.916	52000	14.8	48.8
4	8520	15.2	60.6	1710	0.928	46500	21.8	55.7
5	8520	19.0	75.7	1650	0.940	41000	29.5	61.6
6	8520	22.8	90.9	1570	0.952	35600	37.8	66.4
7	8520	26.6	106.0	1480	0.964	30200	46.6	70.4
8	8520	30.4	121.1	1380	0.976	25100	55.8	73.6
9	8520	34.2	136.3	1260	0.988	20300	65.3	75.6
10	8520	38.0	151.4	1120	1.000	15700	74.9	76.8
11	8520	41.8	166.6	970	1.000	11500	84.5	77.0
12	8520	45.6	181.7	800	1.000	7800	94.0	76.3
13	8520	49.4	196.9	620	1.000	4760	103.4	74.6
14	8520	53.2	212.0	420	1.000	2400	112.4	72.4
15	2980	57.0	210.1	210	1.000	799	121.5	73.0

Table 4.2 Seismic loads and forces for the 4-storey steel plate shear wall

Storey	W_x (kN)	h_x (m)	F_x (kN)	V_x (kN)	J_x	M_x (kN·m)	Δ_x (mm)	Δ_{mx} (mm)
1	8520	3.8	154.3	1140	1.0	11500	2.8	22.7
2	8520	7.6	308.6	990	1.0	7150	5.8	24.0
3	8520	11.4	462.9	680	1.0	3400	8.5	21.3
4	2980	15.2	215.9	220	1.0	820	10.0	11.9

Table 4.3 Stability coefficients and P-Δ amplifications for the SPSWs

	15-storey SPSW				4-storey SPSW			
Storey	$\theta_{x,NBCC}$	$V^*_{x,NBCC}$	$\theta_{x,NEHRP}$	$V^*_{x,NEHRP}$	$\theta_{x,NBCC}$	$V^*_{x,NBCC}$	$\theta_{x,NEHRP}$	$V^*_{x,NEHRP}$
		(kN)		(kN)		(kN)		(kN)
1	0.17	2120	0.035	1870	0.05	1200	0.01	1150
2	0.24	2210	0.047	1870	0.04	1030	0.01	996
3	0.26	2220	0.053	1850	0.03	700	0.01	683
4	0.28	2190	0.057	1810	0.01	219	0.003	216
5	0.30	2140	0.059	1750				
6	0.30	2050	0.060	1670				
7	0.30	1930	0.061	1580				
8	0.30	1790	0.060	1460				
9	0.29	1620	0.059	1330				
10	0.28	1430	0.056	1190				
11	0.26	1220	0.053	1020				
12	0.24	996	0.049	842				
13	0.22	752	0.043	647				
14	0.17	496	0.035	437				
15	0.09	228	0.017	214				

Table 4.4 Summary of steel plate shear wall frame member properties

	15-storey SPSW			4-storey SPSW	
Storey	Column sections	Beam sections	Storey	Column sections	Beam sections
1-3	$W360 \times 990$	$W410 \times 100$	1-3	$W310 \times 226$	$W410 \times 100$
4-6	$W360 \times 900$	$W410 \times 100$	4	$W310 \times 226$	$W760 \times 582$
7-9	$W360 \times 744$	$W410 \times 100$			
10-12	$W360 \times 634$	$W410 \times 100$			
13-14	$W360 \times 592$	$W410 \times 100$			
15	$W360 \times 592$	$W760 \times 582$			

Table 4.5 Periods of steel plate shear walls

| Mode | Periods 15-storey SPSW | | | Periods 4-storey SPSW | | |
	with P-Δ	without P-Δ	NBC 2005/ NEHRP 2000	with P-Δ	Without P-Δ	NBCC 2005/ NEHRP 2000
1st	3.01	2.94	1.04	0.58	0.58	0.385
2nd	0.82	0.81		0.22	0.22	
3rd	0.42	0.41		0.16	0.16	
4th	0.29	0.29		0.13	0.13	

Table 4.6 Maximum inelastic response parameters including P-Δ and strain rate effect for 15-storey steel plate shear wall

| Earthquake records | With strain rate effect | | | Without strain rate effect | | |
	Roof displacement (mm)	Base shear (kN)	Base moment (kN·m)	Roof displacement (mm)	Base shear (kN)	Base moment (kN·m)
El Centro 1940	491	5670	230000	489	5810	228000
Petrolia 1992	465	5550	21900	437	6400	209000
Nahanni 1985	392	7350	20800	387	6950	196000
Parkfield 1966	455	6490	208000	450	6260	197000

Table 4.7 Maximum inelastic response parameters including both P-Δ and strain
rate effect for 4-storey steel plate shear wall

Earthquake records	With strain rate effect			Without strain rate effect		
	Roof displacement (mm)	Base shear (kN)	Base moment (kN·m)	Roof displacement (mm)	Base shear (kN)	Base moment (kN·m)
El Centro 1940	71	5790	58300	62	5260	50600
Petrolia 1992	75	5430	55800	67	5280	51600
Nahanni 1985	73	5560	58200	69	5140	51800
Parkfield 1966	72	5590	58200	66	5230	52500

Table 4.8 Peak seismic response parameters of 15 SPSW with and without P-Δ
effect

Earthquake records	With P-Δ effect			Without P-Δ effect		
	Roof displacement (mm)	Base shear (kN)	Base moment (kN·m)	Roof displacement (mm)	Base shear (kN)	Base moment (kN·m)
El Centro 1940	489	5810	228000	471	6260	224000
1.5*El Centro	568	7090	243000	575	7960	264000
2.0* El Centro	719	7930	256000	705	8690	258000
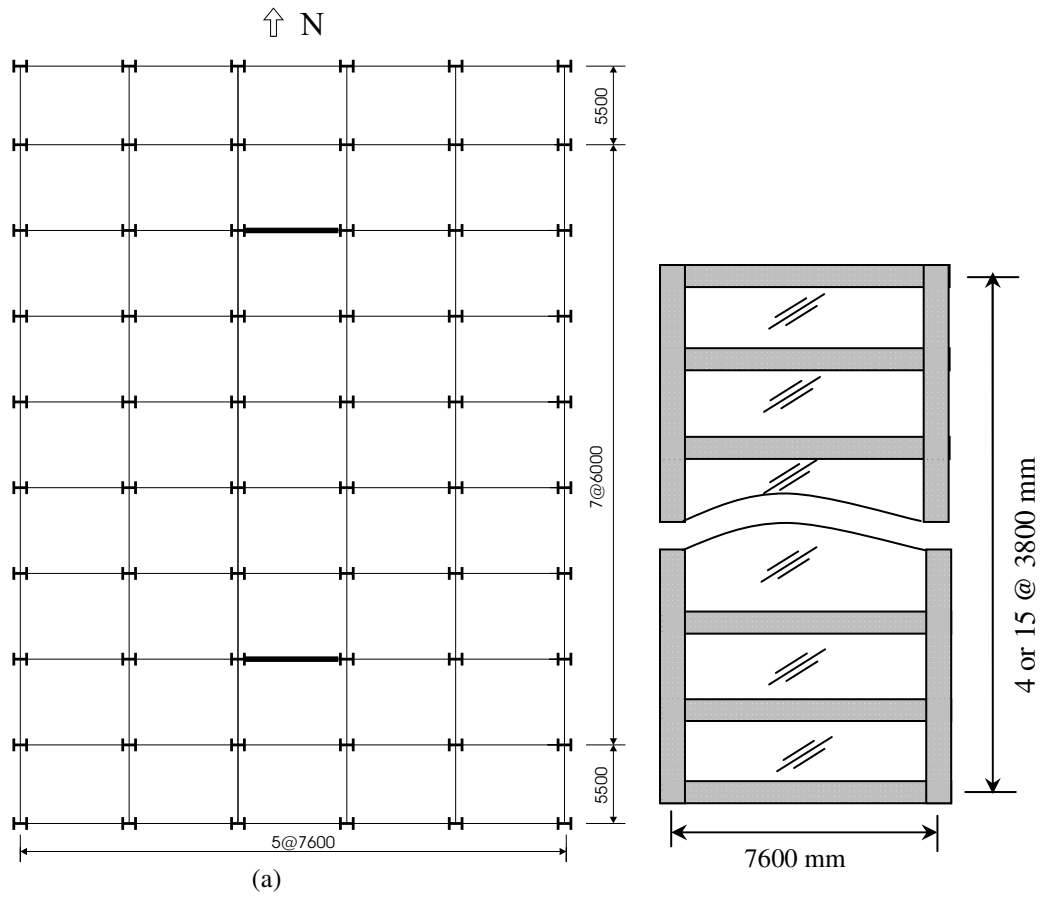
Fig. 4.1 4-storey and 15-storey buildings: (a) Floor plan, (b) Elevation of SPSW
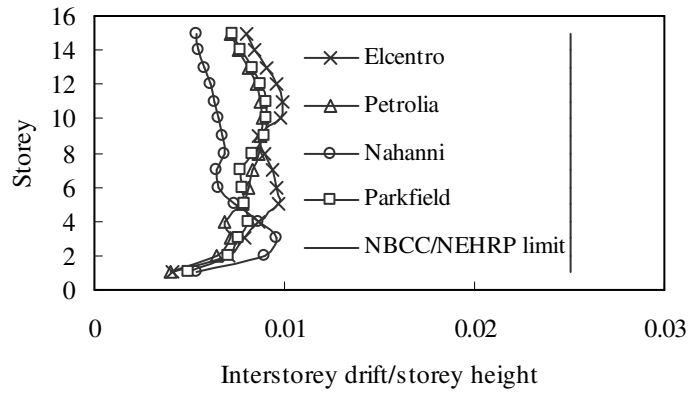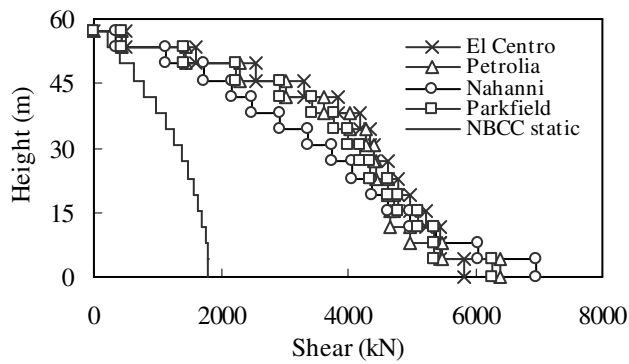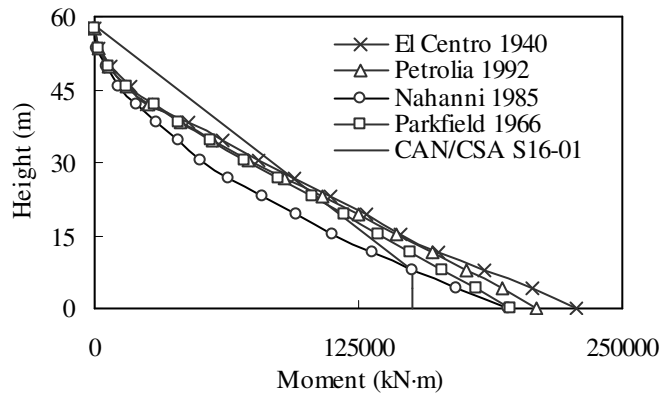
Fig. 4.2. Inelastic response of 15-storey SPSW: (a) peak interstorey drift; (b) peak storey shear forces and (c) peak bending moments

114
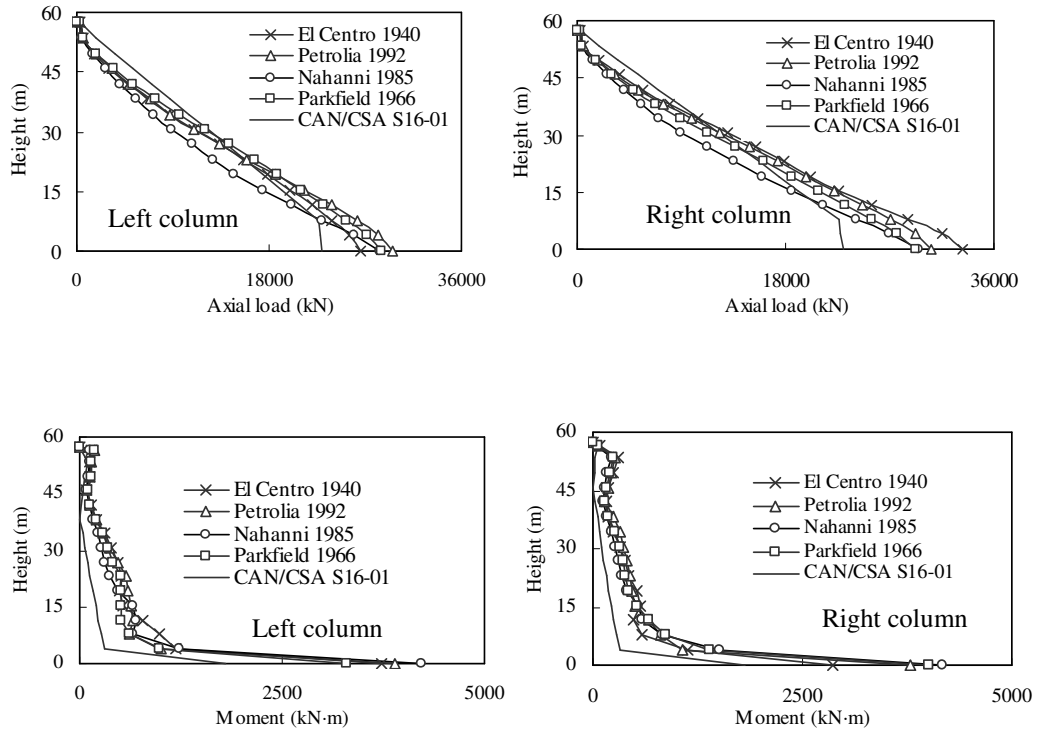
Fig. 4.3 Peak axial forces and bending moments for the left and right columns of the 15 storey SPSW
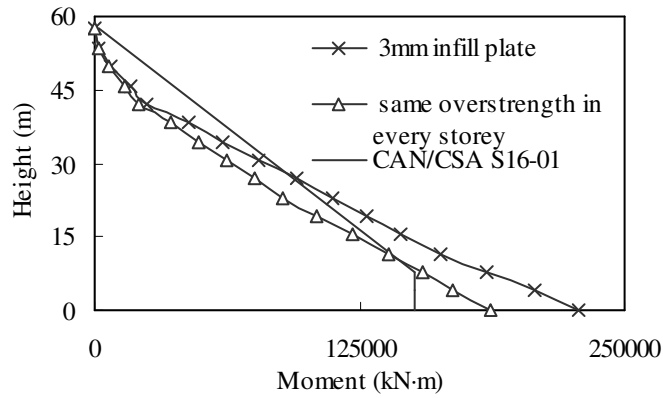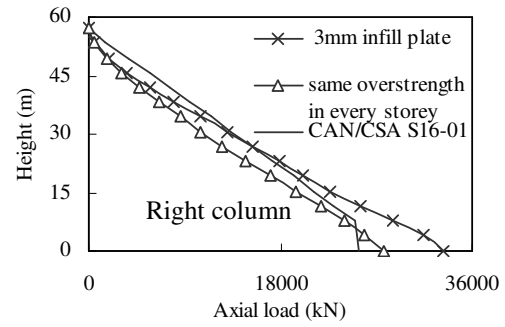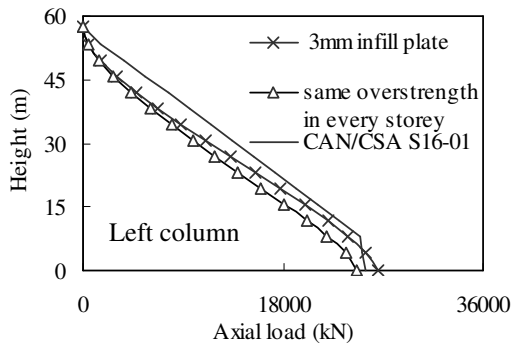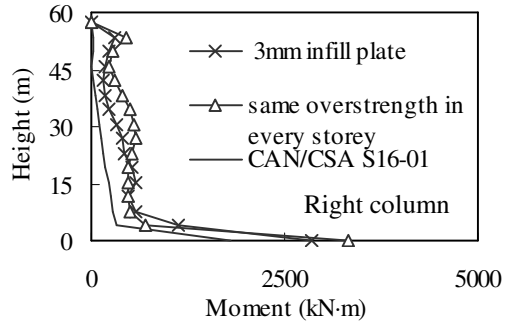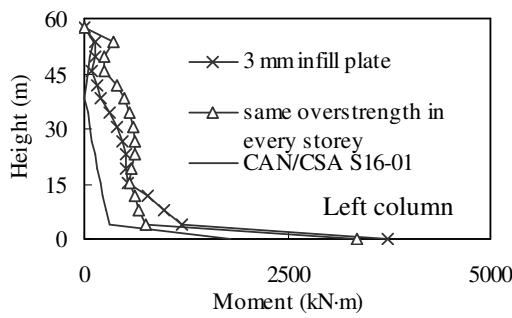
Fig. 4.4 Peak seismic responses of 15-storey SPSW under El Centro earthquake:
(a) bending moments in shear wall; (b) axial forces in columns and (c) bending
moments in column

(a)

(b)

(c)
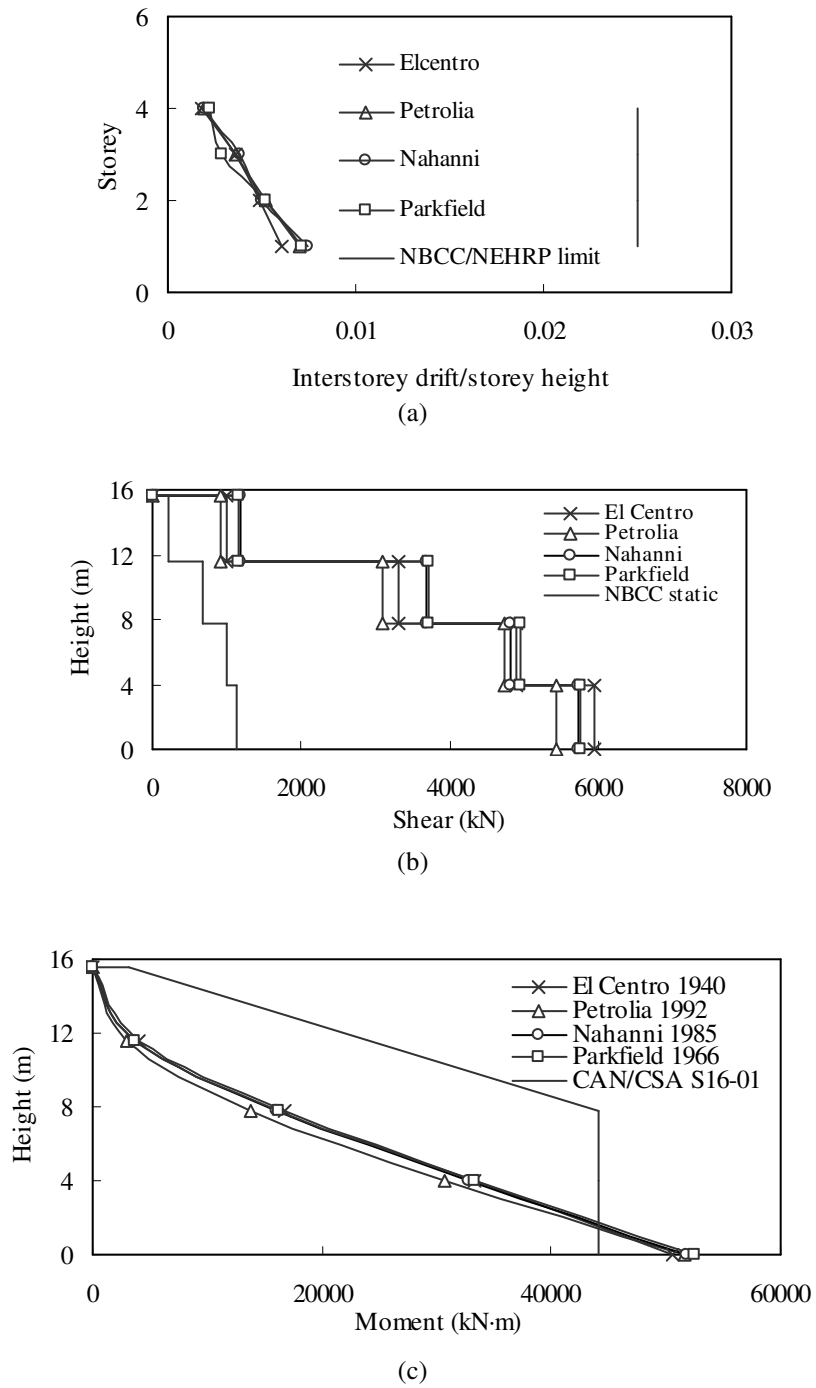
Fig. 4.5 Inelastic response of 4-storey SPSW: (a) peak interstorey drift; (b) peak storey shear forces and (c) peak bending moments

117
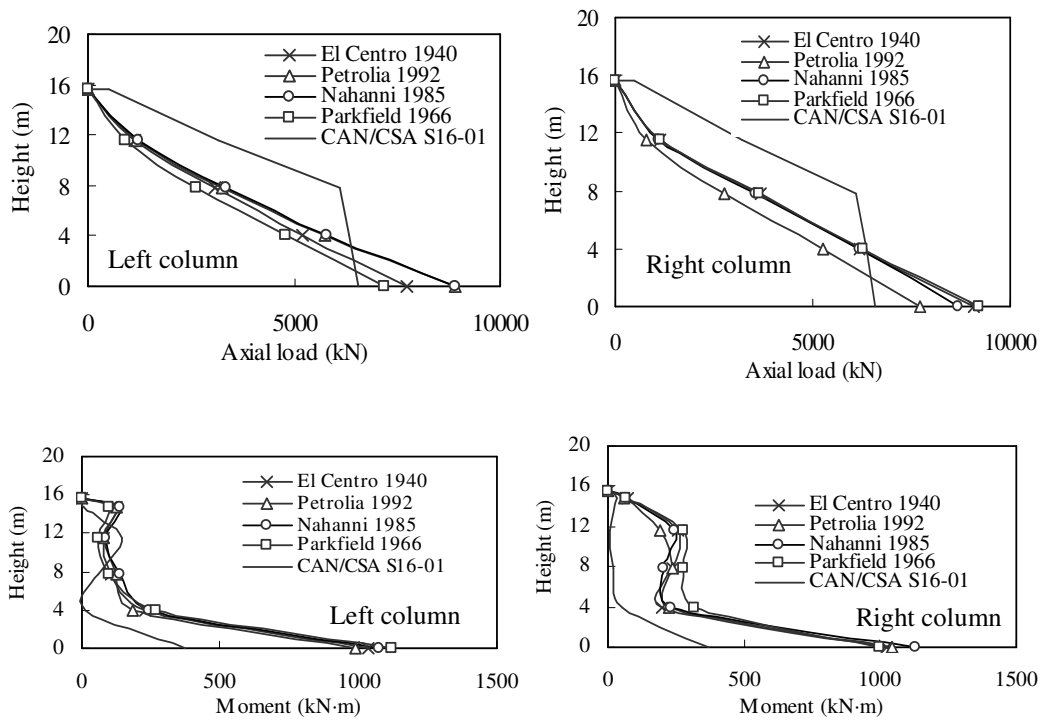
Fig.4.6 Peak axial forces and bending moments for the left and right columns of the 4-storey SPSW
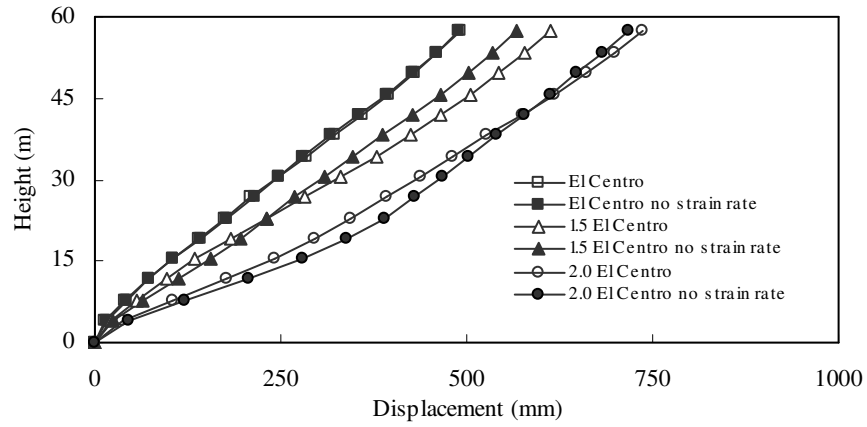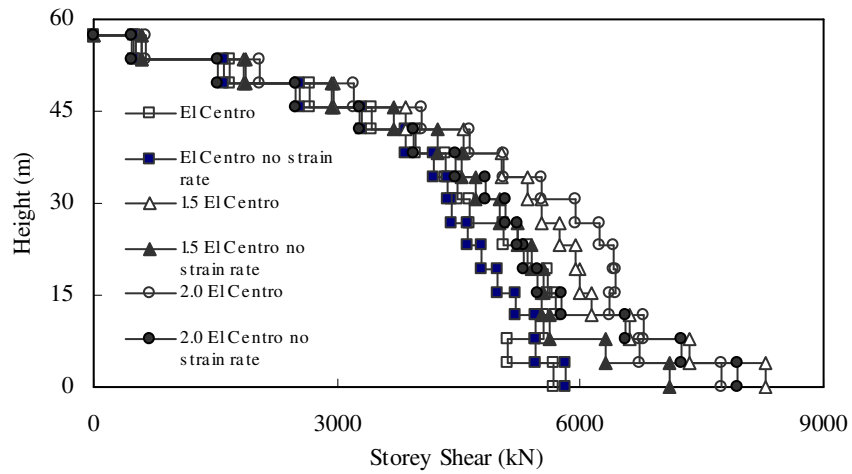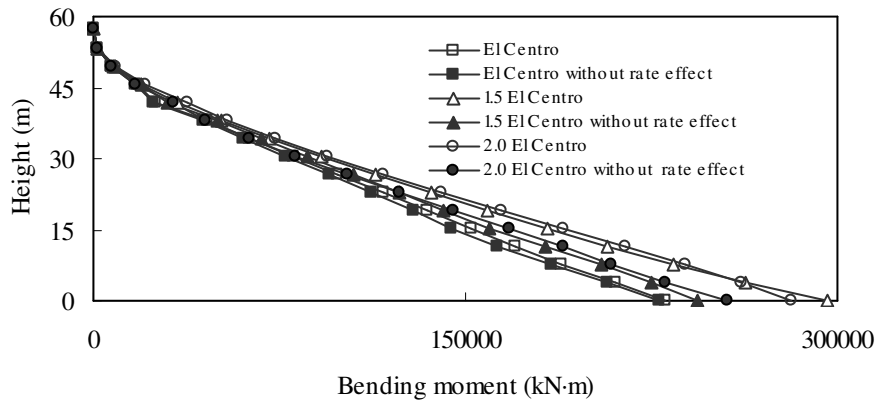
Fig. 4.7 Peak storey (a) displacements; (b) shear forces and (c) bending moments
of 15-storey SPSW (with and without strain rate effects)

119
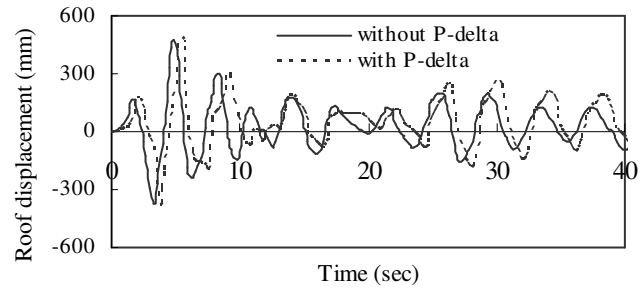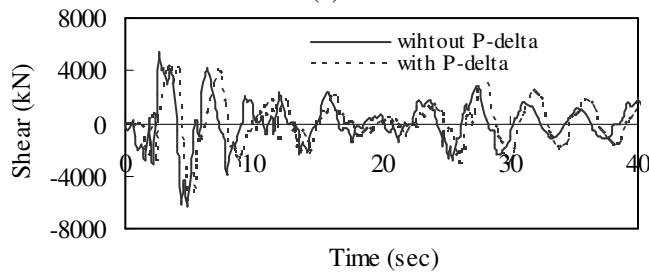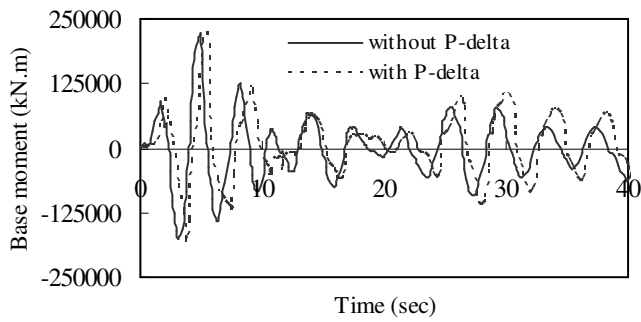
Fig. 4.8 Inelastic seismic response (a) top storey displacement; (b) base shear and (c) base overturning moment for El Centro 1940 earthquake record with and without P-delta effect.

120

References

AISC. 2005. Seismic provisions for structural steel buildings. American Institute of Steel Construction, Chicago, IL.

CSA. 2009. Limit states design of steel structures. CAN/CSA S16-09, Canadian Standards Association, Toronto, ON.

CSA. 2001. Limit states design of steel structures. CAN/CSA S16-01, Canadian Standards Association, Toronto, ON.

Cowper, G.R. and Symonds, P.S. 1957. Strain hardening and strain rate effects in the impact loading of cantilever beams. Brown University Division of Applied Mathematics, Report No. 28.

Dastfan, M. and Driver, R.G. 2008. Flexural stiffness limits for frame members of steel plate shear wall systems. Proc., Annual Stability Conference, Structural Stability Research Council, April 2-5, Nashville, Tennessee, USA.

Driver, R.G., Kulak, G.L., Kennedy, D.J.L., and Elwi, A.E. 1997. Seismic behaviour of steel plate shear walls. Structural Engineering Report No. 215, Department of Civil and Environmental Engineering, University of Alberta, Edmonton, Canada.

Gioncu, V. 2000. Influence of strain-rate on the behaviour of steel members. In behaviour of Steel Structures in Seismic Areas, STESSA 2000 (eds. F.M. Mazzolani, R. Tremblay), Montreal, 21-24 August 2000, Balkema, Rotterdam.

Gupta, A., and Krawinkler, H. 2000. Dynamic P-delta effects for flexible inelastic steel structures. Journal of Structural Engineering, ASCE, 126(1): 145-154.

Hibbitt, Karlsson, and Sorensen. 2007. ABAQUS/Standard User's Manual. Version 6.7, HKS Inc., Pawtucket, RI.

International Code Council (ICC). International building code. International Code Council, Falls Church, Va; 2000.

Kaneko, H. 1997. Influence of strain-rate on yield ratio. In kobe earthquake damage to steel moment connections and suggested improvement. JSSC Technical Report No.39.

Kurobane, Y., Ogawa, K., Ueda, C. 1996. Kobe earthquake damage to high rise Ashiyahama apartment buildings: Brittle tensile failure of box section columns." In Tubular Structures VII (eds I. Farkas and K. Jarmai), Miskolc, 28-30 August 1996, Balkema, Rotterdam, 277-284.

Mahin, A.S., Bertero, V.V., Atalay, M.B., and Rea, C. 1972. Rate of loading effects on uncracked and repaired reinforced concrete members. Report EERC 72-9, University of California, Berkeley.

Manjoine, M.J. 1944. Influence of rate of strain and temperature on yield stress of mild steel. Journal of Applied Mechanics, 11: 211-218.

Montgomery, C.J. 1981. Influence of P-delta effects on seismic design. Canadian Journal of Civil Engineering, 8: 31-43.

Nakamura, K., Mizuno, J., Matsuo, I., Suzuki, A., and Tsubota, H. 1999. Effects of loading rate on reinforced concrete shear walls. Part 1, Dynamic properties of large-size rebars. In Earthquake Resistant Engineering Structures (eds G. Oliveto, C.A. Brebbia), Catania, June 1999, WIT Press, Southampton, 43-52.

Naumoski, N. 2001. Program SYNTH – generation of artificial accelerogram history compatible with a target spectrum. User's manual, Dept. of Civil Engineering, University of Ottawa, Ottawa, ON.

NEHRP (National Earthquake Hazards Reduction Program). 2000. NEHRP recommended provisions for seismic regulations for new buildings and other structures. Building Seismic Safety Council, Washington, D.C. 2 vols., FEMA 368 and 369.

NBCC. 2005. National Building Code of Canada,12th ed, Canadian Commission on Building and Fire Codes, National Research Council of Canada (NRCC), Ottawa, ON, Canada.

Paulay, T. and Priestley, M.J.N. 1992. Seismic design of reinforced concrete and masonry buildings. John Wiley & Sons, Inc., New York, N.Y.

Tremblay, R., Coté, B., and Léger, P. 1999. An evaluation of $P-\Delta$ amplification factors in multi-storey steel moment resisting frames. Canadian Journal of Civil Engineering, 26: 535-548.

Wallace, B.J., and Krawinkler, H. 1989. Small-scale model tests of structural steel assemblies. Journal of Structural Engineering, 115(8): 1999-2015.

5. PROPOSED SEISMIC DESIGN PROCEDURE FOR STEEL PLATE SHEAR WALLS[3]

5.1 General

Seismic design requirements in the current AISC provisions (AISC 2005) and Canadian steel design standard CAN/CSA S16-01 (CSA 2001) specify that steel plate shear walls (SPSWs) be designed under capacity design principles. Capacity design of structures involves pre-selecting a localized ductile fuse (or fuses) to act as the primary location for the dissipation of seismic energy. In SPSWs, it is tension yielding in the infill plates, occurring under the action of the story shear, and plastic hinging at the ends of the beams and bases of the columns that are considered to be the ductile and desirable sources of energy dissipation. Consistent with the principles of capacity design, all other structural elements are protected against actions that could cause failure by providing them with sufficient strength so as to remain essentially elastic. The commentary of the AISC 2005 seismic provisions lists three different capacity design procedures for the design of SPSWs.

This chapter reviews the main published design methods, and a new procedure is proposed for the design of column boundary members of SPSWs, which are the main capacity protected elements in SPSWs. The proposed method first uses the concepts of indirect capacity design principles of CAN/CSA S16-01 to identify the infill plates that would be expected to yield in the design earthquake.

---

[3] A version of this chapter has been submitted for publication in the *Journal of structural engineering*, ASCE

Associated loads from the infill plate tension fields are then applied to the boundary columns, along with vertical shears consistent with plastic hinging of the beams at each story, to determine the design axial loads. Column moments are estimated considering the conditions at each story individually. The proposed method does not require any nonlinear analysis and is simple and efficient to use.

To investigate the performance of the proposed design method, two 4-storey and one 8-storey SPSWs are designed using the proposed method and analyzed for four spectrum-compatible earthquake ground motions for Vancouver, Canada. The resulting seismic loads are compared with the design loads determined by the proposed procedure, as well as by other capacity design procedures.

5.2 Current design methods of steel plate shear walls

Both the AISC Seismic Provisions (AISC 2005) and CAN/CSA S16-01 (CSA 2001) enforce the capacity design approach for SPSWs under earthquake loading. AISC 2005 recognizes three different analytical procedures to achieve capacity design of the columns and beams. These are: nonlinear pushover analysis; indirect capacity design approach, adopted from CAN/CSA S16-01; and combined linear elastic computer programs and capacity design concepts. Berman and Bruneau (2008) proposed another capacity design method for the design of boundary columns. Each of these methods is reviewed briefly here.

5.2.1 Nonlinear pushover analysis

Nonlinear pushover analysis has been widely used as a tool for the seismic design of boundary members of SPSWs. In the pushover analysis, infill plates are assigned a yield strength of $R_y F_y$, where R_y is the ratio of expected-to-nominal yield strength and F_y is the nominal yield strength. The analysis is conducted for a target displacement, generally at the top storey, and axial forces, shears and moments in the framing members are determined. However, as a design tool nonlinear static analysis is very time consuming, as several iterations may be needed to obtain the final member sizes. Nonlinear pushover analysis will not be considered in this chapter.

5.2.2 Indirect Capacity Design (ICD) Approach

CAN/CSA S16-01 indicates that the loads in the vertical boundary members of a SPSW can be determined from the gravity loads, combined with the seismic loads increased by the capacity design amplification factor

$$B = \frac{V_{re}}{V_u} \tag{5.1}$$

where V_{re} is the probable base shear resistance and V_u is the factored seismic design base shear. The probable base shear resistance of a SPSW (V_{re}) is given by

$$V_{re} = 0.5 R_y F_y w L \sin 2\alpha \tag{5.2}$$

where R_y is specified as 1.1 in CAN/CSA S16-01, w is the infill plate thickness, L is the bay width between column centerlines, and α is the angle from the vertical of the tension field developed in the infill plate.

Axial forces in the boundary columns are determined from the overturning moments defined as follows:

(1) The moment at the base is BM_u, where M_u is the factored seismic base overturning moment corresponding to the force V_u;

(2) The moment BM_u extends from the base to a height H, equal to the bay width, L, but not less than two stories; and

(3) The moment decreases linearly above height H to B times the overturning moment at one storey below the top of the wall, but need not exceed R_d times the factored seismic overturning moment corresponding to the force V_u at any storey under consideration, where R_d is the ductility-related force modification factor.

The local column moments due to tension field action in the infill plates are multiplied by the amplification factor B. CAN/CSA S16-01 also provides the following equation to ensure that the columns in SPSWs are sufficiently stiff to develop an essentially uniform tension field in the adjacent infill plate

$$\omega_h = 0.7h \sqrt[4]{\frac{w}{2LI_c}} \qquad (5.3)$$

where I_c is the column moment of inertia, h is the storey height, and ω_h is the column flexibility parameter that may not exceed 2.5.

An evaluation of the CAN/CSA S16-01 approach has been presented previously by Bhowmick et al. (2009). It was observed that it underestimates the design loads for boundary columns, potentially by a large margin. This is principally

because a significant portion of the strength of the surrounding frame is neglected. In SPSWs – especially tall SPSWs – columns at the lower stories contribute a larger portion of total shear strength, and neglecting the shear contribution of the columns in the determination of B results in an underestimation of the boundary column design loads.

5.2.3 Combined Linear Elastic Computer Programs and Capacity Design Concepts (LE+CD)

In this method, the boundary columns are designed for the maximum capacity of the infill plates in combination with the maximum possible axial load due to overturning moment. The axial load in a column at any storey considers the expected strength of the connecting infill plate at that level plus the axial force from the overturning moment multiplied by an overstrength factor, Ω_o. In this procedure, forces equal to the expected yield strength of the infill plates are applied to the boundary framing members in the direction of the tension field, α.

5.2.4 Capacity Design Method by Berman and Bruneau (2008)

Berman and Bruneau (2008) recently proposed a capacity design method for columns of SPSWs. In their method, a uniform plastic collapse mechanism is assumed based on yielding in all infill plates and the development of plastic hinges at the ends of all beams. The loads, including distributed forces from yielding of the infill plates, moments from plastic hinging in the beams, axial forces from the beams, and the applied seismic loads, are applied in a linear model to determine the design load effects in the columns. For expediency, the capacity design method proposed by Berman and Bruneau (2008) is termed the

"CD-BB" method here. Some of the concepts of this method for determining column axial loads are explained in the next section and are adopted into the proposed method. The method of Berman and Bruneau (2008) has been shown to provide a reasonable estimate of column design loads for short SPSWs. However, the method is likely to be overly conservative for mid- to high-rise SPSWs where simultaneous yielding of all the infill plates over the entire wall height is unlikely. For taller SPSWs, thus, it has been suggested (Berman and Bruneau 2008) that the column axial loads obtained from this procedure be reduced following a procedure similar to that proposed by Redwood and Channagiri (1991) for concentrically braced frames, although its application to SPSWs was not discussed further. Incorporating this modification to reduce axial loads, the procedure is called the "MCD-BB" method herein.

5.3 Proposed method for design of boundary members of steel plate shear wall

Any of the methods described above can be used for the design of boundary members of SPSWs; however, all of the methods have limitations, as will be discussed subsequently. Another important consideration of all the current capacity design methods is the top storey beam, which is designed for full yielding of the top storey infill plate, usually requiring a very stiff member. Seismic analyses of SPSWs have shown that the top storey infill plate typically does not experience yielding, especially when the thickness of the top storey infill plate is limited by the use of a minimum practical infill plate thickness based on

129

considerations related to handling and welding. Thus, in addition to a change in the selection criterion for the top storey beam, a reasonably accurate and relatively efficient method for the design of columns of SPSWs under seismic forces is proposed. This method requires a linear analysis only and can be summarized as follows:

(1) Make the initial assumption that 25% of the total design base shear will be resisted by the columns. This assumption is based on experience from seismic analyses of many multi-storey SPSWs, and it is verified or adjusted in the second design iteration. The capacity design amplification factor, B, currently defined in the indirect capacity design provisions of AISC 2005 and CAN/CSA S16-01 as Eq. (5.1), is thus redefined as B_b for the SPSW base as

$$B_b = \frac{V_{re}}{0.75V_u} \tag{5.4}$$

(2) For every storey above the first, amplification factors are calculated assuming that the storey shear will be resisted by the infill plate alone. Therefore, for any storey i, the amplification factor is

$$B_i = \frac{V_{re,i}}{V_{u,i}} \tag{5.5}$$

where $V_{re,i}$ is the probable shear resistance at storey i, and $V_{u,i}$ is the factored lateral seismic design shear at storey i.

At any storey, if $B_i < B_b$, the infill plate is taken as being fully yielded. Considering the storey shear to be carried by the infill plate alone in the calculation of B_i is conservative because in any case the boundary columns will carry some shear, and the calculated value of B_i will therefore always be smaller than the actual value.

(3) The orthogonal distributed load components (x- and y-directions) from the infill plate tension field at storey i to be applied to the adjacent columns $(\omega_{xci}$ and $\omega_{yci})$ and beams $((\omega_{xbi}$ and $\omega_{ybi})$ or $(\omega_{xbi-1}$ and $\omega_{ybi-1}))$ can be obtained by resolving the infill plate tensile forces that act at an angle α from the vertical. (Beam i is the beam at the top of storey i). At any storey i, when the infill plate, with thickness w, is fully yielded, these distributed loads are

$$\left(\omega_{xci}\right)_{yield} = R_y F_y w \left(\sin\alpha\right)^2 \tag{5.6}$$

$$\left(\omega_{yci}\right)_{yield} = 0.5 R_y F_y w \sin2\alpha \tag{5.7}$$

$$\left(\omega_{xbi}\right)_{yield} = \left(\omega_{xbi-1}\right)_{yield} = 0.5 R_y F_y w \sin2\alpha \tag{5.8}$$

$$\left(\omega_{ybi}\right)_{yield} = \left(\omega_{ybi-1}\right)_{yield} = R_y F_y w \left(\cos\alpha\right)^2 \tag{5.9}$$

A value of 45° can be used as an initial value for α. At any storey where the infill plate is expected to remain elastic, or yield only partially, the distributed forces from that infill plate on the surrounding boundary members are estimated by applying a multiplication factor $\dfrac{B_b}{B_i}$, which is less than 1.0, to Eqs. (5.6) to (5.9).

(4) For determining the axial forces and moments in the columns, beam sections must be selected first. These members are selected to resist both factored gravity and lateral forces. The beam at any storey i is designed for transverse distributed forces obtained from the difference in the vertical tension field force components developed in the infill plates at stories i and $i+1$ of $\omega_{bi} = \left(\omega_{ybi} - \omega_{ybi+1} \right)$. The distributed forces are then combined with the gravity loads with the use of appropriate load factors.

(5) Axial forces in the beams can be estimated in a similar way to that proposed by Berman and Bruneau (2008). These forces originate from two sources: the first is due to the inward force applied to the columns by the infill plate, $P_{b(col)}$, and the second is from the difference in the effects of the infill plates above and below, $P_{b(plate)}$. Thus, the axial force in the beam is

$$P_b = P_{b(col)} \pm P_{b(plate)} \tag{5.10}$$

The axial forces at the ends of the beam at storey i are

$$P_{bi} = \left(\omega_{xci} \frac{h_i}{2} + \omega_{xci+1} \frac{h_{i+1}}{2} \right) \pm \left(\omega_{xbi} - \omega_{xbi+1} \right) \frac{L}{2} \tag{5.11}$$

The two components of the axial forces in the beams are additive at the end where the boundary column is in tension.

(6) All the beams are assumed to form plastic hinges at their ends. As noted earlier, in current practice the top beam is designed assuming full tensile yielding of the top storey infill plate. In the proposed method, however, if the top storey infill plate is not expected to yield, the beam is designed for

the distributed loads obtained from an elastic or partially yielded tension field developed at the top storey, resulting in a lighter beam. Although this is apparently inconsistent with capacity design principles, the forces developed in the uppermost infill plate are self-limiting due to the inelastic deformations that would occur in the top beam in the event of an overload. Moreover, except in the shortest SPSWs, the behaviour of the top panel is not greatly influential on the system performance.

(7) Using the design forces determined through the application of steps 1 through 6, axial forces in the columns can be obtained from a free body diagram such as that shown in Fig. 5.1 for a typical right column of a SPSW, when the lateral loads act from left to right on the SPSW. The distributed loads shown in the free body diagram are those from the tension fields developed in the infill plates and are obtained in step (3). The concentrated horizontal forces are those from the beams and are determined in step (5). The applied moments are from plastic hinging in the beams in the presence of the axial forces determined using Eq. (5.11). The reduced plastic moment capacity at the ends of beam i, M_{pi}, can be approximated as (Bruneau et al. 1998)

$$M_{pi} = 1.18 Z_{xi} F_{yb} \left(1 - \frac{P_{bi}}{A_{bi} F_{yb}} \right) \leq Z_{xi} F_{yb} \tag{5.12}$$

where Z_{xi} is the beam plastic section modulus, A_{bi} is the beam cross-sectional area, and F_{yb} is the beam yield strength.

133

Using the reduced plastic moment capacities, the shear forces at the ends of beam i, V_{bi}, can be obtained as

$$V_{bi} = \frac{\sum M_{pi}}{L} \pm (\omega_{ybi} - \omega_{ybi+1}) \frac{L}{2} \tag{5.13}$$

where $\sum M_{pi}$ is the summation of the reduced plastic moment capacities at opposite ends of beam i.

(8) A simple approach to estimate column moments in every storey is presented in AISC Design Guide 20 (Sabelli and Bruneau 2007). Column moments are estimated storey by storey, assuming fixed ends at each floor. In every storey, column moments, M_{col}, are calculated as the sum of those arising from infill-plate tension and those from plastic hinging of the beam, as follows

$$M_{col,i} = M_{plate,i} + MAX(M_{beam,i}; M_{beam,i-1}) \tag{5.14}$$

Although the two moment components oppose each other at one end of the column in a storey and are additive at the other, the summation is conservative. For a column assumed to be fixed against rotation at each end, the moment from the infill plate tension forces is

$$M_{plate,i} = \frac{\omega_{xci} h_i^2}{12} \tag{5.15}$$

where ω_{xci} is calculated in step (3), and for the case where the infill plate is fully yielded, $\omega_{xci} = (\omega_{xci})_{yield}$. For the moment due to plastic hinging in the beam, $M_{beam,i}$ or $M_{beam,i-1}$, one-half of the reduced plastic moment of the beam can be applied to each column segment connected to that beam

(i.e., above and below). Thus, at any storey i, the moment from beam plastic hinging is the greater of $0.5M_{pi}$ and $0.5M_{pi-1}$ (except at the top of the wall, where the full beam moment would be used). In this approach, beam plastic hinges are assumed to form at the centerlines of the columns, which is not the actual case. Plastic hinges typically form about $d_b/2$ from the column face, where d_b is the depth of the beam. The additional moment could easily be calculated, as is done for moment-resisting frames, but it is not included here for simplicity and also because the increase is generally small in comparison to the moments from the infill plate forces and beam plastic hinging.

Plastic hinges generally do not form at the ends of the beam at the base, if present, due to the need for a heavy member there to anchor the tension field in the lowest storey. A simple approximation can be used for determining the column moment at the lowest storey, as follows

$$M_{col,base} = MAX\left(M_{col,1} \; ; \frac{\left(\omega_{yb}\right)_{yield} L^2}{12} \right) \le M_{p,base} \qquad (5.16)$$

where $\left(\omega_{yb}\right)_{yield}$ is the vertical component of the distributed load at the bottom beam coming from yielding in the bottom storey infill plate, $M_{col,1}$ is taken as the column moment at the top of the lowest storey determined using Eq. (5.14), and $M_{p,base}$ is the moment due to plastic hinging in the bottom beam.

(9) With the first trial design, an elastic analysis of the SPSW is carried out under the code-specified seismic loads. Displacements in every storey are estimated to check the P-Δ effects. The stability factor approach specified in either the commentary of the National Building Code of Canada (NRCC 2005) or in the seismic design provisions of the National Earthquake Hazards Reduction Program (NEHRP 2000) can be used to account for the P-Δ effect in the design, although for SPSWs this effect is often relatively small (Bhowmick et al. 2009).

(10) From the elastic analysis, the contribution of the boundary columns in resisting the base shear is estimated and verified against the value of 25% assumed in step (1). A new amplification factor, $B_{b,n}$, is estimated with the revised fraction of the shear contribution, β, by the infill plate at the base as follows

$$B_{b,n} = \frac{0.5 R_y F_y w L_{cf} \sin 2\alpha}{\beta V_u} \tag{5.17}$$

where L_{cf} is the clear horizontal length of the infill plate between the columns. If $B_{b,n}$ is much lower (greater than 10%) than B_b, assumed in step (1), due to a smaller shear contribution from the boundary columns than assumed, and the maximum stability factor, $\theta_{x,\max}$, calculated in the first trial design, is smaller than 0.1, the value of B_b can be revised to $B_{b,n}$, which may lead to more economical columns. If $B_{b,n}$ is lower than B_b but $\theta_{x,\max}$ is greater than 0.1, it is recommended that the amplification

136

factor not be revised to a value lower than B_b. This is because the use of B_b to select column sections in step (1) resulted in a stiffer SPSW, and thus lowered the values of the stability factors calculated to account for P-Δ effects. Instead, the column forces at each storey are to be multiplied by $(1+\theta_x)$ to allow for P-Δ effects. If $B_{b,n}$ is higher than B_b, as the shear contributions from the columns selected are higher than assumed (i.e., greater than 25%), a second trial is needed. It is possible that a third trial will be needed, but typically only one or two trials are required for a complete design.

5.4 Illustrative design example

Two 4-storey and one 8-storey buildings are used to evaluate the efficiency of the proposed design method. The hypothetical symmetrical office buildings are assumed to be located in Vancouver, Canada and have a plan area of 2014 m^2. As shown in Fig. 5.2, the buildings have two identical SPSWs provided to resist lateral forces in the direction under consideration. For simplicity, each shear wall is assumed to resist one-half of the design seismic loads. Each shear wall is 7.6 m wide, measured from center to center of columns, and has a panel aspect ratio of 2.0 (storey height of 3.8 m). The buildings are assumed to contain foundations built on rock. A dead load of 4.26 kPa is used for each floor and 1.12 kPa for the roof. The live load on all floors is taken as 2.4 kPa. Design seismic loads in every storey were calculated using the equivalent lateral load approach specified in the NBCC 2005. An importance factor, I, of 1.0 is used in the design. As prescribed

by NBCC 2005 for ductile SPSWs, a ductility-related force modification factor, R_d, of 5.0 and an overstrength force modification factor, R_o, of 1.6 are used in the design. Although Canadian design provisions have been used, the conclusions based on this illustrative example are considered to be general and apply equally to their U.S. counterparts.

For the two 4-storey SPSWs, cases of constant and variable infill plate thickness over the height of the walls were considered. For the cases of the constant infill plate thickness (4-storey SPSWCT and 8-storey SPSW), 3.0 mm was used in all stories. For the 4-storey SPSW with variable thickness (4-storey SPSWVT), values of 3.0, 2.75, 2.0 and 1.0 mm (bottom to top) were used. Intermediate beam sections were selected following steps (4) and (5) of the proposed approach. For all three SPSWs, a beam section of W760X582 was selected to resist tensile forces from infill plate yielding at the base. The nominal yield strength of the beams, columns and infill plates was assumed to be 350 MPa and all steel was assigned a modulus of elasticity of 200 000 MPa.

Table 5.1 presents the calculated seismic forces, F, and shears, V, in every storey of the 4-storey and 8-storey SPSWs. The preliminary selection of beams and columns was based on the design loads obtained after the first iteration of the proposed method with an assumed tension field angle of 45°. Once preliminary sections for beams and columns were selected, the magnitudes of the tension field angles α in every storey were calculated using the associated equation given in

138

AISC 2005 and CAN/CSA S16-01. Described below are the steps for a second iteration (of the proposed procedure) for designing the 4-storey SPSWCT:

(1) The base shear of the 4-storey SPSWCT was found to be 1150 kN (Table 5.1). Using Eq. (5.2), the probable shear resistance, V_{re}, at the base of the 4-storey SPSWCT is obtained as 4362 kN. Using Eq. (5.4), the amplification factor at the first storey, B_b, was estimated to be 5.06.

(2) Considering the total storey shear in every upper storey $(i = 2 \cdots n)$ to be taken by the infill plates only, the amplification factors in each storey were determined and are presented in Table 5.2. It is observed that the amplification factor of the second storey is lower than B_b. Thus, according to the proposed approach only the first two stories are likely to be fully yielded for an earthquake in Vancouver. The distributed forces, obtained from infill plate tension forces as explained in step (3), to be applied at the beams and columns are also presented in Table 5.2.

(3) Beam sections selected for the 4-storey SPSWs are presented in Table 5.3. Axial forces for beams of the 4-storey SPSWCT were calculated using Eq. (5.11) and are presented in Table 5.4. (For the selected example, the lateral seismic loads are assumed to be acting from left to right on the SPSWs.) In Table 5.4, P_{bL} and P_{bR} represent the axial forces in the beams at the left and right ends, respectively. In the case of the SPSW with constant plate thickness, the net distributed forces on the beams (except at the base of the wall and the top storey) from the infill plates are very small, as the tension forces above and below any intermediate beam

cancel. Additionally, the beams must resist the gravity loads. The beam sections selected satisfy the beam-column requirements of CAN/CSA S16-01. Reduced plastic moments for selected beam sections were calculated using Eq. (5.12). Using reduced plastic moments in the beams, shear forces at the left and right ends of beams were calculated using Eq. (5.13). Table 5.4 presents reduced plastic moments and shear forces at the left and right ends of all beams for the 4-storey SPSWCT.

(4) Since the lateral loads are acting from left to right on the SPSWs, the right column is critical for design. Axial forces in the right column in every storey can be calculated using a free body diagram, as presented generically in Fig. 5.1. The force components of such a free body diagram for the 4-storey SPSWCT are presented in Tables 5.2 and 5.4.

(5) Column design moments in every storey were calculated following the procedure stated in step (8) of the proposed design method. Unlike the CD-BB approach (Berman and Bruneau 2008), where the bottom storey column is designed for a moment equal to the reduced plastic moment of the beam at the base, the column moment at the lower storey was estimated using Eq. (5.16). Design axial forces and moments of the columns of the 4-storey SPSWCT are presented in Table 5.5.

(5) The final beam and column sections selected for the 4-storey SPSWCT are presented in Table 5.3. An elastic analysis was carried out for the seismic loads specified in Table 5.1. From the elastic analysis, it was observed that about 21% of the total base shear was resisted by the boundary columns.

As explained at step (10) of the proposed procedure, the new amplification factor, $B_{b,n}$, was estimated as 4.55, which is 10% lower than B_b estimated at the first step. Thus, no adjustment to B_b is needed, nor is a second design cycle.

Following the same procedure, the other two SPSWs were designed. The final column and beam sections selected for the 4-storey SPSWVT and 8-storey SPSW are presented in Tables 5.3 and 5.6, respectively.

5.5 Seismic responses of shear walls designed with proposed method

A total of four diverse seismic records were chosen for the time history response analyses. These are: (1) N-S component of the El Centro earthquake of 1940; (2) Petrolia station record from the 1992 Cape Mendocino earthquake; (3) Nahanni, Canada 1985 earthquake record; and (4) Parkfield 1966 earthquake record. The seismic records were modified using the software SYNTH (Naumoski 2001) to make them spectrum compatible for Vancouver, Canada. Nonlinear time step dynamic analyses of the three SPSWs were performed using ABAQUS (Hibbitt et al. 2007). In the finite element model, beams, columns, and infill plates were modeled using general purpose four-node doubly-curved shell elements with reduced integration (ABAQUS element S4R). The finite element model includes one SPSW and a gravity "dummy" column carrying the vertical loads supported by all the tributary leaning columns combined. The gravity column is made of bar elements and connected with the SPSW at every storey with pin-ended rigid links. The gravity column was designed so as not to provide any lateral stiffness to the

system, and it carried half of the total mass at each floor. In the finite element analyses, the storey gravity loads were represented as lumped masses on the columns at every floor. Floor slabs were considered rigid. A damping ratio of 5% in Rayleigh proportional damping was selected for all the seismic analyses. For simplicity, an elasto-plastic stress versus strain relation was adopted.

Table 5.7 presents the peak seismic force effects at the column bases of the 4-storey SPSWCT and SPSWVT computed from the nonlinear time history analyses. Fig. 5.3 presents the envelopes of peak column axial forces and peak column moments (which do not necessarily occur simultaneously) obtained from the inelastic time history analyses of the 4-storey SPSWCT. (Note that the maximum axial forces and moments presented in all tables and figures are absolute values.) Fig. 5.3(a) shows that for all ground motions, the axial forces in every storey are lower than the design axial forces obtained from the proposed approach. The maximum column axial force developed at the base of the 4-storey SPSWCT from the time history analyses, 9100 kN for the Parkfield earthquake record, is 14.2% lower than the design axial force determined by the proposed method of 10 600 kN. Fig. 5.3(b) shows that the peak seismic demand for flexure at the base of the columns, 1710 kN·m for the Nahanni earthquake record, is about 44.6% lower than the design moment determined by the proposed method of 3090 kN·m. Also, for the upper stories the design column moments are significantly higher than the column moments developed during the earthquakes. This occurs because of the assumption made in the proposed approach that plastic

hinges form at the ends of all beams. Plastic hinges at the ends of the beams were not observed to form during the seismic analyses of the 4-storey SPSWCT. Thus, proposed design column moments were found to be conservative, as expected.

Fig. 5.4 presents the envelope of peak column axial forces and peak column moments obtained from the inelastic time history analyses of the 4-storey SPSWVT. Like the 4-storey SPSWCT, Fig. 5.4(a) shows that for all ground motions, the peak axial forces in every storey are lower than the design axial forces obtained from the proposed approach. The maximum column axial force developed at the base of the 4-storey SPSWVT from the time history analyses, 8780 kN, is 20.9% lower than the design axial force determined by the proposed method of 11 100 kN. Fig. 5.4(b) shows that the peak dynamic moment at the base of the column of the 4-storey SPSWVT, 1730 kN·m, is 41.6% lower than the design moment at the base determined by the proposed method. For the same reason specified for the 4-storey SPSWCT, the design column moments in the upper stories are significantly higher than the column moments developed under the spectrum compatible earthquake records.

Table 5.8 presents peak seismic force effects at the column bases of the 8-storey SPSW obtained from nonlinear time history analyses. The resulting distributions of peak column axial forces and peak column moments are presented in Fig. 5.5. Fig. 5.5(a) shows that the axial force demands in every storey are lower than the design axial forces obtained from the proposed approach. The maximum column

axial force developed at the base of the 8-storey SPSW from the time history analyses, 16 420 kN, is 14.7% lower than the design axial force determined by the proposed method of 19 250 kN. Fig. 5.5(b) shows that the peak seismic demand for moments at the base of the columns, 2340 kN·m, is 24.5% lower than the design moment determined by the proposed method of 3100 kN·m. Again, the design column moments in the upper stories are significantly higher than those developed during the earthquakes due to the assumption of beam hinging in all stories.

Seismic analyses of all three SPSWs show that the maximum design axial forces are always slightly overestimated using the proposed approach. Also, the column moments (especially in the upper stories) are higher than the moments developed during the selected earthquakes, as discussed previously. The assumption of beam hinging will always overestimate the beam shear forces (if plastic hinges do not form at the ends of the beam) and thereby result in higher axial forces in the columns.

5.6 Comparison with other capacity design procedures

Column design forces were estimated using various currently-available capacity design methods. Figs. 5.6 to 5.8 compare column axial forces and moments from the five different procedures introduced previously (i.e., ICD, LE+CD, CD-BB, MCD-BB, and the proposed procedure) with those from nonlinear seismic analysis (average values) for all three SPSWs. Methods LE+CD, CD-BB, and MCD-BB assume yielding of the infill plates in every storey. Thus, in these

144

methods the top storey beam was designed to anchor the tension field yield forces developed at the top storey infill plate. In the case of both the 4-storey SPSWCT and the 8-storey SPSW, the top storey infill plate is 3.0 mm thick, and a beam section of W760X582 was required for the top storey. For the 4-storey SPSWVT, where the infill plate at the top storey is only 1.0 mm thick, a beam section of W530×150 was selected.

It is observed from Figs. 5.6 to 5.8 that the ICD method underestimates the column moments, as compared to the seismic analysis, in all three SPSWs. Moreover, it underestimates axial forces at the bases of the walls typically by a substantial margin. As explained earlier, this is because the amplification factor used in the ICD method to estimate axial forces and column moments does not include the contribution of the boundary columns to the storey shear capacity. Also, the amplification factor in each storey is based on the bottom storey infill plate only.

The LE+CD method generally underestimates the design column axial force in the bottom stories in all SPSWs. This is mainly because the axial load at any storey does not include the load contributions from possible yielding in the upper stories. To calculate the column moments in the LE+CD method, distributed loads from infill plate yielding are applied to the surrounding moment resisting frames. A linear analysis of this frame will give the moments in the columns in every

storey. Figs. 5.6 to 5.8 show that the column moments are significantly overestimated by the LE+CD method.

Fig. 5.6(a) shows that for the 4-storey SPSWCT, the design column axial forces are generally overestimated by both the CD-BB and MCD-BB methods. The difference between these methods is only in the determination of axial forces in the columns; thus, in Fig. 5.6(b) column moments determined by the MCD-BB method are not presented. Fig. 5.6(b) shows that column moments are overestimated using this method because a stiffer beam was used at the top storey and plastic hinges were assumed to form at the ends of all beams, including the beam at the base. It was observed from seismic analyses that no plastic hinging occurred at the ends of the bottom beam. Figs. 5.6(a) and 5.6(b) indicate that among all the capacity design methods, the proposed approach provides the best and most consistent estimates of the design column axial forces and moments, while remaining on the conservative side. Moreover, it was observed from seismic analyses that only the bottom two infill plates of the 4-storey SPSWCT experienced yielding, as predicted by the proposed approach.

Fig. 5.7(a) indicates that for the 4-storey SPSWVT, both the CD-BB and proposed methods estimate the column axial forces reasonably well. The CD-BB method agrees well with the proposed method because, as predicted by the proposed approach, most of the infill plates (i.e., bottom three infill plates) of the 4-storey SPSWVT experience yielding during seismic analysis. The MCD-BB

method reasonably estimates the column axial forces in every storey. Fig. 5.7(b) also shows that the CD-BB (or MCD-BB) method greatly overestimates the column moments in most of the stories, except at the third storey where the column moment is underestimated by about 76%. The design column moments from the proposed method are somewhat greater than those from the seismic analysis. Also, in this case, as predicted by the proposed approach, no plastic hinges formed at the ends of the bottom beam.

Fig. 5.8(a) shows that for the 8-storey SPSW, the MCD-BB method slightly underestimates the design column axial load in the first storey. The CD-BB method significantly overestimates the column axial forces in every storey, as only the bottom four infill plates of the 8-storey SPSW yielded fully (as predicted by the proposed approach) during the seismic analysis. Design column moments are largely overestimated in most of the stories (with the exception of an underestimation of 3.6% at the second storey) by the CD-BB method, as shown in Fig. 5.8(b). Also, plastic hinges were not observed to form at the ends of the bottom beam as assumed by this method. It is observed from Fig. 5.8 that the design column axial loads and moments obtained from the proposed approach agree well with those from the seismic analysis, while remaining on the conservative side.

5.7 Conclusions

A procedure for determining design forces for the boundary members of SPSWs is presented. One of the distinguishing features of this method is that it identifies the infill plates that are expected to yield during design-level earthquakes. Two 4-storey and one 8-storey SPSWs were designed according to the proposed approach. Design column moments and axial forces from the proposed procedure are shown to agree well with the results from four distinct nonlinear seismic analyses of the three SPSWs, while providing slightly conservative results. Other available capacity design methods presented in the literature are also evaluated. In general, the ICD method underestimates both the design column axial loads at the base of the SPSW and the column moments. The LE+CD method usually overestimates the design column moments by a substantial margin and underestimates the column axial forces. The recently-proposed CD-BB method is found to be generally overly conservative in estimating design moments for columns, although for the 4-storey SPSWVT and 8-storey SPSW cases the column design moment at one storey is underestimated. In general, the CD-BB method was observed to overestimate the design axial loads in columns. Good results are achieved, however, when no minimum plate thickness was specified for handling and welding considerations (4-storey SPSWVT), making the panels much more likely to yield under the seismic analyses. Results also indicate that the MCD-BB method (with modifications to the CD-BB method to reduce design axial load as the number of stories increases) may underestimate the design axial loads in the lower stories. Of all the design methods examined in this research, the

proposed method is the one that predicts the column axial forces and bending moments most reliably and consistently in the cases considered.

Table 5.1 Seismic loads for SPSWs

	8-storey SPSW			4-storey SPSW	
Storey	F (kN)	V (kN)		F (kN)	V (kN)
1	54	1650		155	1150
2	107	1596		311	994
3	161	1489		466	683
4	214	1328		217	217
5	268	1114			
6	321	846			
7	375	525			
8	150	150			

Table 5.2 Distributed forces developed from infill plates for 4-storey SPSWCT

Storey	α (degree)	B	Forces from yielding infill plates (kN/m)			Forces developed from infill plates (kN/m)		
			ω_{yc}, ω_{xb}	ω_{xc}	ω_{yb}	ω_{yc}, ω_{xb}	ω_{xc}	ω_{yb}
1	41.8	5.06	574.0	513.7	641.3	574.0	513.7	641.3
2	41.8	4.4	574.0	513.7	641.3	574.0	513.7	641.3
3	42.2	6.4	574.7	521.1	633.9	455.1	412.6	501.9
4	42.2	20.1	574.7	521.1	633.9	144.7	131.2	159.6

Table 5.3 Summary of 4-storey SPSWs

Storey	4-storey SPSWCT		4-storey SPSWVT	
	Column sections	Beam sections	Column sections	Beam sections
1	W360×634	W460×128	W360×634	W530×219
2	W360×634	W460×128	W360×634	W530×219
3	W360×314	W460×128	W360×382	W530×219
4	W360×314	W460×128	W360×382	W530×150

Table 5.4 Beam end force effects of 4-storey SPSWCT

Beam	P_{bL} (kN)	P_{bR} (kN)	M_{pL} (kN·m)	M_{pR} (kN·m)	V_{bL} (kN)	V_{bR} (kN)
Base	2181	-2181	8330	8330	4629	-245
1	-1952	-1952	831	831	219	219
2	-2212	-1308	774	973	-300	760
3	-2212	146	774	1068	-1058	1543
4	-799	301	1068	1068	-326	888

Table 5.5 Design column forces for 4-storey SPSWCT

Storey	Column axial force (kN)	Column moment (kN·m)
1	10600	3090
2	8030	1100
3	4930	1030
4	1490	1230

Table 5.6 Summary of 8-storey SPSW

	8-storey SPSW	
Storey	Column sections	Beam sections
1-3	W360×900	W460×128
4-6	W360×509	W460×128
7-8	W360×287	W460×128

Table 5.7 Maximum inelastic response at column bases for 4-storey SPSWs

Earthquake record	4-storey SPSWCT				4-storey SPSWVT			
	Column axial force (kN)		Column moment (kN·m)		Column axial force (kN)		Column moment (kN·m)	
	Left	Right	Left	Right	Left	Right	Left	Right
El Centro 1940	7610	8630	1600	1460	8140	8620	1660	1690
Petrolia 1992	7930	7600	1460	1390	8220	7670	1350	1730
Nahanni 1985	8290	8290	1530	1710	8090	7690	1190	1490
Parkfield 1966	7460	9100	1650	1620	7150	8780	1460	1540

Table 5.8 Maximum inelastic response at column bases for 8-storey SPSW

Earthquake record	8-storey SPSWCT			
	Column axial force (kN)		Column moment(kN·m)	
	Left	Right	Left	Right
El Centro 1940	16210	16420	1910	1930
Petrolia 1992	14680	15760	2220	1970
Nahanni 1985	16070	16220	2270	1990
Parkfield 1966	12260	15930	2340	1620
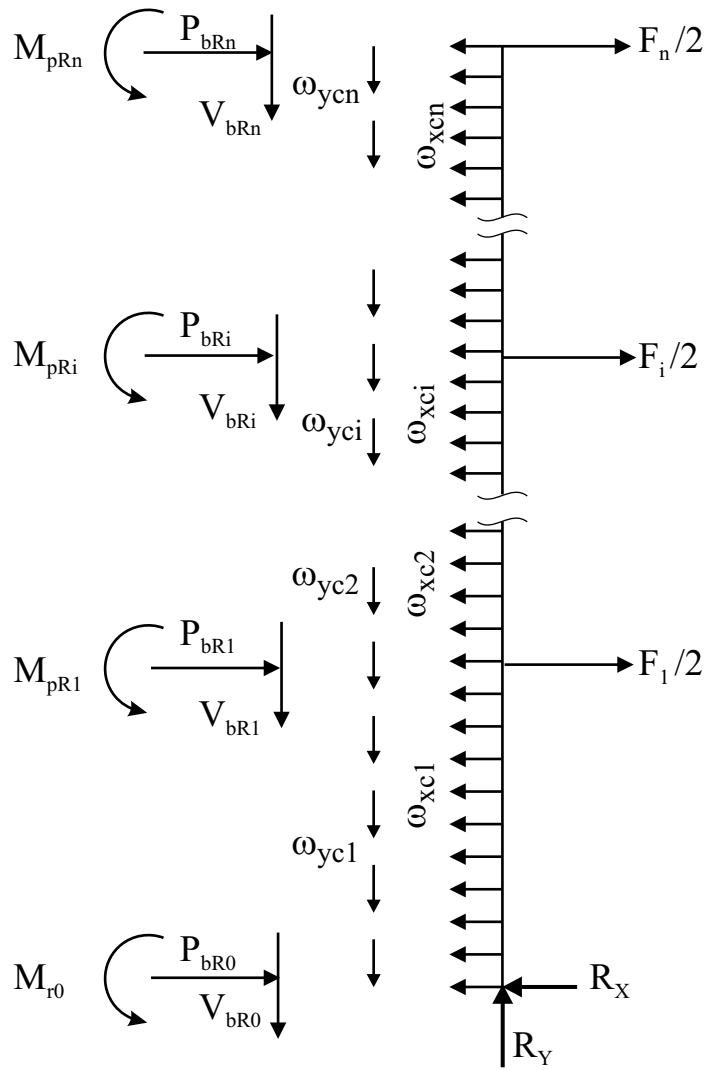
Fig. 5.1 Free body diagram of typical right column of a SPSW

153
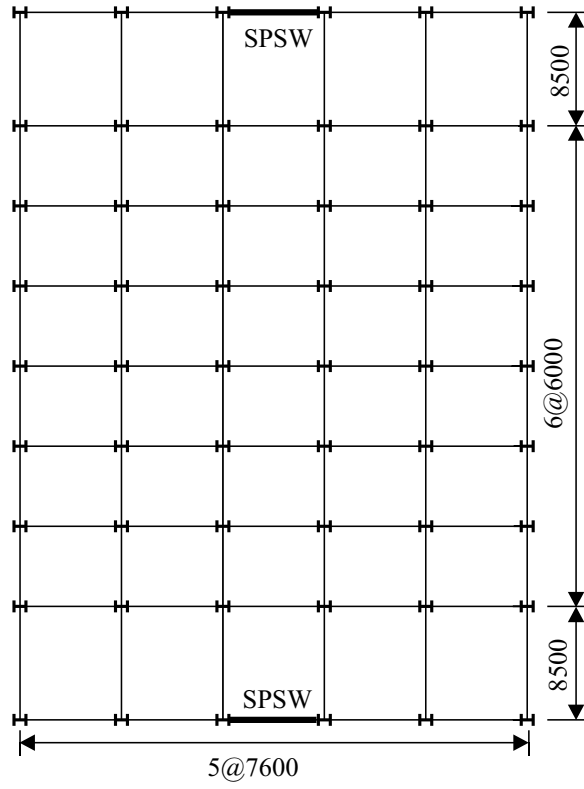
Fig. 5.2 Plan of 4-storey and 8-storey buildings
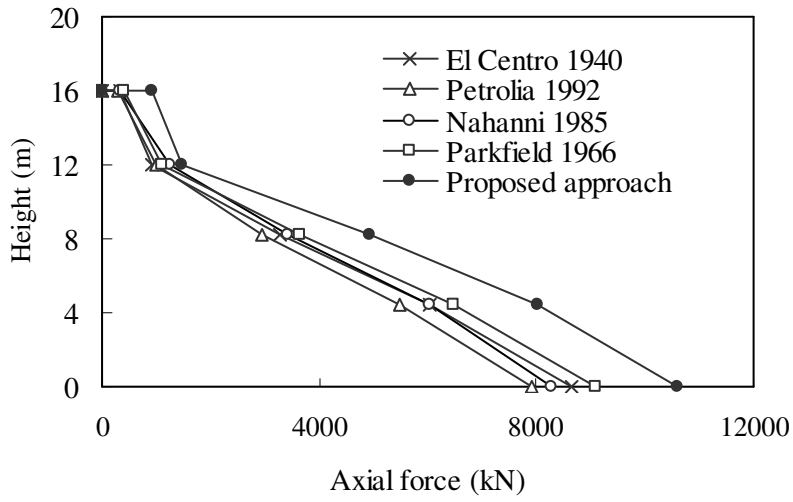
(a)
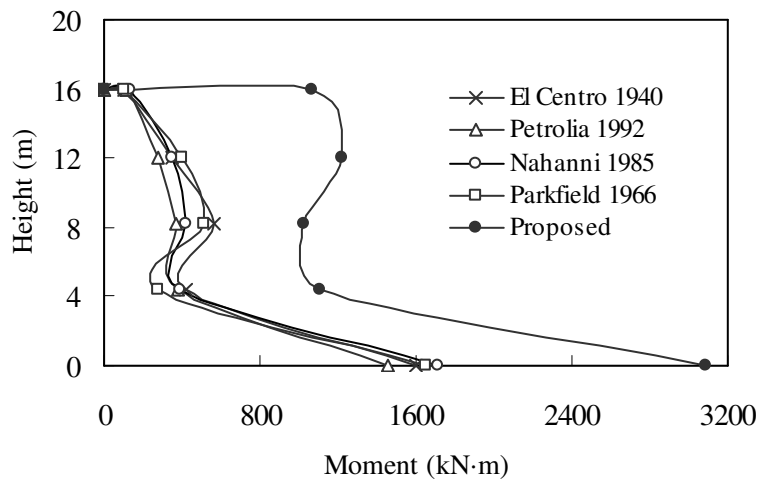
(b)

Fig. 5.3 Inelastic response of 4-storey SPSWCT: (a) peak column axial forces; (b) peak column moments

155
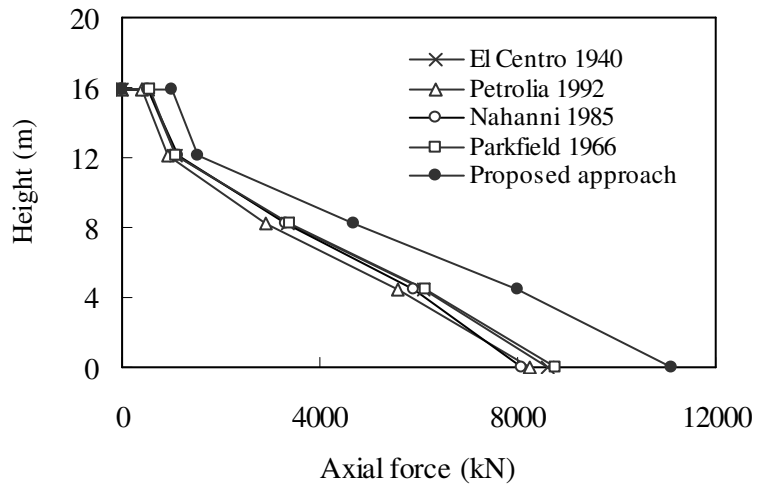
(a)
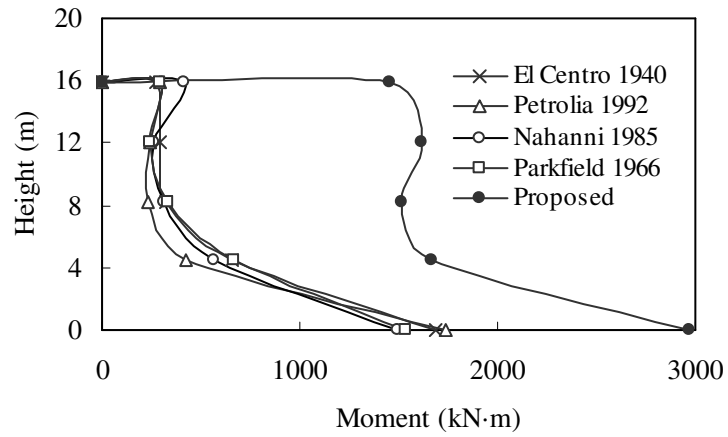
(b)

Fig. 5.4 Inelastic response of 4-storey SPSWVT: (a) peak column axial forces; (b) peak column moments
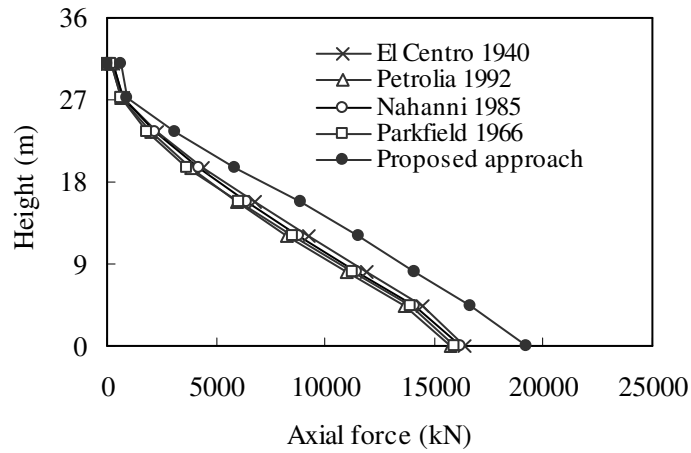
(a)
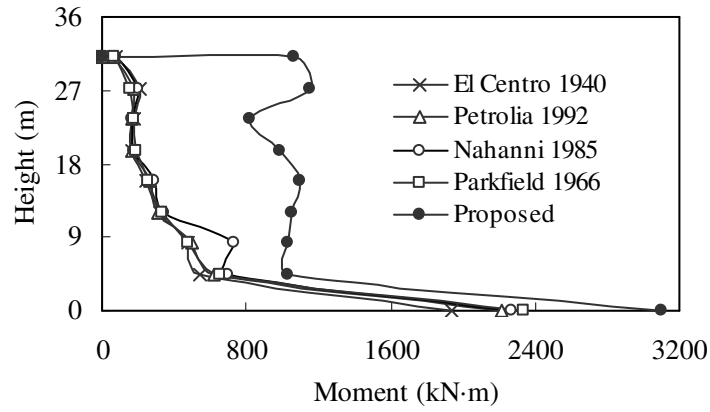
(b)

Fig. 5.5 Inelastic response of 8-storey SPSW: (a) peak column axial forces; (b) peak column moments
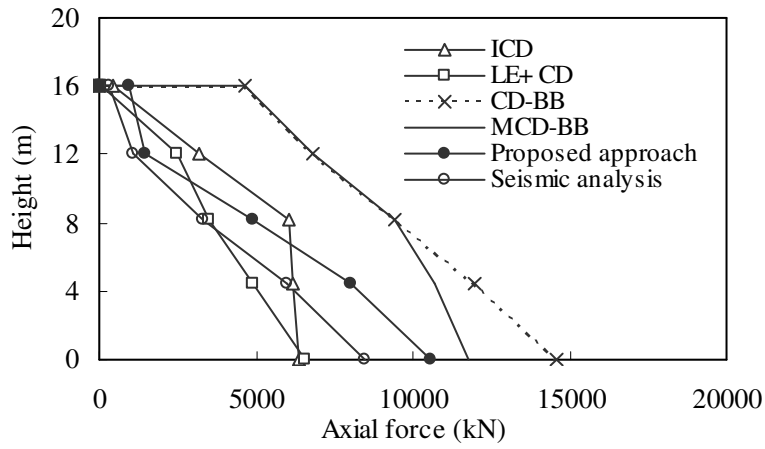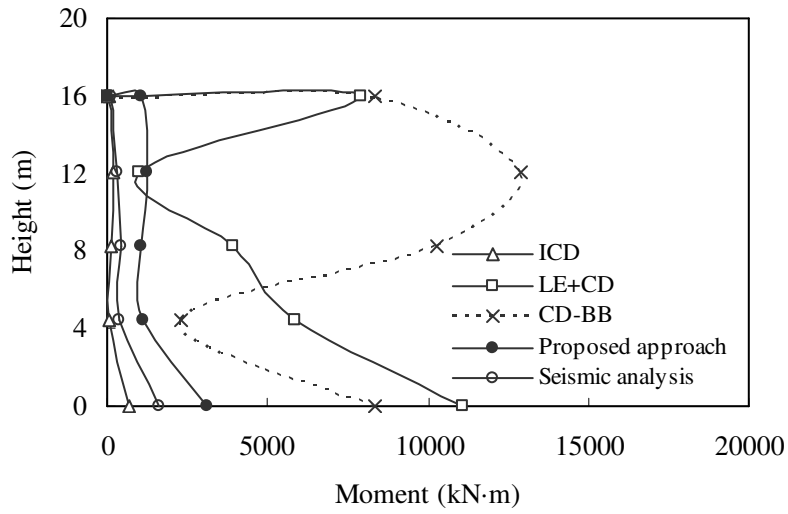
Fig. 5.6 Comparison of column forces from various methods for 4-storey
SPSWCT: (a) peak column axial forces; (b) peak column moments
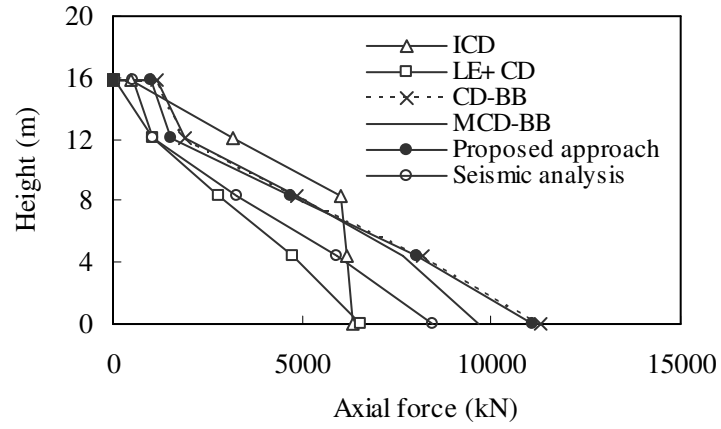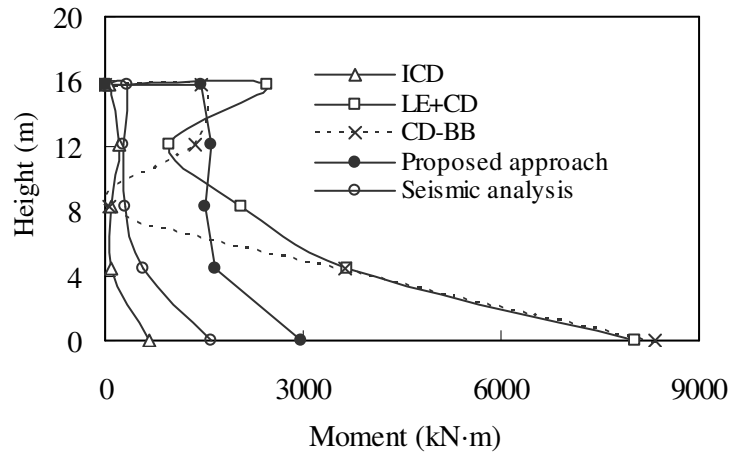
Fig. 5.7 Comparison of column forces from various methods for 4-storey
SPSWVT: (a) peak column axial forces; (b) peak column moments
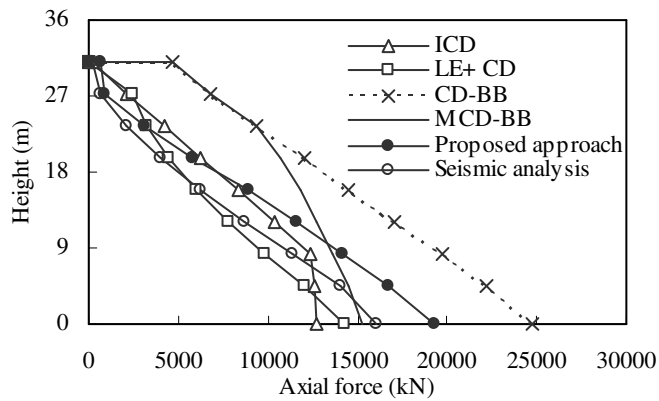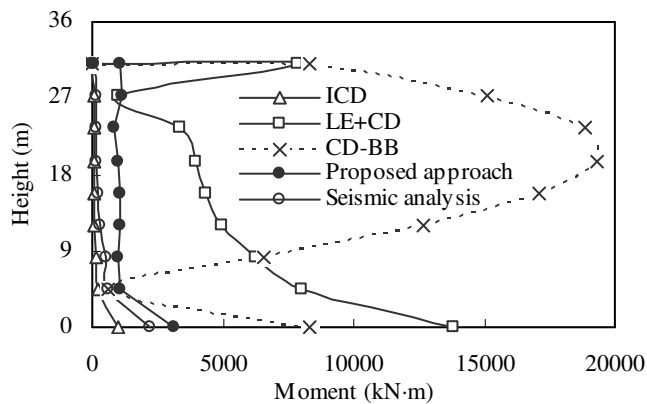
Fig. 5.8 Comparison of column forces from various methods for 8-storey SPSW:
(a) peak column axial forces; (b) peak column moments

References

AISC. 2005. Seismic provisions for structural steel buildings. ANSI/AISC 341-05, American Institute of Steel Construction, Chicago, IL.

Berman, J.W. and Bruneau, M. 2008. Capacity design of vertical boundary elements in steel plate shear walls. Engineering Journal, AISC, first quarter, 57-71.

Bhowmick, A.K., Driver, R.G., and Grondin, G.Y. 2009. Seismic analysis of steel plate shear walls considering strain rate and P-delta effects. Journal of Constructional steel research, 65(5): 149-1159.

Bruneau, M., Whittaker, A.S., and Uang, C.M. 1998. Ductile design of steel structures. McGraw-Hill, New York.

CSA. 2001. Limit states design of steel structures. CAN/CSA S16-01, Canadian Standards Association, Mississauga, ON.

Hibbitt, Karlsson, and Sorensen. 2007. ABAQUS/Standard User's Manual. Version 6.7, HKS Inc., Pawtucket, RI.

Naumoski, N. 2001. Program SYNTH – generation of artificial accelerogram history compatible with a target spectrum. User's manual, Dept. of Civil Engineering, University of Ottawa, Ottawa, ON.

NEHRP (National Earthquake Hazards Reduction Program). 2000. NEHRP recommended provisions for seismic regulations for new buildings and other structures. Building Seismic Safety Council, Washington, D.C., 2 vols., FEMA 368 and 369.

NRCC. 2005. National Building Code of Canada. Canadian Commission on Building and Fire Codes, National Research Council of Canada, Ottawa, ON.

Redwood, R.G. and Channagiri, V.S. 1991. Earthquake-resistant design of concentrically braced steel frames. Canadian journal of civil engineering, 18(5): 839-850.

Sabelli, R. and Bruneau, M. 2007. Steel design guide 20: steel plate shear walls. American Institute of Steel Construction, Chicago, IL.

6. NONLINEAR ANALYSIS OF PERFORATED STEEL PLATE SHEAR WALLS[4]

6.1 General

Steel plate shear walls (SPSWs) are a very effective system for resisting lateral loads due to wind and earthquakes. A properly designed SPSW has high ductility, high initial stiffness, high redundancy, and excellent energy absorption capacity. In North America, the current practice is to use thin unstiffened plates for the infill plates, relying on tension field action to provide high lateral resistance. The surrounding framing members are generally "capacity designed", i.e., designed to develop the infill plate tension field capacity, while themselves remaining essentially elastic.

Very often, the infill plate used in a SPSW is thicker and stronger than that required by the design. In fact, handling and welding considerations are likely to govern the selection of the thickness of the infill plate in the vast majority of cases. Increasing the plate thickness to suit fabrication considerations is often a problem in capacity design, as this will introduce excessive forces to the surrounding frame members, thus increasing their required size. Recent attempts to address this problem have included the use of light-gauge, cold-formed steel infill plates or low yield strength (LYS) steel for infill plates (Berman and Bruneau 2005, Vian 2005), introducing vertical slits in the infill plate (Hitaka and Matsui 2003), or by introducing a regular pattern of circular perforations in the

---

[4] A version of this chapter will be submitted for publication to the *Journal of constructional steel research*.

163

infill plate (vian 2005). Another approach to reduce the demand on boundary members, proposed by Xue and Lu (1994), is to connect the infill plate to the beams of moment resisting frames only. Among all the proposed options, the perforated SPSW recommended by Vian (2005), and shown in Fig. 2.11, represents an attractive system since it also provides a route for the utility systems to pass through the infill plates.

Research on circular perforations in shear panels similar to SPSWs started with Roberts and Sabouri-Ghomi (1992). They conducted a series of quasi-static tests under cyclic diagonal loading on unstiffened steel plate shear panels with centrally-placed circular openings. Based on the results, the researchers proposed the following approximate equation for strength of an unstiffened infill panel with a central circular opening:

$$V_{op} = V_p \left(1 - \frac{D}{d_p} \right) \qquad (6.1)$$

where V_{op} and V_p are the strength of a perforated and a solid shear panel, respectively, D is the perforation diameter, and d_p is the panel height.

Purba (2006) analyzed a 4000 mm by 2000 mm single storey SPSW with multiple regularly-spaced circular perforations of equal diameter, as recommended by Vian (2005). The effects of infill plate thickness and perforation diameter were considered in the analysis. It was observed that for multiple regularly-spaced perforations, Eq. (6.1) provides a conservative estimate of the strength of the

164

perforated infill plate when d_p in Eq. (6.1) is replaced by S_{diag}, the diagonal distance between each perforation line (see Fig. 2.11). Through a calibration study, the following modified equation was proposed to calculate the shear strength of perforated SPSWs with the regular perforation pattern used by Vian (2005):

$$V_{op} = V_p \left(1 - 0.7 \frac{D}{S_{diag}} \right)$$

(6.2)

Purba (2006) also found that results from an individual perforated strip analysis can accurately predict the behaviour of a complete perforated SPSW provided that the hole diameter is less than 60% of the strip width $\left(\dfrac{D}{S_{diag}} \leq 0.6 \right)$. Although Eq. (6.2) was found to provide good strength predictions of SPSWs for the regular perforation pattern proposed by Vian (2005), a more general expression, applicable to any pattern of perforations, is clearly desirable.

This chapter presents a general equation for determining the strength of perforated SPSWs. The proposed equation is based on a strip model, and is derived by discounting the strips that are intercepted by perforations. Finite element models of two single storey SPSWs (with aspect ratios of 2.0 and 1.5) and with eight different types of perforation patterns are analyzed to investigate the effectiveness of the proposed equation. The SPSW strength reductions resulting from the perforation patterns, as determined by non-linear pushover analysis, are compared with the reduction predicted by the proposed equation.

Currently there are no guidelines for the design of boundary columns when perforations are made in the infill plates. AISC Steel Design Guide 20 (Sabelli and Bruneau 2007) presents a capacity design method for the design of SPSW columns with solid infill plates. The method in AISC Steel Design Guide 20 (Sabelli and Bruneau 2007) assumes that all the infill plates over the building height reach their full yield capacity, and plastic hinges are assumed at the ends of all the horizontal members of the frame. Forces from the infill plate tension fields and the force effects from the beams are then applied to a free body diagram of the boundary columns to determine their design axial forces and moments. Column moments are evaluated considering the conditions at each storey individually. The presence of perforations in the infill plates affects the forces and moments in the boundary columns, thus requiring modifications to the current design method. This chapter proposes modifications to the capacity design method of AISC Steel Design Guide 20 (Sabelli and Bruneau 2007) to accommodate SPSWs with circular perforations. The modified capacity design method is used to design the columns of a 4-storey SPSW with four circular perforations. The resulting design forces for the boundary columns are compared with the design forces obtained from a seismic analysis of the 4-storey SPSW under four spectrum-compatible earthquake ground motions for Vancouver, Canada.

6.2 Strength equation for perforated infill plate

To develop a general strength model, it is assumed that the infill plate has negligible buckling capacity and that the shear strength of the SPSW is provided strictly by tension field action. The angle of the tension field, α, developed in the infill plate is obtained from the equation specified both in Canadian standard, CAN/CSA S16-09 (CSA 2009) and AISC seismic Specification (AISC 2005). In the presence of a circular hole of diameter D, as shown in Fig. 6.1, one can discount part of the contribution, β, of the steel within a diagonal strip of width D (Vian 2005). It is assumed, therefore, that only a portion of that tension strip with an equivalent width of $D(1-\beta)$ will be effective. Taking the diagonal strip containing the circular hole to be at the angle of the tension field, α, the horizontal projection of the portion of the strip to be discounted is $\beta \dfrac{D}{\cos \alpha}$. After discounting the strip with the circular perforation, the effective width of the perforated infill plate, $L_{p,eff}$, becomes:

$$L_{p,eff} = L_p - \beta \frac{D}{\cos \alpha} \tag{6.3}$$

where L_p is the width of perforated infill plate.

When more than one strip is perforated and all the strips around the circular perforations are parallel and are inclined at an angle α, the effective width of the perforated infill plate, $L_{p,eff}$, is

$$L_{p,eff} = \left(L_p - N_r \beta \frac{D}{\cos \alpha} \right) \tag{6.4}$$

167

where N_r is the maximum number of diagonal strips (at any section, cut parallel to length L_p, over the height of the panel) with circular perforations to be discounted.

Thus, the shear strength of a perforated infill plate, V_{op} is

$$V_{op} = 0.5\,\sigma\,w\left(L_p - N_r\beta\,\frac{D}{\cos\alpha}\right)\sin 2\alpha \qquad (6.5)$$

where w is the infill plate thickness and σ is the stress in the infill plate (remaining solid) tension strips, taken as the yield stress for design.

The shear strength of a solid infill plate, V_p, is given by

$$V_p = 0.5\,\sigma\,wL_p\sin 2\alpha \qquad (6.6)$$

From Eqs. (6.5) and (6.6)

$$\frac{V_{op}}{V_p} = \left(1 - \beta\,N_r\,\frac{D}{L_p\cos\alpha}\right) \qquad (6.7)$$

A practicing engineer can use the geometry to estimate graphically the value of

$N_r\dfrac{D}{L_p\cos\alpha}$ in the design office. As discussed in the next section, the value of

the constant β is obtained from the analysis of a series of one-storey SPSWs with a variety of perforation patterns.

6.3 Analysis of perforated steel plate shear walls

Nonlinear finite element analyses of a series of single-storey SPSWs were carried out using ABAQUS (Hibbitt, Karlsson, and Sorensen 2007) to determine the magnitude of the constant β. Both material and geometric nonlinearities were

considered. In total, eight different types of perforation patterns were considered in this study. Variation in perforation diameters was also considered for each type of perforation pattern.

6.3.1 Selection of the shear wall system

The single-storey SPSW considered here is a lower storey of a hypothetical multi-storey office building located in Vancouver, Canada. The symmetrical building has a total area of 2014 m^2 and has a storey height of 3.8 m. The building has two identical SPSWs to resist lateral loads in each direction. For simplicity, each shear wall was assumed to resist one half of the design seismic loads. Each shear wall is 7.6 m wide, measured from center to center of columns, and thus the panels have an aspect ratio of 2.0. The building was assumed to be located on rock (site class B according to NBCC 2005). Design seismic load was calculated using the equivalent static force procedure of the National Building Code of Canada (NBCC) 2005 (NRCC 2005). An importance factor, I, of 1.0 was selected for the design. As prescribed by NBCC 2005, a ductility-related force modification factor, R_d, of 5.0 and an overstrength force modification factor, R_o, of 1.6 were used in the design. The NBCC 2005 load combination $D + 0.25S + E$ (where D = dead load, E = earthquake load, and S = snow load) was considered for the design.

An infill plate thickness of 3.0 mm was used. Shishkin et al. (2005) observed that the ultimate base shears of SPSWs varied little when the angle of inclination of the tension field, α, was changed from 38$^\text{o}$ to 50$^\text{o}$. Also, beginning of design of

any SPSW, the column sections are unknown to determine the angle of tension field. Thus, the value of the angle of the diagonal tension field was assumed as 45° in this chapter. With the angle of the tension field known, boundary beams and columns were selected. Even though, the single storey SPSW was the lower storey of a multi-storey building, a beam section of W610X498 was selected for top and bottom beams to anchor the tension forces from the yielded infill plate (in a multi-storey building, the tension field in the bottom storey would be anchored by the infill plate in the storey above). A column section of W360X900 was selected to carry the forces developed in the yielded infill plate and the plastic hinges at the ends of the top beam.

Figures 6.2(a) to 6.2(h) show the eight different perforation patterns used in this investigation. The perforations are placed and selected in such a way so that the behaviours of the SPSWs remain symmetric for the lateral loads applied from both directions. The figures also show that strips are drawn at 45° around the perforations. All the circular perforations shown in Fig. 6.2 have diameters of 500 mm.

6.3.2 Characteristics of the finite element model

The entire infill plate and boundary members (beams and columns) were modeled using a general purpose four-node, doubly-curved, shell element with reduced integration (ABAQUS element S4R). The beams and column were rigidly connected and the infill plate was considered to be connected directly to the

beams and columns. Initial imperfections were applied in the model to help initiate buckling in the infill plate and development of the tension field. The infill plate was taken to have an initial imperfection pattern corresponding to the first buckling mode of the plate wall with a peak amplitude of 1 mm. Thus, an eigenvalue buckling analysis was first run on the perfect SPSW (with a flat infill plate) to extract the first buckling mode. All the SPSWs modeled and analyzed have hinge supports at the bases of the columns, so that their only rotational restraint in the plane of the wall was due to the rigid connection to the base beam. The hinges at the bases of the columns were modeled using rigid beam connections (BEAM-type multi-point constraints in ABAQUS) between the nodes at the base cross-sections of the columns and a reference node at the center of the column. Only rotation about the strong axis of the column was allowed.

All steel members were assumed to have a modulus of elasticity of 200 000 MPa. An elasto-plastic stress versus strain curve was adopted, with a yield strength of 385 MPa for the infill plates, and 350 MPa for the beams and columns. A displacement control solution strategy where the top storey displacement was used as the control parameter was used in this work. A target displacement of 110 mm was selected for all the pushover analyses of the single storey SPSWs.

6.3.3 Pushover analysis and results

SPSWs with the eight different perforation patterns shown in Fig. 6.2 were modeled and analyzed. For comparison purposes, a SPSW with a solid infill plate was also analyzed. It may be more rational, instead of comparing the total shear

171

strengths, which include both the strength of the infill plate and that of the boundary frame, to compare only the infill plate strengths with different perforation patterns. Thus, a model consisting of only the rigid frame of the SPSW was also analyzed. Shear strengths of 9771 kN and 6269 kN were obtained for the single storey SPSW with the solid infill plate and without any infill plate (bare frame), respectively. Resulting pushover curves for all eight cases (with a perforation diameter of 500 mm) are shown in Fig. 6.3. To examine the effect of perforation diameter, all eight perforation patterns illustrated in Fig. 6.2 were re-analyzed for two other perforation diameters, namely, 400 mm and 600 mm. Resulting pushover curves are shown in Fig. 6.4 and Fig. 6.5. The curves for the solid plate and the bare frame cases provide the upper and lower bounds, respectively, to the potential responses of the perforation patterns considered.

The cases designated Type 2, Type 3 and Type 4 have only two circular perforations in different locations, and therefore two strips can be discounted. For any perforation diameter, the pushover analysis results show that the location of the perforations has only a small effect in the total shear strength. For 400 mm and 500 mm holes, the variation in shear strength is less than 1%, and for the 600 mm diameter holes it is 1.3%. Since the Type 1 case has only one perforation at the center of the infill plate, one strip can be discounted. Thus, the base shear for Type 1 was observed to be higher than for the other perforation types, where more strips are discounted. It can be observed from Fig. 6.2 that for Type 5 and Type 8 arrangement of perforations, there are some overlapping between strips. For Type

5 and Type 8 perforations, about 3.3 and 7.3 equivalent strips are discounted respectively. Since for Type 8 perforation pattern, maximum numbers of strips are discounted (in this study), for all three perforation diameters, the Type 8 case resists a lower base shear than any other perforation type considered here. Table 1 presents the base shears for all the perforation patterns. As expected, for every perforation pattern, there is a reduction in the shear strength of the SPSW as the perforation diameter increases.

By assuming that the overall SPSW strength can be approximated by the summation of the base frame and the infill plate strengths, it is possible to estimate the infill plate strength by subtracting the bare frame strength from the total strength at the same displacement level, namely, 110 mm, as selected here. Thus, ratios of perforated infill plate strengths to the solid infill plate strength, V_{op}/V_p, were calculated for all perforation configurations and are presented in Table 2. The number of diagonal strips to be discounted, N_r, is also presented in Table 2. The ratios of V_{op}/V_p for the three different perforation diameters were then used in Eq. (6.7) to evaluate the constant β. As specified earlier, a value of $\alpha = 45^o$ was used for the angle of inclination of the tension field for all hole patterns investigated. Estimated values of β for the 24 cases considered are plotted against V_{op}/V_p in Fig. 6.6. Except for the wall with a single perforation, Type 1 (where the values of beta range from 1.3 to 1.4), it was observed that the β values are very similar. For Type 1 cases, it was observed from pushover

analysis that more than the one strip containing the hole was discounted, which is contrary to all the other cases. To investigate further the effect of placing a single perforation in the infill plate, Type 2 and Type 3 cases with a hole diameter of 400 mm were reanalyzed with only one perforation (the left perforation for Type 2 and Type 3). The ratios of V_{op}/V_p for these two cases were the same, 0.93, which gives a value of β equal to 0.88. Thus, for the 400 mm diameter case, the shear strength of the infill plate reduced more (4.3% for the cases studied) when the single perforation is placed at the center of the infill plate. Nevertheless, since there is only one hole, unless it is very large the increased impact on the overall wall capacity is relatively small. The mean of all β values in Fig. 6.6, excluding the three values obtained for the infill plate with a single perforation at the center, is 0.7. Thus, a value of 0.7 was selected for the constant β to use in Eq. (6.7) to calculate the ratio of perforated infill plate strength to the solid infill plate strength, V_{op}/V_p.

Figure 6.7 presents ratios of perforated infill plate strengths to the solid infill plate strength, as determined from finite element analysis (FEA), compared to the ratios predicted using Eq. (6.7). For all the cases, except the Type 1 cases, excellent agreement is observed between the FEA results and Eq. (6.7). For the Type 1 case, when the value of 0.7 is used for β, Eq. (6.7) overestimates the value of V_{op}/V_p by only 6.4% for the 400 mm diameter case, 7.2% for the 500 mm diameter case, and 8.4% for the 600 mm diameter case.

The proposed equation (Eq. (6.7)) with the value of β as derived above was used to predict the reduction in shear strength for a SPSW with an aspect ratio of 1.5 (SPSW width of 5.7 m). The single storey SPSW was designed for the same conditions as the SPSWs with an aspect ratio of 2.0; that is, the single storey panel is a part of the theoretical building described previously. Again, an infill plate thickness of 3.0 mm was used. In this case, a W530X272 section was selected for the top and bottom beams and a column section of W360X509 was selected to carry the forces developed from infill plate yielding and plastic hinging at the ends of the top beam. Similar eight perforation patterns, as analyzed for an aspect ratio 2.0, were also considered for the SPSWs with an aspect ratio of 1.5. The detailed layout for the perforation patterns for the SPSWs with an aspect ratio of 1.5 is presented in Fig. 6.8.

Nonlinear pushover analyses of all the eight perforation patterns were carried out for a storey displacement of 110 mm. Ratios of perforated infill plate strengths to the solid infill plate strength, V_{op}/V_p, were calculated and are compared with the values obtained from Eq. (6.7) in Fig. 6.9. Again, excellent agreement between the finite element analysis results and those from Eq. (6.7) is observed. The maximum difference between the predicted V_{op}/V_p values obtained from Eq. (6.7) and the V_{op}/V_p values obtained from the finite element analysis was 9% (for the infill plate with a single perforation at the center of the SPSW (Type 1)).

Finally, the proposed equation, Eq. (6.7), was applied to the perforation pattern used by Vian (2005) (shown in Fig. 2.11). The equation proposed by Purba (2006), Eq. (6.2), to determine the reduction in shear strength for this specific perforation layout, was compared with Eq. (6.7). A value of 6 was used for N_r in the proposed equation to reflect the presence of six diagonal rows of holes. It is observed from Fig. 6.10 that for the regular perforation layout, the reduction in shear strength from the proposed equation, Eq. (6.7), is nearly identical to that obtained from the equation recommended by Purba (2006). Thus, the proposed equation can be used for relating the shear strength of a SPSW with a solid infill plate to an analogous SPSW with a perforated infill plate (with circular perforations).

6.4 Design of boundary columns of perforated steel plate shear walls

As stated earlier, a need exists to develop an accurate and efficient method for estimating design forces on boundary columns of SPSWs with perforations in the infill plates. The presence of the perforations serves to reduce the demand on the columns, which can have a significant effect on economics under capacity design. A simple and efficient capacity design method for design of columns of SPSWs with solid infill plates is presented in AISC Steel Design Guide 20 (Sabelli and Bruneau 2007). The method is modified here to include the effects of circular perforations in arbitrary locations. The modified design method can be summarized as follows:

176

(3) For a selected perforation layout, the ratio of perforated infill plate strength to the solid infill plate strength, V_{op}/V_p, is calculated using Eq. (6.7). While designing the boundary columns for a given infill plate thickness and perforation pattern, it is suggested that the N_r value be rounded to the lower integer to use in Eq. (6.7). This is a conservative approach since the boundary columns are to be designed to yield the remaining solid infill plates.

(2) The distributed loads developed from yielding of the perforated infill plates, as shown in the free body diagram in Fig. 6.11 of a typical column from an n-storey SPSW, can be obtained by multiplying the distributed loads developed from yielding of solid infill plates by V_{op}/V_p. Thus, the distributed loads applied to the columns $\left(\omega_{yci} \text{ and } \omega_{xci}\right)$ and beams $\left(\left(\omega_{ybi} \text{ and } \omega_{xbi}\right) \text{ and } \left(\omega_{ybi-1} \text{ and } \omega_{xbi-1}\right)\right)$ at any storey i can be determined as:

$$\omega_{xci} = \left(V_{op}/V_p\right)_i R_y F_y w \left(\sin\alpha_i\right)^2 \; ; \; \omega_{yci} = \left(V_{op}/V_p\right)_i 0.5 R_y F_y w \sin 2\alpha_i \qquad (6.8)$$

$$\omega_{xbi} = \omega_{xbi-1} = \left(V_{op}/V_p\right)_i 0.5 R_y F_y w \sin 2\alpha \qquad (6.9)$$

$$\omega_{ybi} = \omega_{ybi-1} = \left(V_{op}/V_p\right)_i R_y F_y w \left(\cos\alpha\right)^2 \qquad (6.10)$$

It is assumed that the distributed loads calculated in this way will act uniformly over the length of beams and columns in every storey.

(3) The beam at any storey i is designed for distributed loads obtained from the difference between the tension forces developed in the infill plates at

177

storey i and $i+1$, namely, $\omega_{bi} = \left(V_{op} / V_p \right)_i \left(\omega_{ybi} - \omega_{ybi+1} \right)$. The distributed loads are then combined with the gravity loads using appropriate load factors.

(4) Axial forces in the beams can be estimated using the approach outlined in AISC Steel Design Guide 20. Axial forces are obtained from two sources: the first is due to the inward force from the infill plate applied to the columns, $P_{b(col)}$, and the second is from the difference in the effects of the infill plates above and below the beam, $P_{b(plate)}$. Thus, the axial force in the beam is

$$P_b = P_{b(col)} \pm P_{b(plate)} \tag{6.11}$$

The axial force at the ends of the beam at storey i is

$$P_{bi} = \left(\omega_{xci} \frac{h_i}{2} + \omega_{xci+1} \frac{h_{i+1}}{2} \right) \pm \left(\omega_{xbi} - \omega_{xbi+1} \right) \frac{L}{2} \tag{6.12}$$

At the end where the column is in tension, the above two components of the axial force in the beams are additive.

(5) All the beams are assumed to form a plastic hinge at their ends. The reduced plastic moment capacity at the ends of beam i, M_{pri}, can be obtained from the approximate equation (Bruneau et al. 1998)

$$M_{pri} = 1.18 Z_{xi} F_{yb} \left(1 - \frac{P_{bi}}{A_{bi} F_{yb}} \right) \le Z_{xi} F_{yb} \tag{6.13}$$

where Z_{xi} is the beam plastic section modulus, A_{bi} is the beam cross-sectional area, and F_{yb} is the beam yield strength.

178

Using the reduced plastic moment capacities, the shear forces at the ends of beam i, V_{bi}, can be obtained using the following equation:

$$V_{bi} = \frac{\sum M_{pri}}{L} \pm \left(\omega_{ybi} - \omega_{ybi+1} \right) \frac{L}{2} \tag{6.14}$$

where $\sum M_{pri}$ is the summation of the reduced plastic moment capacities at opposite ends of beam i.

With all the force components determined for the column free body diagrams, design axial forces for the columns can be easily calculated.

(6) Column moments are estimated storey by storey, assuming they are rigidly connected to the beams at each floor. In every storey, column moments, M_{col}, are calculated as the sum of those arising from infill plate tension and those from plastic hinging of the beam, as follows:

$$M_{col,i} = M_{plate,i} + MAX \left(M_{beam,i}; M_{beam,i-1} \right) \tag{6.15}$$

For a column assumed to be fixed against rotation at each end, the moment from the infill plate tension field is

$$M_{plate,i} = \frac{\omega_{xci} h_i^2}{12} \tag{6.16}$$

where ω_{xci} is calculated from Eq. (6.8). For the moment due to plastic hinging in the beam, $M_{beam,i}$ or $M_{beam,i-1}$, one-half of the reduced plastic moment of the beam can be applied to each column segment connected to that beam (i.e., above and below).

Similar to AISC Steel Design Guide 20, the column moments at the top and bottom storey are taken as the moment due to plastic hinging at the ends of the top and bottom beam.

6.5 Design Example

A 4-storey SPSW was selected to evaluate the accuracy of the proposed design method. The 4-storey building is assumed to have the same plan area as the building considered above, from which the 1-storey SPSWs were taken for determining the factor β. The building has two identical 4-storey SPSWs to resist lateral forces in one direction. Each shear wall is 5.7 m wide, measured from center to center of columns, with an aspect ratio of 1.5 (storey height of 3.8 m). A dead load of 4.26 kPa was used for each floor and 1.12 kPa for the roof. The live load on all floors was taken as 2.4 kPa. Design seismic loads at every storey were calculated using the equivalent static force procedure of NBCC 2005 (NRCC 2005). The base shear for one 4-storey SPSW was calculated as 1150 kN. Distribution of the base shear up the height of the SPSW resulted in lateral loads of 155 kN, 311 kN, 466 kN, and 217 kN, at each storey from the first to the fourth, respectively. For the 4-storey building used for this investigation, variable infill plate thicknesses were selected over the height of the SPSW, as shown in Fig. 6.12. The figure also shows the beam and column sections selected for the frame. In every storey, the top two and the bottom two perforations are located at the same distance from the beam flange closest to the perforations. A yield strength of 385 MPa was selected for the infill plates, whereas the yield strength

180

for the beams and columns was taken as 350 MPa. All steel members were assumed to have a modulus of elasticity of 200 000 MPa.

For the perforation pattern selected, a value of 3 was used for N_r value. Using Eq. (6.7), the value of V_{op}/V_p was calculated as 0.72. The preliminary selection of beams and columns was based on the design loads that were obtained after the first iteration of the proposed method with an assumed tension field inclination angle of 45°. The calculations for the second iteration of the proposed procedure are described in the following. The distributed forces, obtained from yielding of the infill plates, were obtained from Eqs. (6.8), (6.9) and (6.10) and are presented in Table 6.3. The angle of inclination of the tension field presented in Table 6.3 was obtained from the equation in Canadian standard CAN/CSA S16-09.

Axial forces for the beams of the 4-storey SPSW were calculated using Eqs. (6.12) and are summarized in Table 4. The values of P_{bL} and P_{bR} are the axial force at the beams left and right ends, respectively. The reduced plastic moments for the selected beam sections were calculated using Eq. (6.13). Using the reduced plastic moment capacity of the beams (M_{prL} and M_{prR}), shear forces at the left and at right ends of beams (V_{bL} and V_{bR}) were calculated using Eq. (6.14). Table 4 tabulates the reduced plastic moments and shear forces at the left and right ends of all beams for the 4-storey perforated SPSW.

Finally, axial forces and bending moments in the boundary columns in every storey were calculated and are presented in Table 6.5.

6.6 Comparison with Seismic Analyses

Four different seismic records were chosen for the time history response analysis. These are: (1) N-S component of the El Centro earthquake of 1940; (2) Petrolia station record from the 1992 Cape Mendocino earthquake; (3) Nahanni, Canada 1985 earthquake record; and (4) Parkfield 1966 earthquake record. The seismic records were modified using the software SYNTH (Naumoski 2001) to make them spectrum compatible for Vancouver, Canada. Nonlinear time step dynamic analyses of the 4-storey SPSW were performed using ABAQUS. As for the single storey SPSWs described above, the beams, columns, and infill plates were modelled using the shell element S4R from ABAQUS. The finite element model includes one steel plate shear wall and a gravity "dummy" column carrying the vertical load supported by half of the leaning columns in the building. The gravity column is made of rigid bar elements and connected to the steel plate shear wall at every storey, with pin-ended rigid links. The boundary conditions and material properties are the same as for the single storey SPSWs described earlier. In the finite element analyses, the storey gravity loads were represented as lumped masses on the columns at every floor. A damping ratio of 5% in Rayleigh proportional damping was selected for all the seismic analyses.

Axial forces and bending moments for the boundary columns of the 4-storey SPSW were obtained from nonlinear seismic analysis. Figures 6.13 and 6.14 present the envelopes of absolute maximum column axial forces and column moments obtained from the seismic analyses. Figure 6.13 shows that for all ground motions, the axial forces in every storey are lower than the design axial

forces obtained from the proposed method. The maximum column axial force developed at the base of the 4-storey perforated SPSW from the time historey analyses, 7450 kN, for the Petrolia 1992 earthquake record, is only 3.3% lower than the proposed design axial force, 7700 kN. Figure 6.14 shows that the peak seismic demand for flexure at the base of the columns, 1340 kN·m, for the Petrolia 1992 earthquake record, is 34.3% lower than the proposed design moment of 2040 kN·m. Also, the design column moments for the upper stories are much larger than the column moments determined from the seismic analyses.

One of the objectives of introducing perforations into the infill plates was to reduce the overstrength and, thereby, reduce the design forces for capacity design of the boundary members of the SPSWs. To demonstrate how perforations help reduce the design forces, design forces were calculated for the same 4-storey SPSW with solid infill plates, following the capacity design method presented in the AISC Steel Design Guide 20. Beam sections in every storey for the 4-storey SPSW with solid infill plates were the same as the 4-storey perforated SPSW, except the beam at the base, which was selected as W530X300 to resist the yield capacity of the full infill plate.

The design forces calculated for the 4-storey SPSW with solid infill plates are compared with the design forces for the 4-storey SPSW with perforated infill plates in Fig. 6.13 and Fig. 6.14. Figure 6.13 shows that the design column axial forces in every storey of the perforated SPSW are lower than those for the SPSW with no perforations. The design column axial force at the base of the 4-storey perforated SPSW, 7700 kN, is 23% lower than the design axial force for the

SPSW with no perforations. Figure 6.14 shows that the maximum bending moment at the base of the column of the perforated SPSW, 2040 kN·m, is 33% lower than the design moment for the SPSW with no perforations. The significant benefit of the plate weakening from the four perforations selected for each storey is evident.

6.7 Conclusions

A series of finite element analyses of unstiffened SPSWs with different perforation patterns was performed. The analyses show that the shear strength of an infill plate with circular perforations can be calculated by reducing the shear strength of the solid infill plate by the factor given by Eq. (6.7). The equation was found to give excellent predictions of reduced shear strengths of SPSWs with different patterns of perforations, different perforation diameters, and different infill plate aspect ratios.

A procedure for calculating the design force effects for columns of SPSWs with circular perforations in the infill plates is presented. Design column moments and axial forces from the proposed procedure were shown to agree very well with the results of nonlinear seismic analyses of 4-storey SPSWs with circular perforations in the infill plates. Furthermore, the advantages of having perforations in the infill plates were demonstrated.

Table 6.1 Total base shear for different perforation patterns

Perforation pattern	Total shear strength (kN)		
	Perforation diameter		
	400 mm	500 mm	600 mm
Type 1	9378	9311	9232
Type 2	9381	9304	9240
Type 3	9316	9222	9111
Type 4	9359	9262	9162
Type 5	9166	9030	8887
Type 6	9205	9060	8915
Type 7	9026	8860	8702
Type 8	8439	8153	7891

Table 6.2 Ratios of perforated to solid infill plate strengths

Perforation pattern	N_r	$\dfrac{V_{op}}{V_p}$ from FE analysis		
		Perforation diameter		
		400 mm	500 mm	600 mm
Type 1	1	0.89	0.87	0.85
Type 2	2	0.89	0.87	0.85
Type 3	2	0.87	0.84	0.81
Type 4	2	0.88	0.85	0.83
Type 5	3.3	0.83	0.79	0.75
Type 6	3	0.84	0.80	0.76
Type 7	4	0.79	0.74	0.69
Type 8	7.3	0.62	0.54	0.46

Table 6.3 Distributed loads from perforated infill plates

Storey	α (degree)	Loads from yielding infill plates (kN/m)		
		ω_{yc} or ω_{xb}	ω_{xc}	ω_{yb}
1	42.9	415	385	447
2	41.0	378	329	434
3	41.9	276	247	308
4	43.2	138	130	147

Table 6.4 Beam end forces of 4-storey SPSW

Beam	P_{bL} (kN)	P_{bR} (kN)	M_{prL} (kN·m)	M_{prR} (kN·m)	V_{bL} (kN)	V_{bR} (kN)
Base	1180	-1180	2040	2040	1900	-465
1	-1460	-1250	939	985	300	375
2	-1380	-803	956	1070	-5	715
3	-1110	-325	1020	1070	-91	822
4	-641	148	1070	1070	-46	795

Table 6.5 Design column forces for 4-storey SPSW

Storey	Column axial force (kN)	Column moment (kN·m)
1	7703	2044
2	5630	929
3	3356	831
4	1356	1224
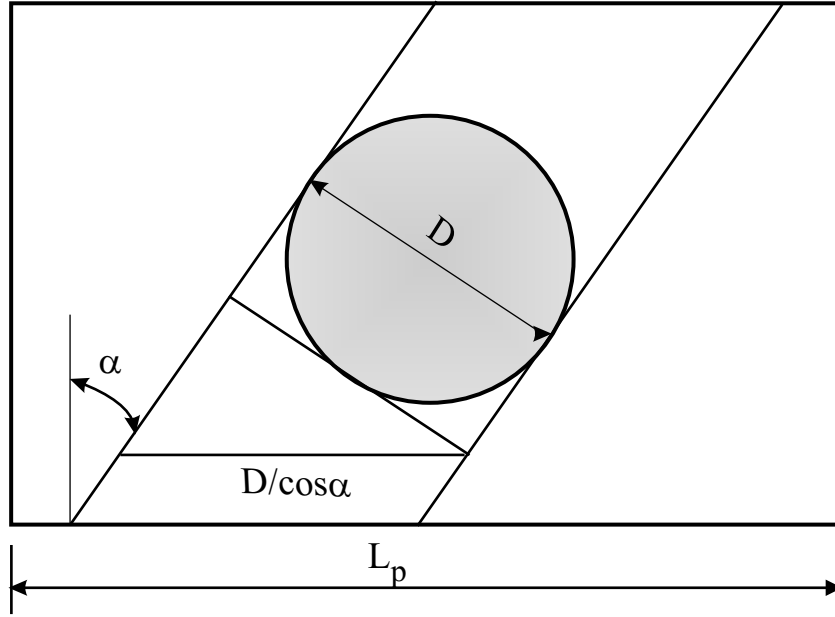
Fig. 6.1 Strip model for perforated infill plate

(a)

(b)

(c)

(d)

(e)

(f)

189
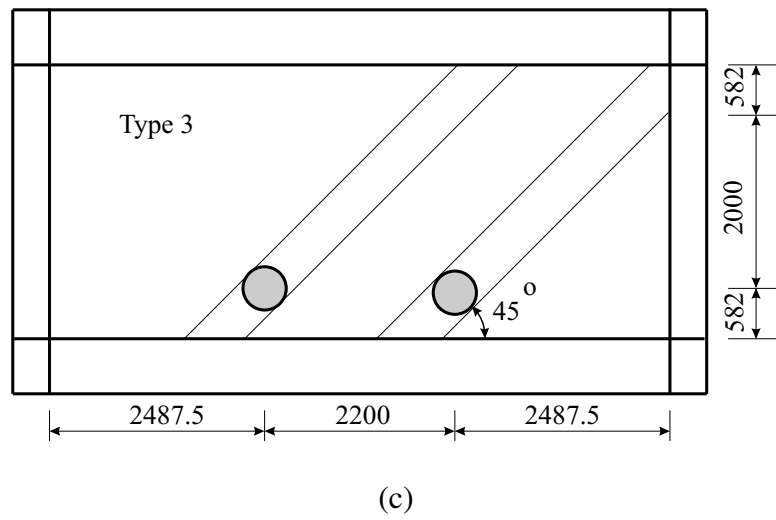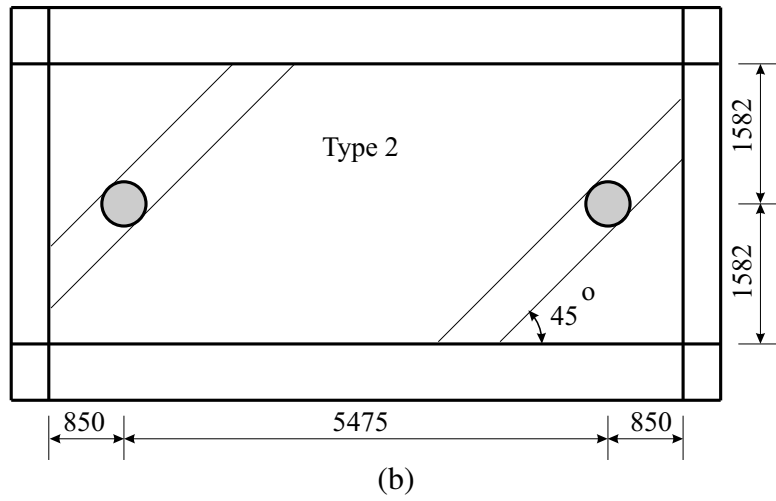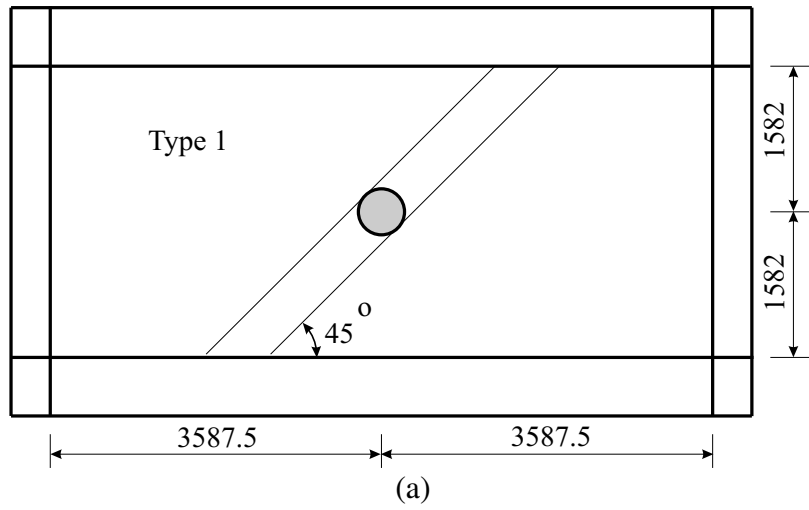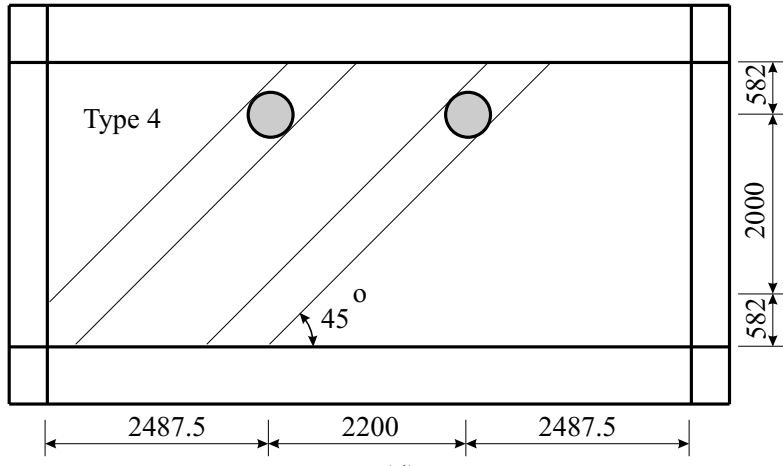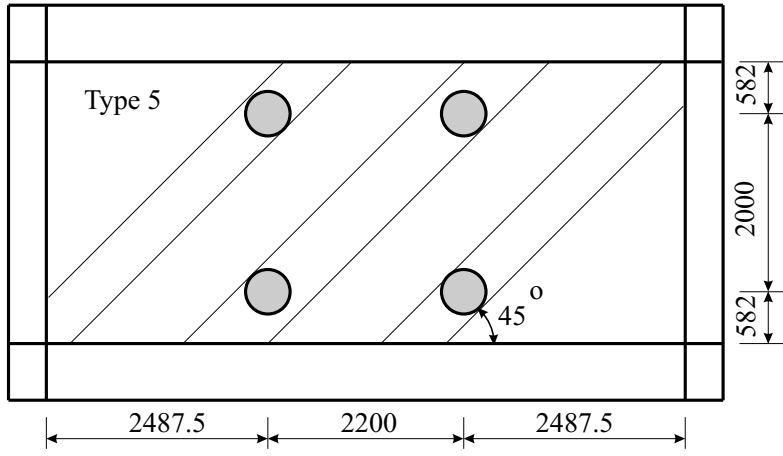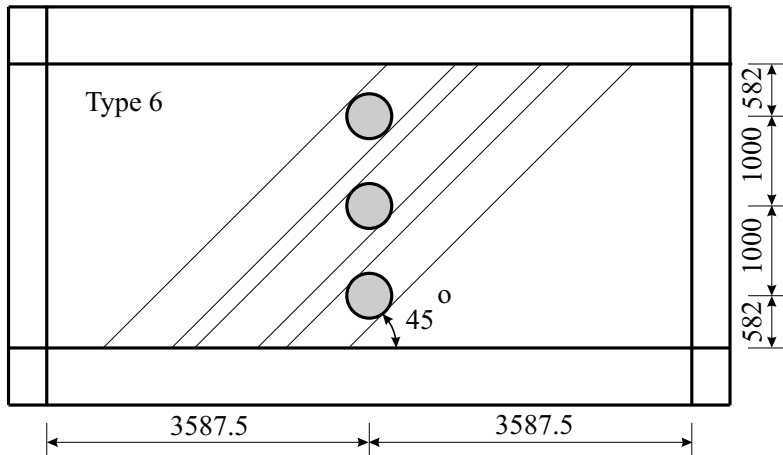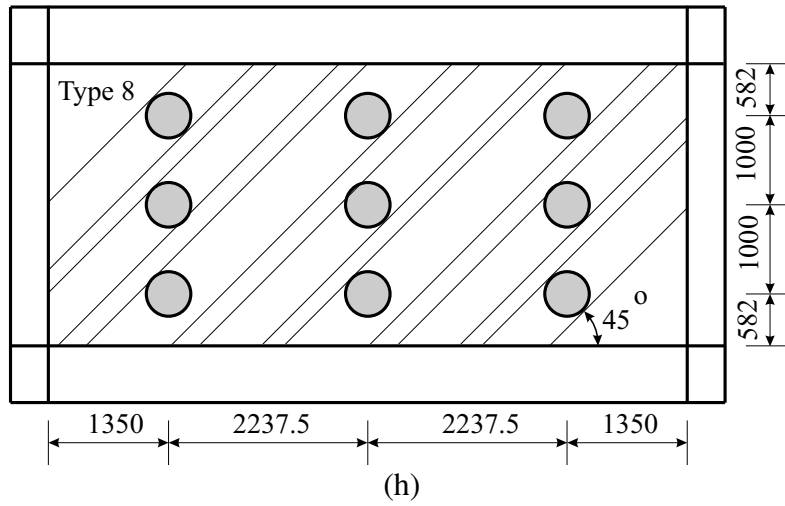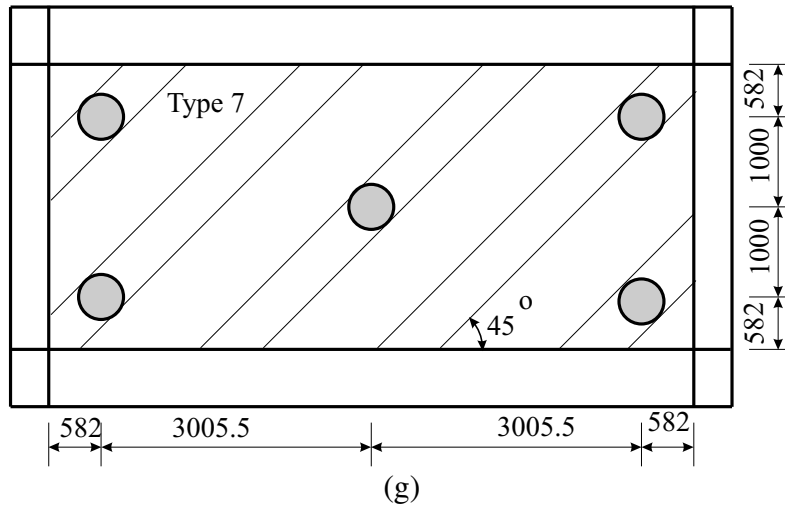
Fig. 6.2 Selected perforation layouts for aspect ratio 2.0 (a) Type 1; (b) Type 2; (c) Type 3; (d) Type 4; (e) Type 5; (f) Type 6; (g) Type 7; (h) Type 8
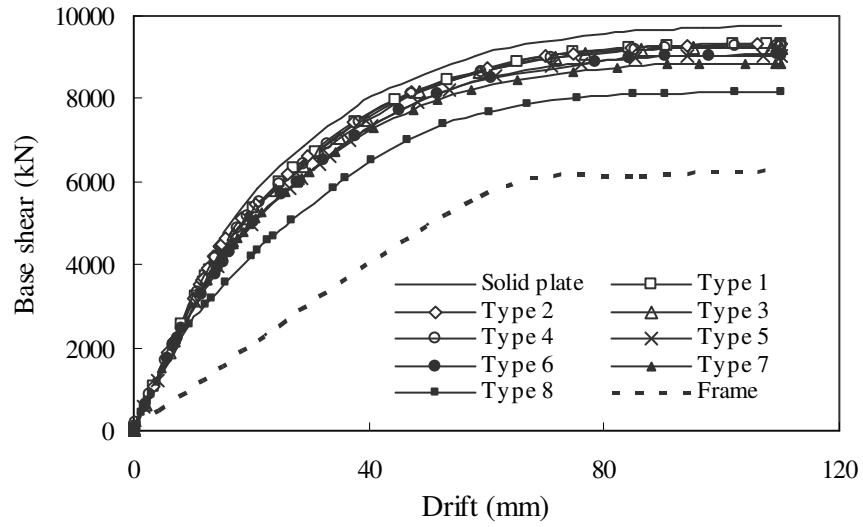
Fig. 6.3 Pushover curves for 500 mm diameter perforations
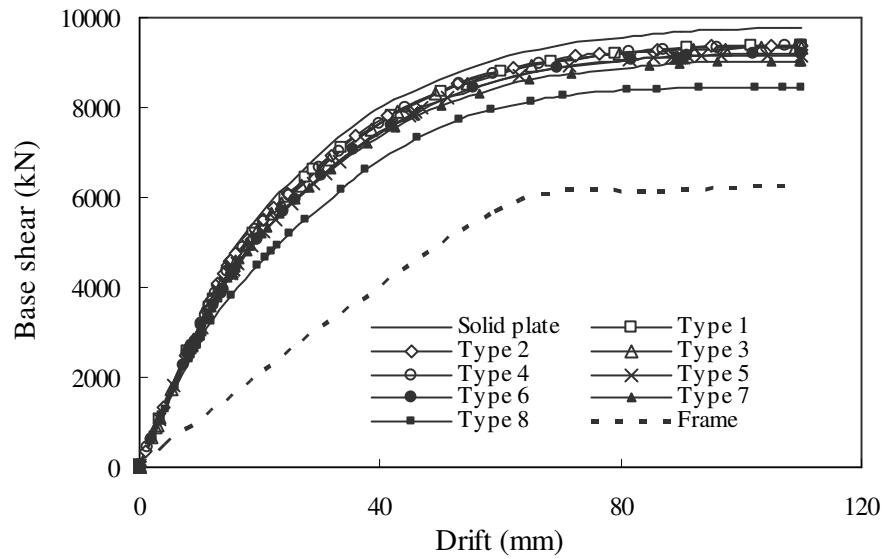
Fig. 6.4 Pushover curves for 400 mm diameter perforations
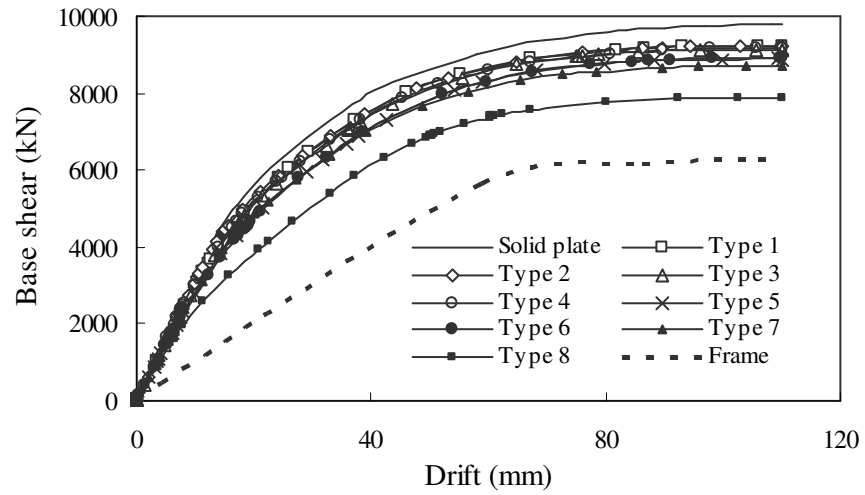
Fig. 6.5 Pushover curves for 600 mm diameter perforations
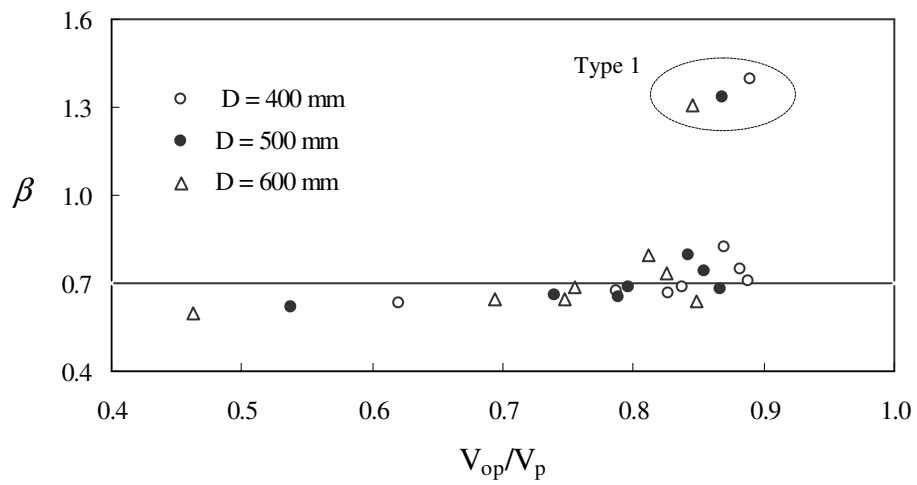
Fig. 6.6 Estimation of constant β
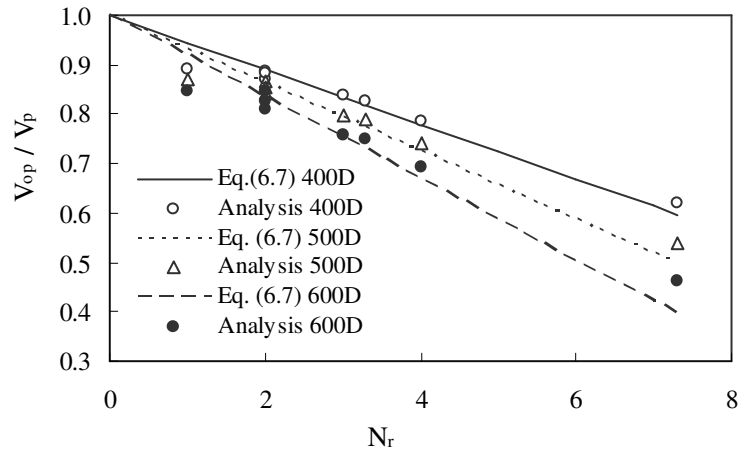
Fig. 6.7 Strength ratios of perforated infill plate to solid infill plate (aspect ratio 2.0)

(a)

(b)

(c)

194

(d)

(e)

(f)

(g)

(h)
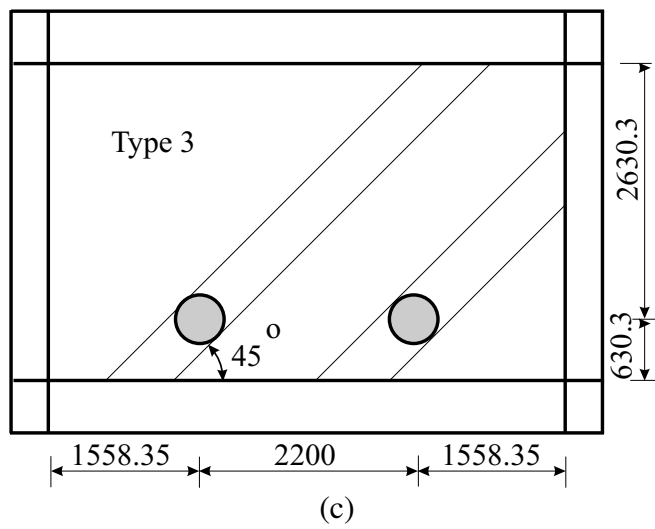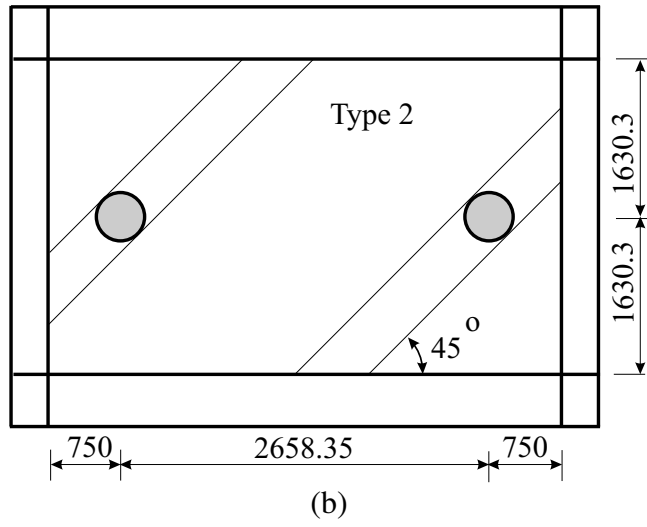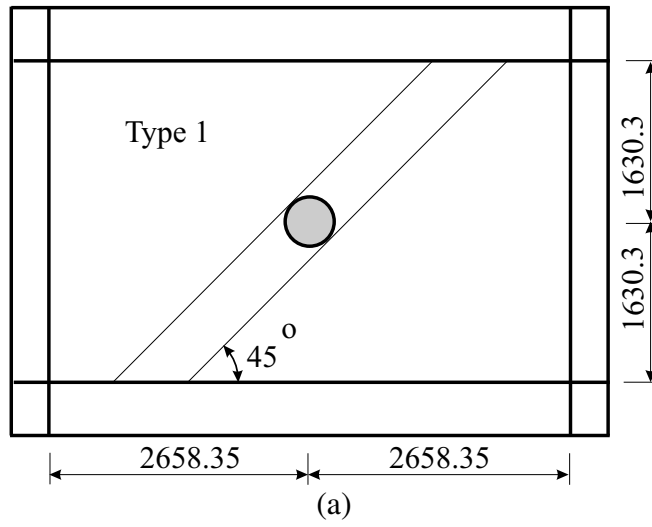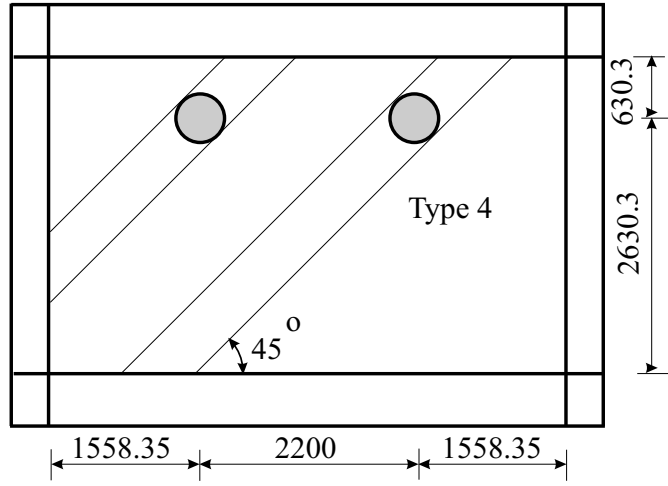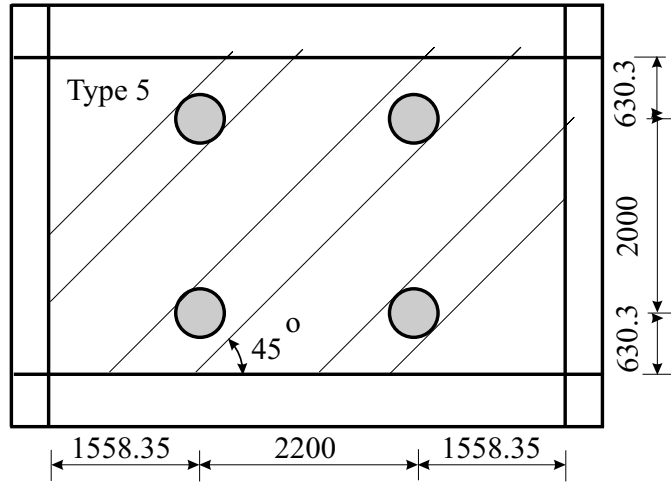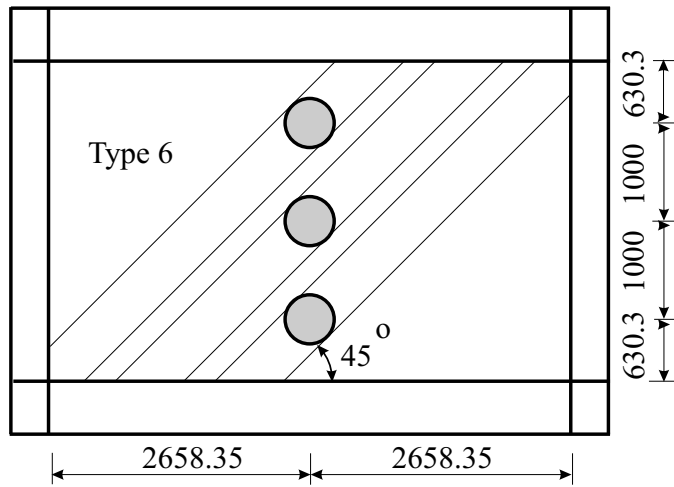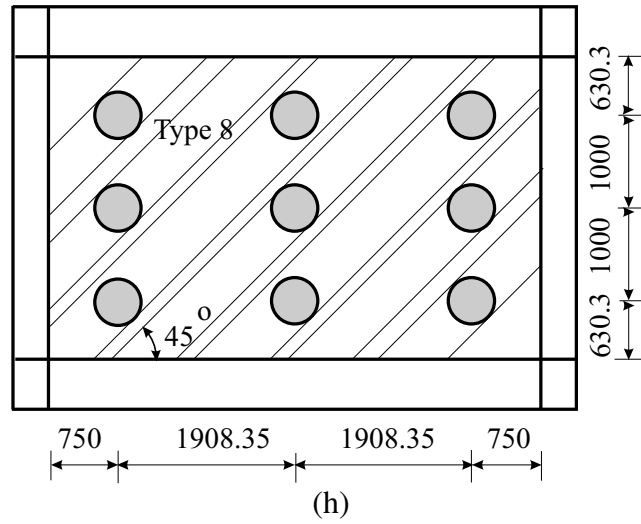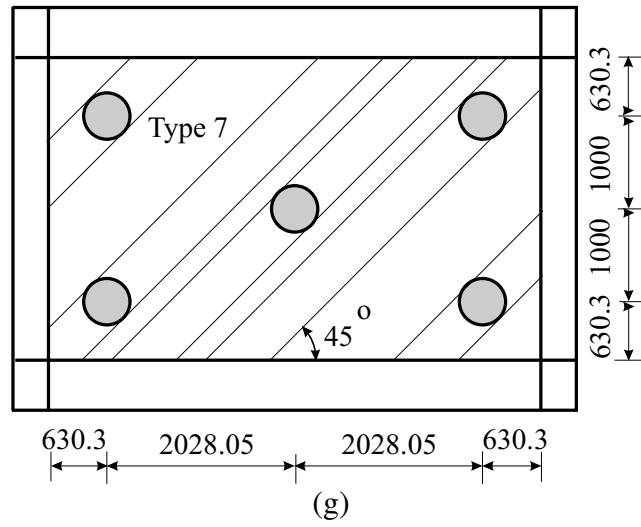
Fig. 6.8 Selected perforation layouts for aspect ratio 1.5 (a) Type 1; (b) Type 2;
(c) Type 3; (d) Type 4; (e) Type 5; (f) Type 6; (g) Type 7; (h) Type 8
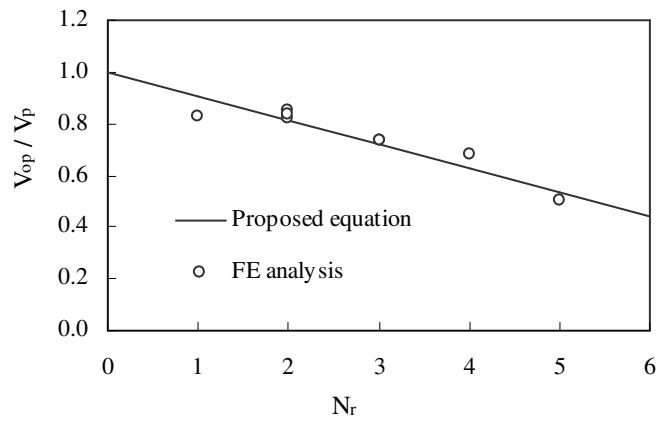
Fig. 6.9 Strength ratios of perforated infill plate to solid infill plate (aspect ratio 1.5)
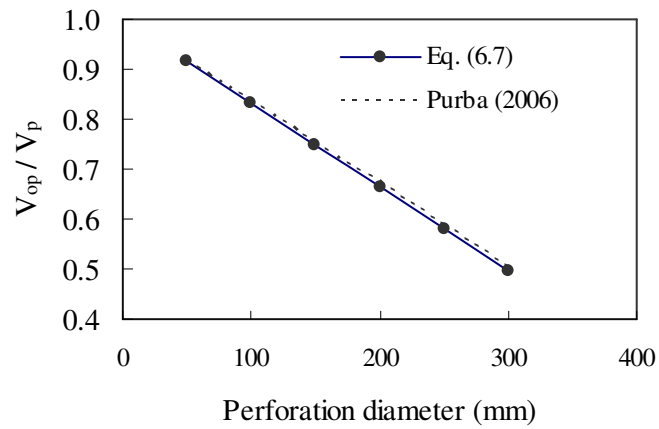
Fig. 6.10 Comparison of Eq. (7) with the equation proposed by Purba (2006)
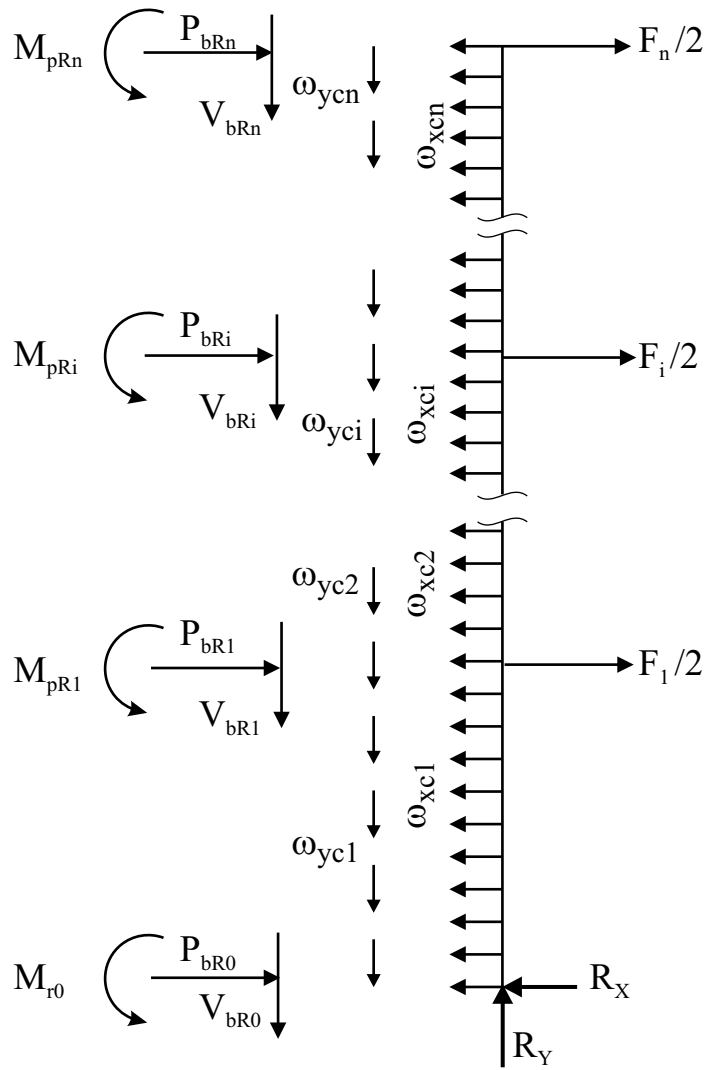
Fig. 6.11 Free body diagram of typical right column of a SPSW

198
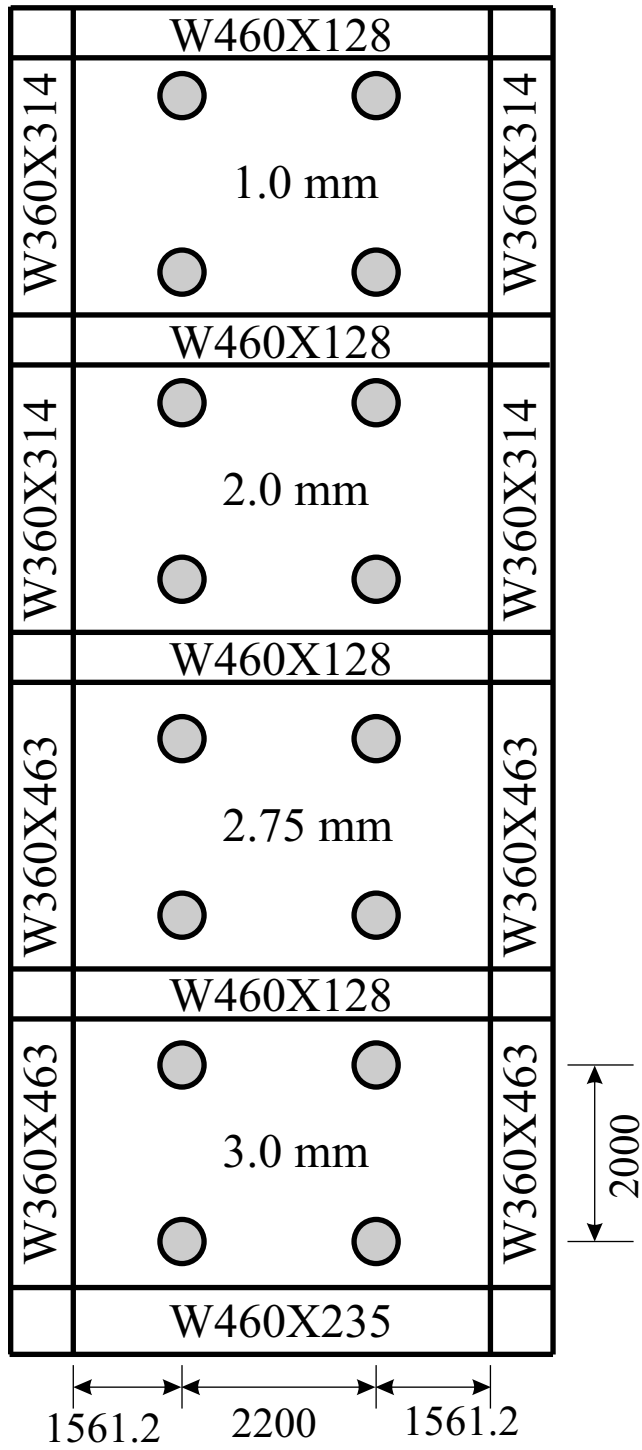
Fig. 6.12 4-storey SPSW with perforations
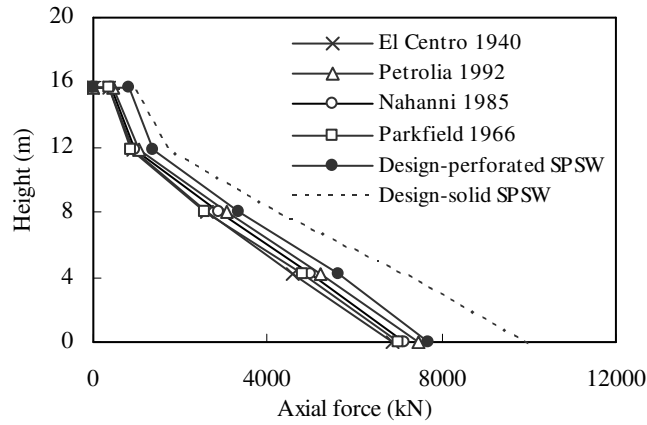
Fig. 6.13 Peak column axial forces for 4-storey SPSWs
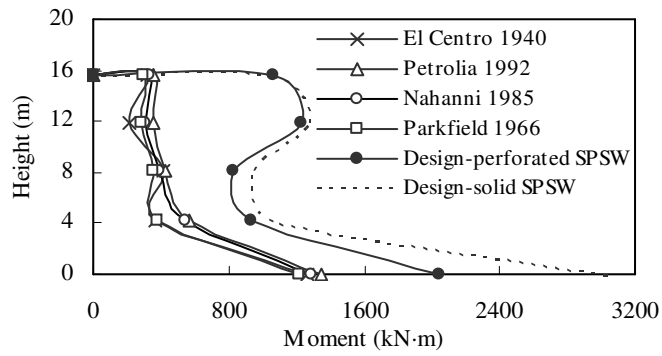
Fig. 6.14 Peak column moments for 4-storey SPSWs

References

AISC. 2005. Seismic provisions for structural steel buildings. American Institute of Steel Construction, Chicago, IL.

Berman, J. W., and Bruneau, M. 2005. Experimental investigation of light-gauge steel plate shear walls. Journal of structural engineering, ASCE,131(2):259-267.

Bruneau, M., Whittaker, A.S., and Uang, C.M. 1998. Ductile design of steel structures. McGraw-Hill, New York.

CSA. 2009. Limit states design of steel structures. CAN/CSA S16-09, Canadian Standards Association, Toronto, ON.

Hibbitt, Karlsson, and Sorensen. 2007. ABAQUS/Standard User's Manual. Version 6.7, HKS Inc., Pawtucket, RI.

Hitaka, T. and Matsui, C. 2003. Experimental study on steel shear walls with slits. ASCE Journal of Structural Engineering, 129 (5):586-595.

Naumoski, N. 2001. Program SYNTH-generation of artificial accelerogram historey compatible with a target spectrum. User's manual, Dept. of Civil Engineering, University of Ottawa, Ottawa, ON, Canada.

NRCC. 2005. National Building Code of Canada. Canadian Commission on Building and Fire Codes, National Research Council of Canada (NRCC), Ottawa, ON, Canada.

Purba, R. H. 2006. Design recommendations for perforated steel plate shear walls. M.Sc. Thesis, State University of New York at Buffalo, Buffalo, N.Y.

Roberts, T.M. and Sabouri-Ghomi, S. 1992. Hysteretic characteristics of unstiffened perforated steel plate shear panels. Thin Walled Structures, 14: 139-151.

Sabelli, R., and Bruneau, M. 2007. Steel design guide 20: steel plate shear walls. American Institute of Steel Construction, Chicago, IL.

Shishkin, J.J, Driver, R.G., and Grondin, G.Y. 2005. Steel plate shear walls using the modified strip model. Structural Engineering Report No. 261, Department of Civil and Environmental Engineering, University of Alberta, Edmonton, Canada.

Vian, D. 2005. Steel plate shear walls for seismic design and retrofit of building structures. PhD dissertation, State Univ. of New York at Buffalo, Buffalo, N.Y.

Xue, M. and Lu, L-W. 1994. Interaction of infilled steel shear wall panels with surrounding frame members. Proceedings, Annual Task Group Technical Session, Structural Stability Research Council, Lehigh University, Bethlehem, PA.

7. FUNDAMENTAL PERIODS OF STEEL PLATE SHEAR WALLS

7.1 Introduction

Accurate estimation of the fundamental period of a structure is a prime consideration in calculating the design base shear and lateral forces for seismic design. Most building codes propose simple empirical expressions to evaluate the fundamental period from the structures geometry. Since the actual period cannot be calculated accurately until a first trial design is performed, these formulae are very useful for the first design iteration. Generally, code specified formulae are adjusted to give lower-bound estimates so that design seismic forces are not underestimated. Design specifications generally also permit the use of established methods of analysis to determine the fundamental periods.

Code period formulas for different lateral load resisting systems have been derived or validated against measured building periods during earthquakes. Unfortunately, up to this day there is no measured period database available for steel plate shear walls (SPSWs). Also the amount of analytical research on the determination of fundamental periods for SPSWs is still very limited. Rezai (1999) conducted low-amplitude vibration tests on two 4-storey SPSWs to determine the frequencies of the specimens. Recently, Topkaya and Kurban (2009) performed frequency analysis of 40 SPSWs (with 2 to 10 stories) to determine their natural periods. They concluded that code specified formulae usually underestimate the fundamental periods of SPSWs. However, no modification or recommendation was suggested to the simple empirical formula currently available in the building codes.

The 2000 National Earthquake Hazards Reduction Program (NEHRP) (NEHRP 2000) recommended provisions for new buildings and other structures. The following expression was proposed for calculating the building period:

$$T = C_r h_n{}^x \tag{7.1}$$

where T is the fundamental period, h_n is the height of the structure above the base, and C_r and x are constants. Design specifications such as NEHRP (NEHRP 2000), National Building Code of Canada (NRCC 2005), and Eurocode (Eurocode 2003), all use $C_r = 0.05$ and $x = 0.75$ for both reinforced concrete shear walls and SPSWs. Thus, in the current building design codes the fundamental period of vibration of a SPSW is given as

$$T = 0.05 (h_n)^{0.75} \tag{7.2}$$

It will be shown in this chapter that this equation, which was originally developed for reinforced concrete shear walls, underestimates the fundamental period of SPSWs of various geometries and mass properties. An improved formula to estimate fundamental periods of SPSWs for use in the equivalent lateral force method specified in the building codes is thus required and presented in this chapter.

Seismic provisions in design codes, such as NEHRP (NEHRP 2000) and the National Building Code of Canada (NRCC 2005), specify limits on the expected interstorey drifts in a structure, with a view to limiting the non-structural damage,

as well as controlling the impact of the $P - \Delta$ forces on seismic performance. The non-mandatory commentary to NBCC 2005 endorses a method based on the stability approach proposed by Paulay and Priestley (1992) to account for $P - \Delta$ effects. To check the interstorey drift limit and account for $P - \Delta$ effects, it is generally required to build detailed finite element models of SPSWs, which is a time consuming process. This chapter examines the effectiveness of using a simple shear flexure cantilever, instead of a full SPSW, to determine the fundamental periods, interstorey drifts, and the stability factors to account for $P - \Delta$ effects. Finally, the effect of support conditions at the base of the columns on the fundamental period is studied. Two support conditions, pinned and fixed bases, are considered in the analytical study.

7.2 Finite element model for frequency analysis

A finite element modelling approach with an implicit integration algorithm is adopted in this research. The SPSWs have been modelled and analyzed using ABAQUS (Hibbitt et al. 2007). Beams, columns, and infill plates were modelled using general purpose four-node shell elements with reduced integration (ABAQUS element S4R). This element has six degrees of freedom per node: three translations and three rotations, defined in a global coordinate system. The storey gravity loads were represented as lumped masses on the columns at every floor and the floor slabs were considered rigid in their plane. An eigenvalue extraction technique was used to calculate the natural frequencies and the corresponding mode shapes of SPSWs.

The finite element model thus developed was validated by comparing published test results with the corresponding frequency analysis results. Two 4-storey SPSW specimens, 4-storey specimen of Driver et al. (1997) and another 4-storey SPSW specimen of Rezai (1999), were modelled using the method outlined above. For the Driver et al. (1997) specimen, a gravity load of 720 kN was applied at the top of each column, as in the test itself. For the 4-storey specimen tested by Rezai (1999), 1700 kg of mass was applied at each floor, resulting in a total mass of 6800 kg. Details of these two test specimens are presented elsewhere (Driver et al. 1997, Rezai 1999). Frequency analyses were carried out for these two specimens and the first two fundamental periods were determined. Table 7.1 compares the first two fundamental periods of the two 4-storey specimens with the periods obtained from low-amplitude vibration tests (Rezai 1999). It is observed that the analytical model agrees well with the test results. For the 4-storey SPSW specimen of Rezai (1999), the first fundamental period, 0.16 sec, is underestimated by only 10% and for the test specimen of Driver et al. (1997), the first fundamental period is underestimated by only 8.75%. The natural periods for the second mode are underestimated by only 8% and 1.5% for the test specimens of Rezai (1999) and Driver et al. (1997), respectively. From a seismic design point of view, the finite element model gives conservative estimates of the fundamental periods for both the test specimens. Figure 7.1 shows the finite element (FE) mesh and the first two longitudinal modes obtained from frequency analysis of the Driver et al. (1997) specimen.

7.3 Evaluation of code formula

A series of SPSWs were designed and analysed to evaluate the code specified period formula for SPSWs. Two typical floor plans shown in Fig. 7.2 were used for this evaluation. Floor plan 1, shown in Fig. 7.2(a), has a total plan footprint area of 2014 m^2. Hypothetical symmetrical office buildings of one to nine stories with a constant interstorey height of 3.8 m were considered for this plan area. Each building, except for the eight and nine storey buildings, has two identical SPSWs provided to resist lateral forces in the E-W direction. For the eight and nine storey buildings, four identical SPSWs were provided in the E-W direction to limit the interstorey drift and $P - \Delta$ effects in every storey. For simplicity, torsion was neglected in the design of all SPSWs. In order to cover a wide range of aspect ratios, shear wall panels with three different widths (3.8 m, 5.7 m, and 7.6 m), measured from centre to centre of columns, were considered. The gravity loads applied on each column of the SPSW include dead, live, and snow loads. A dead load of 4.26 kPa was used for each floor and 1.12 kPa for the roof. The live load on all floors was taken as 2.4 kPa. Snow loads applied on the roof are calculated following the provisions of NBCC 2005, without drifting.

For floor plan 2, shown in Fig. 7.2(b), as adapted from Kulak et al. (2001), symmetrical office buildings of two, four, six, and eight stories were considered. Each building has two identical SPSWs to resist lateral forces in each direction. Two 6 m wide SPSWs are provided in the N-S direction and two 8 m wide SPSWs are provided in the E-W direction. All buildings with floor plan 2 have a

207

storey height of 4.5 m in the first storey and a constant storey height of 3.6 m for the remaining stories. The gravity loads for these buildings include: dead load of 5.0 kPa for each floor and the roof, live load of 2.4 kPa on all floors, and snow load of 1.66 kPa on the roof.

Between the two floor plans shown in Figs. 7.2(a) and 7.2(b), a total of 30 buildings were considered and they were assumed to be located in Vancouver, Canada. The buildings were assumed to contain foundations built on bedrock. The NBCC 2005 load combination $D + 0.5L + 0.25S + E$ (where $D =$ dead load, $L =$ live load, $S =$ snow load, and $E =$ earthquake load) was considered. The equivalent static force procedure was used in the design of the SPSWs. All 30 SPSWs designed in this study have a constant infill plate thickness of 3 mm, which is considered to be the minimum practical infill thickness required for handling and welding considerations. Both the AISC Seismic Provisions (AISC 2005) and CAN/CSA S16-09 (CSA 2009) enforce the capacity design approach for SPSWs under earthquake loading. Thus, the capacity design approach proposed in AISC Design Guide 20 (Sabelli and Bruneau 2007) was used to design the boundary columns and beams of all 30 SPSWs. Table 7.2 presents the final columns and beams of all SPSWs. A pinned support condition was initially assumed for the columns at the base for all the shear walls designed. The effect of the column base support condition is discussed subsequently.

Frequency analyses were carried out to determine the fundamental periods, which are presented in Table 7.2. In addition to the 30 cases presented in Table 7.2, two other sets of data, including computed periods for SPSWs from other sources, are presented in Tables 7.3 and 7.4. Thus, a total of 83 fundamental period data points for SPSWs with different heights and different geometries are used to evaluate Eq. (7.2). Figure 7.3 presents the computed periods as a function of building height, h_n, for all 83 SPSWs. Building codes usually specify an upper limit on fundamental periods calculated based on methods of structural mechanics in order to prevent the use of seismic loads that are too low due to simplified modelling assumptions. NBCC 2005 specifies that, for SPSWs, periods calculated by any established analytical method must not exceed 2.0 times the value determined by Eq. (7.2). In the 2000 NEHRP provisions, this multiplication factor varies from 1.4 for high seismic zones to 1.7 for low seismic zones. These upper limits, specified by the NBCC and NEHRP, are also illustrated in Fig. 7.3. It is observed from Fig. 7.3 that, the computed periods are shorter than the code specified fundamental periods for six cases only. The data suggest that the empirical expression in NBCC and NEHRP tends to give very conservative period estimates for SPSWs, leading to higher seismic design forces. Figure 7.3 also shows that if the NBCC upper limit for fundamental period is used in seismic design, it can be unconservative.

7.4 Alternative empirical formula for periods of steel plate shear walls

Although it is observed from Fig. 7.3 that the code-specified formula provides periods that are, in general, much shorter than the computed periods, this formula can be improved to provide better correlation with the computed periods. The generalized Equation 7.1 can be adopted, with the constants C_r and x adjusted to improve the correlation between computed and empirical values. The constants C_r and x depend on building properties and are determined by linear regression of the numerical analysis period data, as was done by Goel and Chopra (1997) for other lateral load resisting systems. Equation (7.1) can be rewritten as

$$Y = \alpha + \beta X \tag{7.3}$$

where $Y = \log(T)$, $\alpha = \log(C_r)$, $\beta = x$, and $X = \log(h_n)$. Values of α and β are determined by minimizing the squared error between available analytical periods and the computed periods. Thus, the expressions to calculate the values of α and β are

$$\alpha = \frac{\left(\sum Y\right)\left(\sum X^2\right) - \left(\sum XY\right)\left(\sum X\right)}{N\left(\sum X^2\right) - \left(\sum X\right)^2} \tag{7.4}$$

$$\beta = \frac{N\left(\sum XY\right) - \left(\sum X\right)\left(\sum Y\right)}{N\left(\sum X^2\right) - \left(\sum X\right)^2} \tag{7.5}$$

where N is the total number of period data points. The values of α and β calculated from the available SPSW periods are -1.49 and 1.066. Thus, the resulting expression to represent the best-fit to the period data of SPSWs is given by

$$T = 0.033 h_n^{1.066} \tag{7.6}$$

The best-fit expression is illustrated in Fig. 7.4. The standard error of estimate is

$$S = \sqrt{\frac{\sum_{i=1}^{n}[Y_i - (\alpha + \beta X_i)]^2}{(N-2)}} \qquad (7.7)$$

where $Y = \log(T_i) = $ computed period value ; $(\alpha + \beta X_i) = \log(C_r) + \beta \log(h_{ni})$.

The standard error, S, represents scatter in the data and approaches the standard deviation for large values of N. The value of the standard error, S, for the selected period data points was calculated as 0.106. For building codes, the period formula should provide conservative values of the period. This can be obtained by lowering the best-fit line by one standard deviation without changing its slope. Thus, the lower value of C_r, is computed from

$$\log(C_r)_L = \log(C_r) - S \qquad (7.8)$$

The best fit minus one standard deviation curve $\left(T_L = 0.026 h_n^{1.066}\right)$ is also shown in Fig. 7.4. Goel and Chopra (1997) recommended that the value of x from Eq. (7.1) lie between 0.5 and 1.0. Thus, three constrained regression analyses to determine C_r, with x fixed at 0.5, 0.75, 0.9 and 1.0, were carried out. The results from these additional analysis are presented in Table 7.5. It is observed that the values of S are significantly larger at $x = 0.5$ and $x = 0.75$, as expected. Among all the choices, for estimating fundamental periods of SPSWs, the best choice of x is 1.0, with the associated C_r value of 0.04. For seismic design of SPSWs, the best fit minus one standard deviation equation is recommended.

$$T_L = 0.03 h_n \qquad (7.9)$$

Nakashima et al. (2000) found that the period of high-rise buildings could be approximated by $T = 0.026h_n$, which is consistent with the expression obtained in this study.

As mentioned previously, building codes also specify an upper limit on the period calculated from any rational method. This upper limit in the codes is obtained by raising the best-fit line by S without changing its slope. Thus, the upper value of C_r, $(C_r)_U$, is computed from

$$\log(C_r)_U = \log(C_r) + S \tag{7.10}$$

Using Eq. (7.10), $(C_r)_U$ for SPSWs is determined as 0.05, leading to best fit plus one standard deviation curve

$$T_U = 0.05h_n \tag{7.11}$$

Both the upper limit (T_U) and the lower limit (T_L) of the period with x constrained to 1.0 are plotted in Fig. 7.5. It is observed from Fig. 7.5 that very few data points fall below the proposed period formula, Eq. (7.9), for SPSWs. The proposed empirical formula is also compared with the current building code formula, Eq. (7.2), in Fig. 7.5. It is observed that the current code formula gives lower fundamental periods, which is more conservative in terms of seismic design, especially for taller shear walls. Also, the upper limit for the proposed formula is determined as 1.7 (= 0.05/0.03) times the proposed design curve. Thus, when any rational method is used for determining the fundamental period of SPSWs, it should not be taken as longer than 1.7 times the period obtained from Eq. (7.9).

7.5 Effect of support conditions at the base of columns of steel plate shear wall

In practice, the support conditions at the base of the columns of SPSWs fall between fixed and pinned. A numerical study was also conducted to investigate the effect of column base support conditions on the fundamental periods of SPSWs. Frequency analyses of the same 30 SPSWs, initially analysed with pinned column bases, were carried out after fixing the bases of the columns. Results of these analyses are presented in Fig. 7.6. In this figure, the ratios of the fundamental periods for fixed column to pinned column support conditions are presented for all 30 models. It is observed the fixed column support condition decreases the fundamental period by an average of only 3%. The maximum period shortening was 8% for the 2-storey SPSW (case no. 6 of Table 7.2).

7.6 Shear flexure beam model for steel plate shear wall

A simple shear-flexure cantilever model to approximate the behaviour of SPSWs was developed to simplify the calculation of the fundamental period of SPSWs. The development of this model is presented in the following.

The equivalent shear-flexure cantilever, shown in Fig. 7.7 for a four-storey SPSW, includes one node per floor, and the nodes are connected by linear beam elements. Each node has a horizontal and a vertical displacement degree of freedom. The floor masses are concentrated at each node. Each beam, representing a storey, has to have flexural and shear stiffnesses equivalent to the corresponding SPSW storey.

For a simple cantilever beam the effective shear area, A_v, is given by (Charney et al. 2005):

$$A_v = \frac{I^2}{\int \frac{Q^2(y)dy}{t(y)}} \tag{7.12}$$

where Q is the first moment of the area with respect to the neutral axis, $t(y)$ is the width of the cross section at y. By analogy, the effective shear area at any storey i of a SPSW can be computed as:

$$A_{v,i} = \frac{I_{SW,i}^2}{\int \frac{Q_i^2 dA}{b^2}} = \frac{I_{SW,i}^2}{\beta_i} \tag{7.13}$$

where $I_{SW,i}$ is the equivalent moment of inertia of the SPSW at any storey i,

$\beta_i = \int \frac{Q_i^2 dA}{b^2}$, and b is the width of the section.

The exact calculation of β_i in Eq. (7.13) requires the integration of higher order polynomials and is not practical for design applications. Atasoy (2008) developed a simpler approximation for computing the value of β_i by assuming a linear variation of $\frac{Q}{b}$ along continuity regions. At any storey i, the value of β_i is taken as the sum of the contribution of the columns, $(\beta_1)_i$, and the contribution from the infill plate, $(\beta_2)_i$. This is expressed as (Atasoy 2008):

$$\beta_i = (\beta_1)_i + (\beta_2)_i \tag{7.14}$$

where

$$(\beta_1)_i = \frac{(Q_1)_i^2 + (Q_2)_i^2}{w_{c,i}} d_{c,i}$$

$$(\beta_2)_i = \frac{(Q_3)_i^2 + (Q_4)_i^2}{2w_i} b_w$$

$$(Q_1)_i = A_{cf,i}\left(0.5b_w + d_{c,i}\right) \tag{7.15}$$

$$(Q_2)_i = (Q_1)_i + A_{cw,i}0.5\left(b_w + d_{c,i}\right)$$

$$(Q_3)_i = A_{c,i}0.5\left(b_w + d_{c,i}\right)$$

$$(Q_4)_i = (Q_3)_i + \frac{(b_w)^2}{8} w_i$$

and $A_{cw,i}$ is the area of each column web at storey i; $A_{cf,i}$ is the area of the each column flange at storey i; $A_{c,i}$ is the area of each column at storey i; w_i is the infill plate thickness at storey i; $w_{c,i}$ is the web thickness of each column at storey i.

At any storey i, the equivalent moment of inertia for the SPSW, $I_{SW,i}$, is calculated as

$$I_{SW,i} = \frac{w_i\left(L - d_{c,i}\right)^3}{12} + 2I_{c,i} + \frac{1}{2}A_{c,i}(L)^2 \tag{7.16}$$

where $I_{c,i}$ is the moment of inertia of each column at storey i.

Once the shear and flexural properties for the equivalent beam are determined, frequency analysis and elastic analysis of the cantilever beam can be conducted.

7.7 Estimation of fundamental period and $P - \Delta$ effects using the shear-flexure cantilever model

A total of eight SPSWs were used to evaluate the efficiency of the shear-flexure model for estimating fundamental periods of SPSWs. These consisted of: case numbers 1, 5, 9, 18, and 22 from Table 7.2, and numbers 1, 2, and 7 from Table 7.3. The eight selected SPSWs have fixed support conditions at the bases of the columns. With the method described in the previous section, equivalent shear areas and moments of inertia in every storey were determined. Equivalent shear areas and moments of inertia for the 15-storey SPSW (No. 2 in Table 7.3) are presented in Table 7.6.

Frequency analyses of the eight equivalent shear-flexure cantilevers were carried out using ABAQUS to determine their fundamental periods. Table 7.7 shows a comparison of the fundamental periods obtained from the simple shear-flexure cantilever models with the fundamental periods obtained from the detailed finite element models of the selected SPSWs. Table 7.7 demonstrates that the fundamental period obtained from the simplified shear-flexure beam model is in excellent agreement with the fundamental period obtained from the shell element model. The maximum difference between the two periods is only 5%, obtained for the 6-storey SPSW.

The interstorey drift limit recommended in both NBCC 2005 and NEHRP 2000 is $0.025h_{sx}$, where h_{sx} is the storey height. Also, seismic design standards require that seismic-induced shears and overturning moments calculated at each storey be

amplified to account for the $P - \Delta$ effect (NEHRP 2000, NRCC 2005). According to the recommendation in the NBCC commentary, the design storey shear, V_x^*, at any level is taken as:

$$V_x^* = V_x \left(1 + \theta_{x,NBCC}\right) \tag{7.17}$$

where $\theta_{x,NBCC} = \dfrac{P_x \Delta_{mx}}{R_o V_x h_{sx}}$ is the stability factor; P_x is the total gravity load on the structure at and above the level x under consideration; Δ_{mx} is the maximum inelastic interstorey drift at level x, and h_{sx} is the storey height at that level. The NBCC commentary suggests that the $P - \Delta$ effect can be neglected if the stability factor is less than 0.10 and recommends that the structure be stiffened if $\theta_{x,NBCC} > 0.40$.

In the seismic design provision of the NEHRP 2000, the $P - \Delta$ effect is accounted for by increasing the storey shear by

$$V_x^* = V_x \big/ \left(1 - \theta_{x,NEHRP}\right) \tag{7.18}$$

where $\theta_{x,NEHRP} = \dfrac{P_x \Delta_{ex}}{V_x h_{sx}}$ is the stability factor; P_x is as defined above; and Δ_{ex} is the elastic interstorey drift corresponding to the shear force V_x. The provisions for $P - \Delta$ effects in the international building code 2000 (ICC 2000) are identical to those in the NEHRP provisions.

To investigate the effectiveness of the simple shear-flexure cantilever model for estimating interstorey drift and stability factors to account for $P - \Delta$ effects, a 4-storey and a 15-storey SPSW (case numbers 1 and 2 from Table 7.3) were

considered. Interstorey drifts and stability factors for these two SPSWs were determined using the three dimensional shell element model and were presented by Bhowmick et al. (2009). Storey displacements at each level of the equivalent shear-flexure models of the selected SPSWs were obtained from the linear elastic analysis for code specified equivalent lateral loads. Table 7.8 presents the equivalent lateral forces and the storey displacements obtained from elastic analyses of the 4-storey and 15-storey SPSWs. The elastic displacements in every storey were multiplied by $R_d R_0$ to account for the inelastic action, where R_d is a ductility-related force modification factor and R_o is an overstrength-related force modification factor. The values of R_d and R_o are specified in NBCC 2005 as 5.0 and 1.6, respectively, for ductile SPSWs. Table 7.9 and Table 7.10 compare the interstorey drifts of the 4-storey and the 15-storey SPSWs obtained using the shear-flexure beam model with those obtained from the shell element models of the full SPSW structures. For both SPSWs, the interstorey drifts obtained from the two models are in excellent agreement. For the 4-storey SPSW, the maximum ratio of interstorey drifts obtained from the two different models is 1.17 at the fourth storey, and for the 15-storey SPSW, the maximum ratio of interstorey drifts obtained from the two models is 1.18, obtained at the first storey, with the shear-flexure beam model predicting higher storey drifts in both cases. For both 4-storey and 15-storey SPSWs, the anticipated inelastic interstorey drifts (Δ_{mx}) were well below the NBCC 2005 and NEHRP 2000 drift limit of $0.025h_{sx}$ (95 mm).

218

Stability factors to account for $P - \Delta$ effects in the NBCC and NEHRP provisions were calculated and are presented in Table 7.9 and Table 7.10. It is observed from Table 7.9 that for the 4-storey SPSW, the stability factors determined using either the NBCC 2005 and NEHRP 2000 provisions are the same for the shear-flexure cantilever model and the shell element model. For the 15-storey SPSW (Table 7.10), the maximum ratio of stability factors obtained from the two different models is at the first storey and is 1.23 for the NBCC method and 1.17 for the NEHRP method, with the simplified shear-flexure cantilever model giving higher predictions. Thus, the shear-flexure cantilever model gives slightly higher values for the stability factors for the 15-storey SPSW. From a seismic design point of view, this outcome is conservative as seismically- induced shears and moments must be amplified for these higher stability factors, resulting in a stiffer SPSW system.

7.8 Conclusions

A series of SPSWs of different configurations were designed and analysed to determine their fundamental period. The periods obtained from detailed finite element models were compared with those obtained from a code-specified period formula. An improved formula based on a regression analysis of the available period data was proposed. The effectiveness of a simple shear-flexure cantilever model to determine the fundamental period and the $P - \Delta$ effects was also evaluated. Furthermore, the effects of column base support conditions on the

fundamental period of SPSWs were investigated. The main findings of the study are summarized as follows:

(1) Fundamental periods obtained from the current code empirical formula are generally lower than those obtained from a detailed frequency analysis. The code formula was found to provide a significantly lower estimate of the fundamental periods of SPSWs, especially for tall SPSWs. This can lead to excessively conservative estimates of the design seismic forces in the current codes. It is recognised that the proposed period formula derived in this study is based on the stiffness of the SPSW alone. With stiffness contributions from other structural and non-structural components in the building, the period will become slightly shorter. Thus, it is suggested that the proposed formula be re-evaluated should field measurements of periods on SPSW buildings become available.

(2) The proposed formula for determining fundamental periods for SPSWs, $T = 0.03h_n$, which is based on a regression analysis, is very simple and convenient for engineering design applications.

(3) A simple shear-flexure cantilever model was found to predict the fundamental periods of SPSWs accurately.

(4) The shear-flexure beam model was found to predict interstorey drifts accurately when compared to the interstorey drifts obtained from a detailed finite element model of SPSWs.

(5) Stability factors to account for $P - \Delta$ effects determined using the simple shear-flexure model are in excellent agreement with the stability factors obtained from detailed finite element models.

(6) The effect of column base support conditions on the fundamental period of SPSWs is generally not significant.

Table 7.1 Periods of 4-storey steel plate shear wall specimens

Specimen	First fundamental period (sec)		Second fundamental period (sec)	
	Test	Analysis	Test	Analysis
4-storey SPSW (Rezai 1999)	0.164	0.147	0.055	0.051
4-storey SPSW (Driver *et al.* 1997)	0.027	0.025	0.008	0.008

Table 7.2 Properties of SPSWs (results from FEA)

Case no.	No. of stories	Building height (m)	SPSW width (m)	Column section	Top/base beam section	Fundametnal period (sec)
1	1	3.8	3.8	W360x382	W530x150	0.16
2	1	3.8	5.7	W360x592	W610x285	0.13
3	1	3.8	7.6	W360x900	W610x498	0.11
4	2	7.6	3.8	W360x382	W530x150	0.35
5	2	7.6	5.7	W360x592	W610x285	0.28
6	2	7.6	7.6	W360x900	W610x498	0.24
7	3	11.4	3.8	W360x421	W530x150	0.56
8	3	11.4	5.7	W360x634	W610x285	0.43
9	3	11.4	7.6	W360x990	W610x498	0.36
10	4	15.2	3.8	W360x551	W530x150	0.78
11	4	15.2	5.7	W360x818	W610x285	0.58
12	4	15.2	7.6	W1000x748	W610x498	0.48
13	5	19.0	3.8	W360x551	W530x150	1.06
14	5	19.0	5.7	W360x818	W610x285	0.77
15	5	19.0	7.6	W1000x748	W610x498	0.63
16	6	22.8	3.8	W360x677	W530x150	1.31
17	6	22.8	5.7	W360x900	W610x285	0.95
18	6	22.8	7.6	W1000x883	W610x498	0.78
19	8	30.4	3.8	W360x818	W530x150	1.38
20	8	30.4	5.7	W360x990	W610x285	1.00
21	9	34.2	3.8	W360x1086	W530x150	1.53
22	9	34.2	5.7	W360x1086	W610x285	1.14
23	2	8.1	6.0	W360x551	W610x241	0.33
24	2	8.1	8.0	W360x744	W610x372	0.28
25	4	15.3	6.0	W360x744	W610x241	0.58
26	4	15.3	8.0	W360x900	W610x372	0.49
27	6	22.5	6.0	W360x900	W610x241	0.87
28	6	22.5	8.0	W360x1086	W610x372	0.72
29	8	29.7	6.0	W360x1086	W610x241	1.19
30	8	29.7	8.0	W1000x883	W610x372	1.00

All intermediate beams are W460x128, Case nos. (1-22) are for floor plan 1 and Case nos. (23-30) are for floor plan 2.

Table 7.3 SPSWs period database-1

No.	Reference	No. of stories	Height (m)	Period (sec)
1	Bhowmick et al.(2009)	4	15.2	0.58
2	Bhowmick et al.(2009)	15	57.0	2.94
3	Type D Vancouver	4	15.2	0.57
4	Type D Montreal	4	15.2	0.59
5	Type LD Vancouver	4	15.2	0.63
6	Type LD Montreal	4	15.2	0.64
7	Type D Vancouver	8	30.4	1.09
8	Type D Montreal	8	30.4	1.40
9	Type LD Vancouver	8	30.4	1.25
10	Type LD Montreal	8	30.4	1.65
11	4-storey SPSWCT	4	15.2	0.52
12	4-storey SPSWVT	4	15.2	0.53
13	8-storey SPSWCT	8	30.4	1.19

Table 7.4 SPSWs periods database-2 (Topkaya and Kurban (2009))

No.	No. of stories	Height (m)	Period (sec)	No	No. of stories	Height (m)	Period (sec)
1	2	6	0.289	21	6	18	0.645
2	2	6	0.373	22	6	18	0.832
3	2	6	0.203	23	6	18	0.412
4	2	6	0.262	24	6	18	0.532
5	2	6	0.208	25	8	24	1.285
6	2	6	0.268	26	8	24	1.66
7	2	6	0.148	27	8	24	0.796
8	2	6	0.191	28	8	24	1.028
9	4	12	0.563	29	8	24	0.901
10	4	12	0.727	30	8	24	1.163
11	4	12	0.373	31	8	24	0.564
12	4	12	0.481	32	8	24	0.728
13	4	12	0.402	33	10	30	1.692
14	4	12	0.518	34	10	30	2.185
15	4	12	0.267	35	10	30	1.032
16	4	12	0.345	36	10	30	1.332
17	6	18	0.885	37	10	30	1.196
18	6	18	1.143	38	10	30	1.544
19	6	18	0.567	39	10	30	0.735
20	6	18	0.731	40	10	30	0.949

Table 7.5 Results from regression analysis of periods of SPSWs

Regression analysis type	Period formula			S
	Best-fit	Best-fit-1 σ	Best-fit +1 σ	
Constrained with $x = 0.50$	$T = 0.17h_n^{0.5}$	$T_L = 0.11h_n^{0.5}$	$T_U = 0.26h_n^{0.5}$	0.185
Constrained with $x = 0.75$	$T = 0.08h_n^{0.75}$	$T_L = 0.06h_n^{0.75}$	$T_U = 0.11h_n^{0.75}$	0.136
Constrained with $x = 0.9$	$T = 0.05h_n^{0.9}$	$T_L = 0.04h_n^{0.9}$	$T_U = 0.069h_n^{0.9}$	0.115
Constrained with $x = 1.0$	$T = 0.04h_n$	$T_L = 0.03h_n$	$T_U = 0.05h_n$	0.108

Table 7.6 Shear-flexure properties for 15-storey SPSW

Storey	Column sections	Moment of inertia, I_{SW} (mm^4)	Effective shear area A_V (mm^2)
1-3	W360x990	3.74×10^{12}	24 886
4-6	W360x900	3.42×10^{12}	24 834
7-9	W360x744	2.83×10^{12}	24 810
10-12	W360x634	2.43×10^{12}	24 718
13-15	W360x592	2.28×10^{12}	24 708

Table 7.7 Fundamental periods evaluated by two different analytical models

No. of stories	Fundamental period (sec)	
	Shell element model	Simple shear-flexure beam model
1-storey	0.16	0.16
2-storey	0.26	0.27
3-storey	0.35	0.36
4-storey	0.58	0.57
6-storey	0.74	0.78
8-storey	1.09	1.10
9-storey	1.13	1.14
15-storey	2.94	2.98

Table 7.8 Seismic loads and forces for the steel plate shear walls

| Storey | 15-storey SPSW | | | | 4-storey SPSW | | | |
	W_x (kN)	h_x (m)	F_x (kN)	Δ_x (mm)	W_x (kN)	h_x (m)	F_x (kN)	Δ_x (mm)
1	8520	3.8	15.1	4.2	8520	3.8	154.3	2.7
2	8520	7.6	30.3	9.7	8520	7.6	308.6	5.6
3	8520	11.4	45.4	16.1	8520	11.4	462.9	8.2
4	8520	15.2	60.6	23.5	2980	15.2	215.9	9.9
5	8520	19.0	75.7	31.7				
6	8520	22.8	90.9	40.5				
7	8520	26.6	106.0	49.9				
8	8520	30.4	121.1	59.7				
9	8520	34.2	136.3	69.8				
10	8520	38.0	151.4	80.1				
11	8520	41.8	166.6	90.4				
12	8520	45.6	181.7	100.6				
13	8520	49.4	196.9	110.6				
14	8520	53.2	212.0	120.3				
15	2980	57.0	210.1	129.6				

Table 7.9 Interstorey drift and stability factors for the 4-storey SPSW

Storey	Shell element model			Shear-flexure cantilever model		
	Δ_{mx} (mm)	$\theta_{x,NBCC}$	$\theta_{x,NEHRP}$	Δ_{mx} (mm)	$\theta_{x,NBCC}$	$\theta_{x,NEHRP}$
1	22.72	0.05	0.01	21.29	0.05	0.01
2	24.00	0.04	0.01	23.33	0.04	0.01
3	21.28	0.03	0.01	20.65	0.03	0.01
4	11.92	0.01	0.003	13.97	0.02	0.003

Table 7.10 Interstorey drift and stability factors for the 15-storey SPSW

Storey	Shell element model			Shear-flexure cantilever model		
	Δ_{mx} (mm)	$\theta_{x,NBCC}$	$\theta_{x,NEHRP}$	Δ_{mx} (mm)	$\theta_{x,NBCC}$	$\theta_{x,NEHRP}$
1	28.7	0.17	0.035	33.8	0.21	0.041
2	41.2	0.24	0.047	43.4	0.25	0.050
3	48.8	0.26	0.053	51.7	0.28	0.056
4	55.7	0.28	0.057	59.1	0.30	0.060
5	61.6	0.30	0.059	65.5	0.31	0.063
6	66.4	0.30	0.060	70.6	0.32	0.064
7	70.4	0.30	0.061	75.0	0.32	0.065
8	73.6	0.30	0.060	78.6	0.32	0.064
9	75.6	0.29	0.059	80.9	0.31	0.063
10	76.8	0.28	0.056	82.2	0.30	0.060
11	77.0	0.26	0.053	82.6	0.28	0.057
12	76.3	0.24	0.049	81.8	0.26	0.052
13	74.6	0.22	0.043	80.1	0.23	0.046
14	72.4	0.17	0.035	77.6	0.19	0.037
15	73.0	0.09	0.017	74.4	0.09	0.017

(a) FE mesh (b) First longitudinal mode (c) Second longitudinal mode
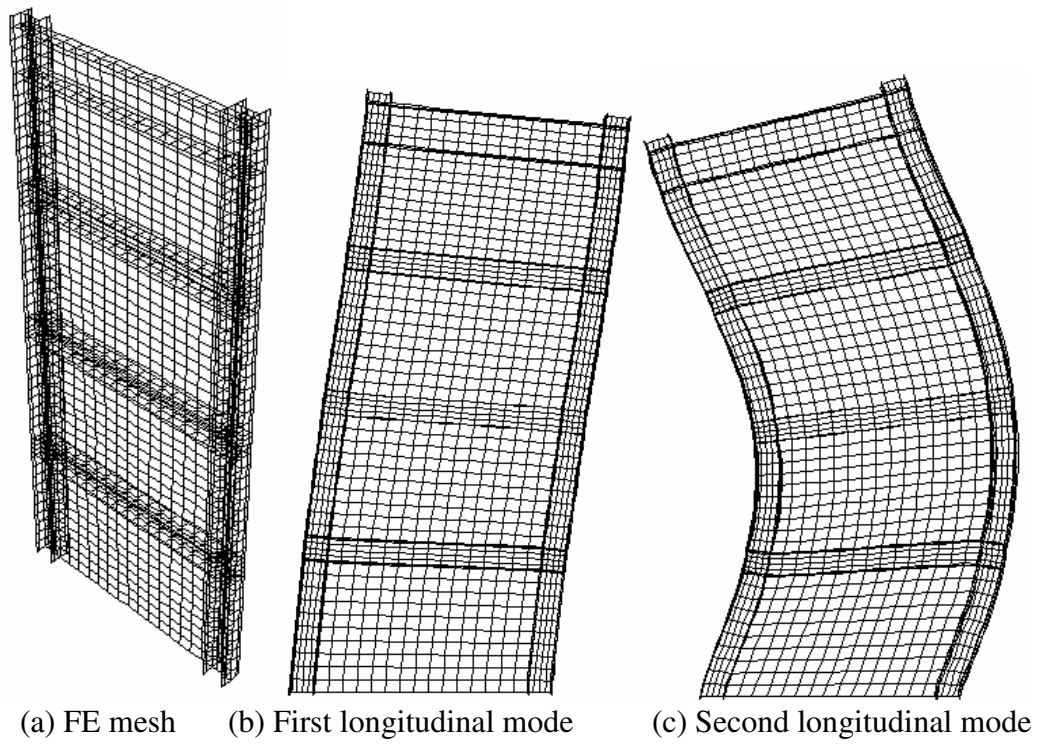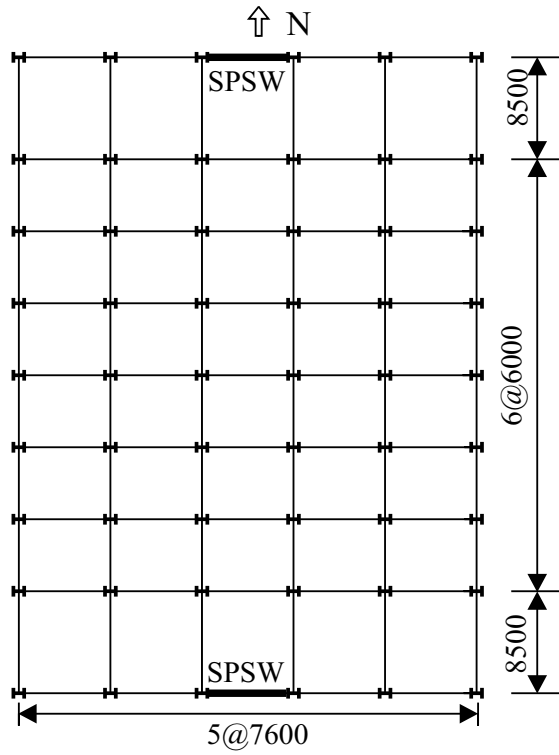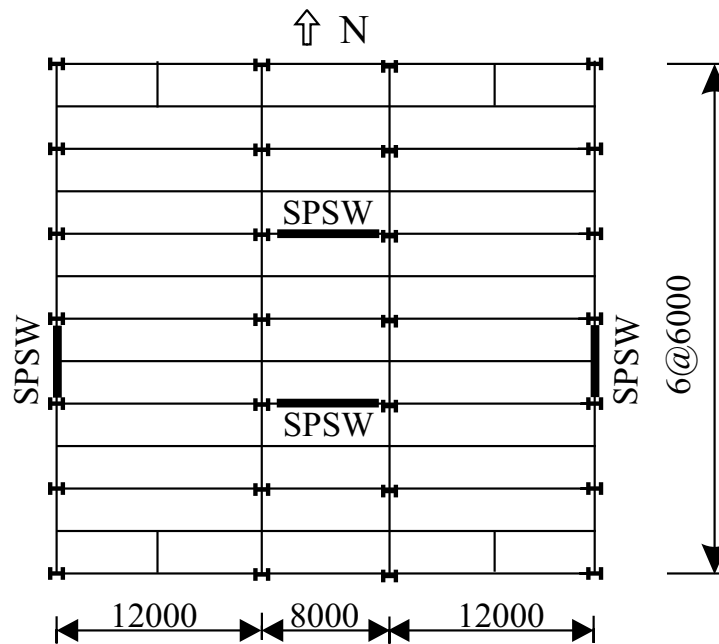
Fig. 7.1 FE mesh and longitudinal modes of Driver *et al.* (1997) specimen

(a) Floor plan 1

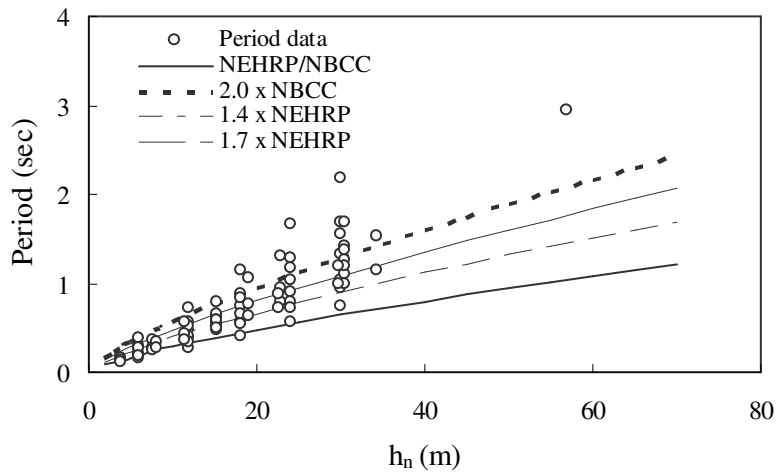(b) Floor plan 2

Fig. 7.2 Selected floor plans

Fig. 7.3 Computed and code predicted periods for steel plate shear walls
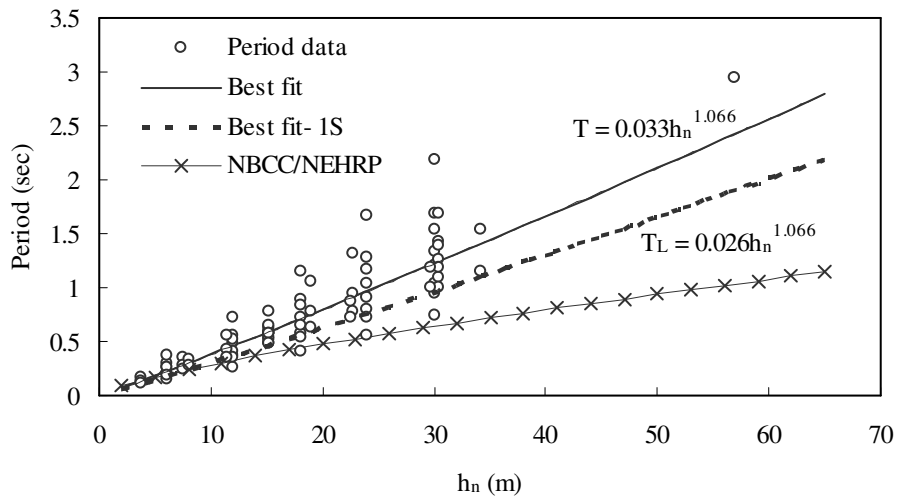

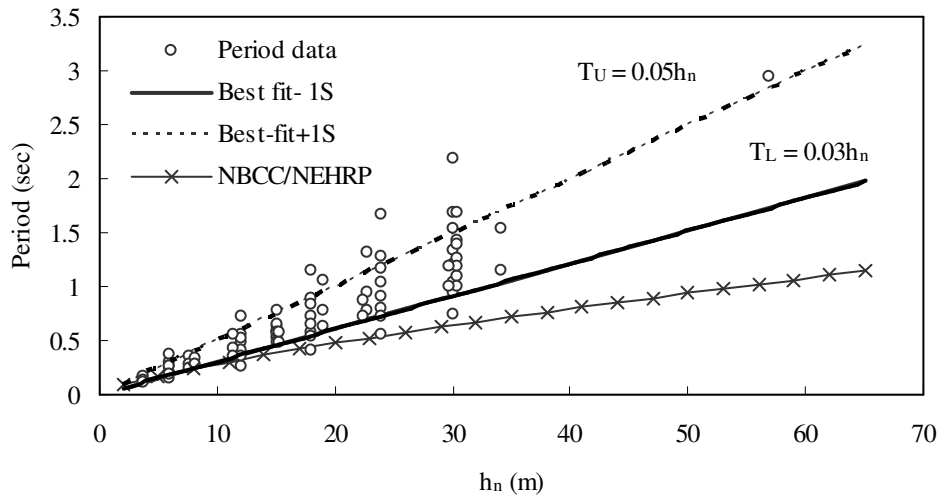Fig. 7.4 Regression analysis for periods of steel plate shear walls

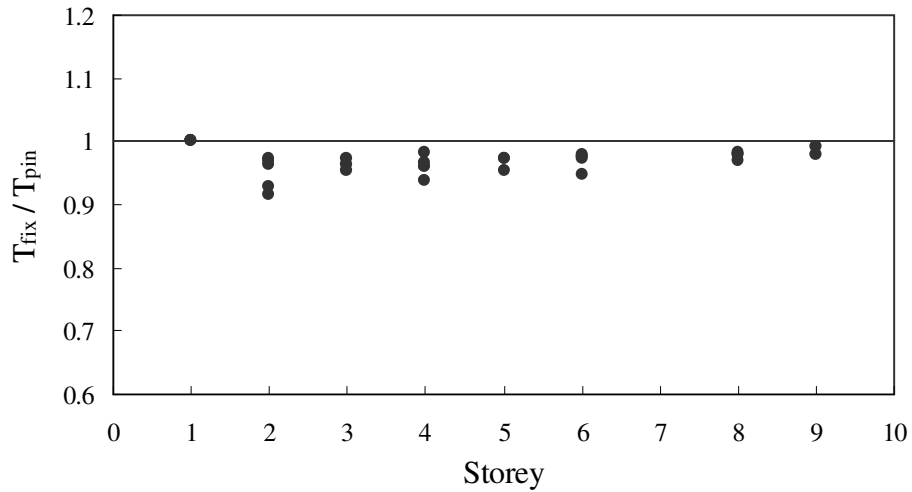Fig. 7.5 Proposed period formula and upper limit for steel plate shear walls

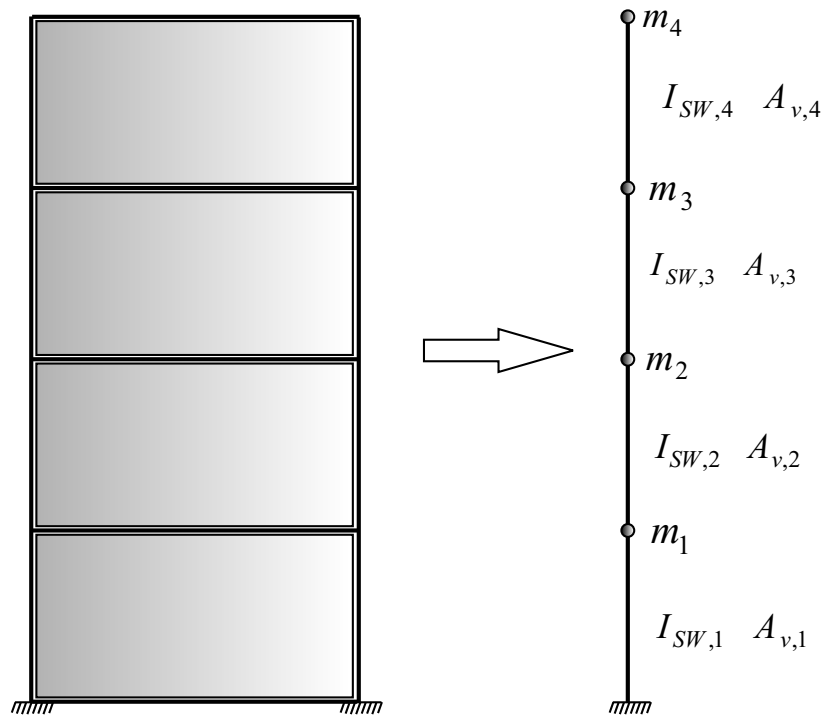Fig. 7.6 Effect of column base support conditions on fundamental periods

Fig.7.7 Shear-flexure cantilever idealization of SPSW

References

AISC. 2005. Seismic provisions for structural steel buildings. American Institute of Steel Construction, Chicago, IL.

Atasoy, M. 2008. Lateral stiffness of unstiffened steel plate shear walls. MS thesis, Middle East Technical University, Ankara, Turkey.

Bhowmick, A.K., Driver, R.G., and Grondin, G.Y. 2009. Seismic analysis of steel plate shear walls considering strain rate and P-delta effects. Journal of Constructional Steel Research, 65(5): 1149-1159.

CSA. 2009. Limit states design of steel structures. CAN/CSA S16-09, Canadian Standards Association, Toronto, ON.

Driver, R.G., Kulak, G.L., Kennedy, D.J.L., and Elwi, A.E. 1997. Seismic behaviour of steel plate shear walls. Structural Engineering Report No. 215, Dept. of Civil and Environmental Engineering, University of Alberta, Edmonton, AB.

Eurocode 8. 2003. Design of structures for earthquake resistance. Part 1: General rules, seismic actions and rules for buildings. Brussels.

Charney, Finley A., Iyera, Hariharan, and Spears, Paul W. 2005. Computation of major axis shear deformations in wide flange steel girders and columns, Journal of constructional steel research, 61: 1525-1558.

Goel, R.K., and Chopra, A.K. 1997. Period formulas for moment-resisting frame buildings. Journal of Structural Engineering, ASCE, 123(11): 1454-1461.

Hibbitt, Karlsson, and Sorensen. 2007. ABAQUS/Standard User's Manual. Version 6.7, HKS Inc., Pawtucket, RI.

International Code Council (ICC). 2000. International building code. International Code Council, Falls Church, Va.

Kulak, G.L., Kennedy, D.J.L., Driver, R.G., and Medhekar, M. 2001. Steel plate shear walls-an overview. AISC Engineering Journal, first quarter, pp. 50-62.

Nakashima, M., Yanagi, H., and Hosotsuji, J. 2000. Simple expressions for predicting fundamental natural periods of high-rise buildings. Proceedings, 1st International conference on constructional steel design, Acapulco, Mexico, pp. 385-394

NEHRP (National Earthquake Hazards Reduction Program). 2000. NEHRP recommended provisions for seismic regulations for new buildings and other structures. Building Seismic Safety Council, Washington, D.C. 2 vols., FEMA 368 and 369.

NRCC. 2005. National Building Code of Canada. Canadian Commission on Building and Fire Codes, National Research Council of Canada, Ottawa, ON.

Paulay, T. and Priestley, M.J.N., 1992, "Seismic design of reinforced concrete and masonry buildings." John Wiley & Sons, Inc., New York, N.Y.

Rezai, M. 1999. Seismic behaviour of steel plate shear walls by shake table testing. PhD Dissertation, Dept. of Civil Engineering, University of British Columbia, Vancouver, BC.

Sabelli, R. and Bruneau, M. 2007. Steel design guide 20: steel plate shear walls. American Institute of Steel Construction, Chicago, IL.

Topkaya, Cem and Kurban, Can Ozan. 2009. Natural periods of steel plate shear wall systems. Journal of Constructional Steel Research, 65(3): 542-551.

8. SUMMARY, CONCLUSIONS, AND RECOMMENDATIONS

8.1 Summary

A finite element model based on nonlinear dynamic implicit formulation was developed to study the behaviour of unstiffened steel plate shear walls. The model includes both material and geometric non-linearities and strain rate effects. The finite element model was validated using the results from a series of quasi-static and dynamic experimental programs. The validated finite element model was then used to study the performance of 4-storey and 8-storey Type D (ductile) and Type LD (limited-ductility) steel plate shear walls with moment-resisting beam-to-column connections under spectrum compatible seismic records Vancouver and Montreal.

Steel plate shear walls designed according to the NBCC 2005 and CAN/CSA S16-01 seismic provision were analyzed under spectrum compatible ground motions. Strain rate effects and $P - \Delta$ effects on the inelastic seismic responses were evaluated. Dynamic shear and moment envelopes were compared with the capacity design approaches currently available in existing literature. A seismic design procedure for determining design forces for the boundary members of SPSWs was presented. Two 4-storey and one 8-storey SPSWs, designed according to the proposed designed method were studied under design earthquake records.

Finite element analyses of unstiffened steel plate shear walls with different perforation patterns were performed. Using the concepts of strip model, developed for solid infill plate, an equation for shear strength of perforated infill plate with circular perforations was developed. A design method for the design of boundary members for perforated SPSWs was also presented.

Finally, a series of steel plate shear walls with different geometries were designed and analysed to determine the fundamental periods. The periods obtained from numerical analysis were compared against the periods obtained from code specified period formula. An improved period formula is proposed. The effectiveness of use of simple shear flexure cantilever model instead of a complete finite element model to determine fundamental periods and $P - \Delta$ effects were also evaluated. Furthermore, the effects of column base support conditions on the fundamental period of SPSWs are investigated.

The key findings from different studies on steel plate shear walls are briefly restated below.

8.2 Conclusions

The non-linear finite element model was found to be very effective to study the behaviour of SPSWs. The finite element model developed was able to provide very good predictions for quasi-static and dynamic analyses of SPSW specimens with different geometry and configurations. For quasi-static tests, the model captured all essential features of the test specimens analysed: initial stiffness, peak

load, and the post-peak behaviour. For the dynamic test of the 4-storey SPSW, the model provided excellent representations of the in-plane frequencies and storey displacements.

SPSWs with moment-resisting beam-to-column connections provided excellent structural performance in terms of stiffness and ductility. For the severe Parkfield earthquake record, the 8-storey Type LD SPSW in Vancouver experienced significant yielding in first, second, and fourth storey columns (right column). However, no soft storey was developed because of the limited plasticity in the other (left) column and partially elastic infill plate at the fourth storey. Thus, the system behaved in a robust manner.

Nonlinear seismic analysis showed that Type D SPSWs performed in a more ductile manner than Type LD SPSWs. For the 8-storey Type D SPSW in Vancouver under the severe Parkfield earthquake, yielding started at the base of one column after five bottom storey infill plates were yielded. In any case, no yielding in either column in any intermediate floor was observed for Type D walls.

It was observed from seismic analysis that the ductility demand in the 4-storey and 8-storey Type D and Type LD SPSWs in Montreal is very low. Even under the severe Parkfield 1966 earthquake record, the behaviour of the 8-storey Type

LD wall was fully elastic. Thus Type LD SPSW can be used for low to medium rise (8-storey or lower) buildings in a seismic region like Montreal or lower.

The interstorey drift distributions obtained from all inelastic time history analyses conducted were well within the 2005 NBCC limit of 2.5% of the storey height, so low to medium rise buildings with SPSWs are unlikely to be governed by drift considerations.

Since capacity design principles are not used in the design of Type LD SPSWs, in high seismic regions there is always a chance of plastic hinge formation in the boundary columns in any intermediate floor. This was observed in the analysis of the 8-storey Type LD SPSW in Vancouver under the severe Parkfield earthquake record. Plastification in boundary columns other than at the base may trigger a soft storey mechanism. Thus, it is recommended that Type LD SPSWs not be used for medium to high rise (over 8-storey) buildings in high seismic regions until the lack of capacity design requirements for this type of SPSW is rectified.

The capacity design approach in CAN/CSA S16-01 underestimates the probable shear strength at the base of the steel plate shear wall. From inelastic dynamic analyses, it was observed that flexural seismic demand at the base of the steel plate shear wall is underestimated in the current code. This is because current practice does not include the shear strength contribution from the boundary columns. It should be noted that in a taller steel plate shear walls where the

boundary columns are large at the bottom storeys, the columns may carry a larger portion of the total shear strength. Due to an underestimation in probable shear strength at the base, a lower value of the amplification factor B is estimated, which leads to a lower value of bending moment at the base of the steel plate shear wall. The analytical work also showed that for the same reason, axial force and bending moment demands in the boundary columns are underestimated.

Strain rate has an effect in the dynamic response of steel plate shear walls. With higher strain rates the ductility of the steel plate shear wall reduces and the average flexural demand at the base of the wall is increased. For seismic design of a steel plate shear wall in Vancouver, the strain rate effect increased the overturning moment by about 11% for the 4-storey and about 4% for 15-storey steel plate shear wall.

The NBCC 2005 approach for accounting for $P - \Delta$ effects is more stringent than the NEHRP 2000 approach. According to the current Canadian stability factor approach, the flexural capacity of the steel plate shear wall had to be increased by as much as 30% in one storey. The inelastic seismic analysis of the shear wall designed without any amplification for $P - \Delta$ effects showed that the $P - \Delta$ effect on the response of the structure is very small. Thus, the stability approach in NBCC 2005 seems overly conservative.

Design column moments and axial forces from the proposed procedure are shown to agree well with the results from four distinct nonlinear seismic analyses of the three SPSWs. The LE+CD method usually overestimated the design column moments and underestimates the column axial forces. The recently-proposed CD-BB method was found to be generally overly conservative in estimating design moments and axial loads for columns. Results also indicated that the modified CD-BB method may underestimate the design axial loads in the lower stories. Of all the design methods examined, the proposed method was the one that predicted the column axial forces and bending moments most reliably and consistently.

Finite element analysis showed that shear strength of an infill plate with circular perforations can be calculated by reducing the shear strength of the solid infill plate by a factor of $\left(1 - 0.7\,N_r\,\dfrac{D}{L\,\cos\alpha}\right)$. The equation gave excellent predictions of reduction in shear strengths due to perforations for SPSWs with different aspect ratios and different perforation patterns.

Results from the proposed method for design of boundary members for perforated SPSWs were observed to agree very well with the results from nonlinear seismic analysis of SPSW with circular perforations in the infill plates.

Fundamental periods obtained from the current code empirical formula are generally lower than that obtained from a detailed frequency analysis. The code

formula was found to provide a signficantly lower estimate of the fundamental periods of SPSWs, especially for tall SPSWs.

The proposed formula for determining fundamental periods for SPSWs, $T = 0.03h_n$, is very simple and convenient for engineering applications. When compared with the existing building code formula, the proposed empirical formula provided better estimates of the periods of SPSWs.

A shear-flexure cantilever model was found to predict the fundamental periods and interstorey drifts of SPSWs accurately. Stability factors to account for $P - \Delta$ effects determined by using a simple shear-flexure model were in excellent agreement with the stability factors obtained from detailed finite element models.

8.3 Recommendations for future Research

For any steel plate shear wall design, welding and handling considerations limit the infill plate thickness. Use of thicker than required infill plate thickness requires use of stiffer and stronger boundary members for capacity design approach. Experimental investigations are needed to study the effect of use of thinner infill plates on SPSWs. Also, the welding technique of a thinner infill plate should be investigated.

The proposed equation for reduction in shear strength due to circular perforations in the infill plates is based on numerical investigation. Experimental studies on

SPSWs with circular perforations in different locations in the infill plates, would verify the proposed equation as well as the proposed design method of SPSWs with circular perforations.

The study on perforation was limited to circular perforations. Therefore the results of this investigation cannot be used indiscriminately to SPSWs with perforations of other shapes. For other perforation geometries, more study is required. Also, the current study on circular perforations was conducted with only perforation diameters varying from 400 mm to 600 mm. The results of this study should be used with caution for perforations of larger diameters   More analytical studies are needed to investigate the effects of larger perforation sizes.

The proposed fundamental period formula in this study for steel plate shear walls can be progressively modified and improved, and its uncertainties can be reduced by expanding the SPSW period database with experimental and more analysis data.

The boundary columns of taller SPSWs experience large axial loads caused by high overturning moments. One way to resist that high axial loads is to encase each steel column with concrete. This will increase the sectional area of each column and decrease out-of-plane buckling of the columns. To date, very limited research has been done in this area and thus requires further study.

Experimental investigations should be carried out for SPSWs with low-yield infill plates to investigate the effectiveness of low yield infill plates in reducing the size of the boundary columns of SPSWs designed according to capacity design principles.